ANL-6794
Meteorology
Engineering and Equipment
(TID-4500, 26th Ed.)
AEC Research and
Development Report

ARGONNE NATIONAL LABORATORY
9700 South Cass Avenue
Argonne, Illinois 60440

A LABORATORY INVESTIGATION OF THE LAGRANGIAN AUTOCORRELATION FUNCTION IN A STRATIFIED FLUID

by

Paul Frenzen

Radiological Physics Division

November 1963

Reproduced from a thesis submitted to
the Faculty of the Graduate School of
The University of Chicago
in partial fulfillment of the
requirements for the degree of
Doctor of Philosophy

Operated by The University of Chicago
under
Contract W-31-109-eng-38
with the
U. S Atomic Energy Commission

DISCLAIMER

PREFACE

During the earlier portion of the relatively brief fifty-year history of the study of turbulent diffusion in the atmosphere, simplified concepts of the problem presupposing the existence of quasi-constant transfer coefficients analogous to those of molecular theory were widely employed. In more recent years, however, it has been realized that the value of these so-called "K-theories" to meteorological problems is inherently limited, and alternative, statistical methods of analysis have come into increasing use. Whereas early diffusion studies were principally confined to the consideration of the slowly changing mean values of fluctuating quantities found in turbulent fields, modern developments in both theory and instrumentation have made it possible to investigate the nature of the rapidly changing fluctuations themselves.

The continuation of this trend in the past decade can be seen in the change in emphasis that appears in the proceedings of two international diffusion symposia convened seven years apart. Papers presented at the first of these, held at M.I.T. in 1951, largely dealt with the design of instruments and the development of experimental techniques capable of exploring the structure of the turbulent atmosphere in minute detail. On the other hand, at least partly because these experimental methods had sufficiently progressed by the time of the second symposium in 1958, conferees at Oxford turned to the theoretical aspects of the problem. What is more, a significant number of these later presentations made use of the method of Lagrangian statistics originally set forth by G. I. Taylor in his now classical treatment of "Diffusion by Continuous Movements" (1921). In fact, had there

been any prior doubt, the discussions of the Oxford symposium should have firmly established this particular statistical approach in the forefront of modern concepts of turbulent diffusion.

In the current paper, experimental results are presented which demonstrate the stability dependence exhibited by the Lagrangian autocorrelation function, the principal statistical characteristic contained in the Taylor theory. A detailed review of the statistical representation of the diffusion process introduces the discussion, but the historical framework provided by the earlier K-theories has been omitted. For this background material the reader may refer to one or more of the excellent resumés which are to be found in the literature (e g., Meteorology and Atomic Energy, 1955; Sutton, 1953).

TABLE OF CONTENTS

LIST OF TABLES

LIST OF ILLUSTRATIONS

ACKNOWLEDGMENTS

This investigation was carried out under the supervision of Professor Dave Fultz of the Department of the Geophysical Sciences, The University of Chicago; his personal friendship as well as his technical advice over a long period of association has been genuinely appreciated. The writer would also like to express his sincere thanks to Mr. Leonidas D. Marinelli and Dr. John E. Rose, present and former Directors of the Radiological Physics Division, and to Mr. Harry Moses, leader of the Meteorology Section of that division, for their continued support and encouragement.

The completion of the extensive series of experiments described in this report, preceded by the development of the requisite apparatus and techniques of observation and analysis, could not have been carried out without the generous contributions of many people; their efforts in this regard are gratefully acknowledged by the author. Special thanks are due to Messrs. Eugene K. Gutowski, Robert C. Sablotni, and Lawrence O. Nippa of the Physics Shop who, along with an inexperienced assistant in the person of the writer, constructed the Argonne towing tank. Many details in the original design were suggested by Professor Gordon H. Strom of the Department of Aeronautical Engineering, New York University, while the driving mechanism, carriage, and numerous subsequent additions and modifications were due to Richard F. Selman, Edwin J. Fudala, and the late Alois J. Bragagnolo of the Staff Shop, Radiological Physics Division.

The experiments themselves were carried out with the very able assistance of Mr. William Prepejchal of the Radiological Physics Division, who also contributed a number of improvements both to the

experimental apparatus and to the methods of data reduction; the internal consistency and overall quality of the numerical results obtained owe a great deal to his skill and diligence in the operation of the analog to digital conversion apparatus.

The author is particularly indebted to Mrs. Cynthia Chamot, who, initially under the supervision of Dr. Joseph M. Cook, developed the computer program; even more importantly, she successfully kept the changing requirements of the experimental analysis commensurate with the changing facility of the Argonne digital computer GEORGE by periodically modifying the program during the extended period required to complete the investigation. The skillful assistance rendered by other members of the Applied Mathematics Division in data-tape preparation and computer operation has also been sincerely appreciated.

Particular thanks are extended to Mrs. Barbara J. Dyer and Miss Lee Cherven of the Radiological Physics Division who typed the first complete manuscript, and also to Mrs. Lesley Masson of the Division of Meteorological Physics, CSIRO, Melbourne, Australia, who prepared the final version. Similarly, a word of thanks is due the Graphic Arts Department for their work in preparation of this report.

Finally, the author would like to express his sincere appreciation to his wife, Helen, who, in her wisdom, largely overlooked the writer's throes during the preparation of this report, and so encouraged him to preserve a proper perspective during his travail.

Symbol	
M	the mesh length, the distance between component bars of the grid.
n	an eddy frequency in the power spectrum nF(n); (47). Also the stability parameter of Sutton; (14).
n_k	the frequency of the peak in the power spectrum; (49) or (53).
N^2	the Brunt-Vaisala stability parameter; (50) or (59).
N/	designates the neutrally stratified cases.
p	a pressure.
p_0	the pressure at the reference level for a potential temperature or potential density; (55).
Pr	the Prandtl number; (35).
Q	the source strength in diffusion relations; (15).
R	a correlation estimate.
Re_g	the grid Reynolds number = $\bar{U}M/\nu$.
Ri	the standard Richardson number; (54) or (56).
Ri*	the Richardson number of turbulence; (57) or (58).
$R_k(\xi)$	the k component of the Lagrangian autocorrelation function; (12).
S/	designates the stably stratified cases.
t	the decay time measured from the virtual origin t_0.
$\mathcal{t}_k$	the k component of the Lagrangian scale time; (23).
$\mathcal{t}_{ke}$	the k component of the Lagrangian scale time based upon the exponential approximation; (40).
t_0	the time of the virtual origin of the first period of homogeneous turbulent decay.
$\mathcal{t}_{zg}$	the vertical component of the Lagrangian scale time based upon the Gaussian approximation; (52).
T	the grid time measured from the time of grid passage; also, a total diffusion time as in (11).
T*	a characteristic time scale of turbulence; (33).
u,v,w	total velocities in the x,y, or z direction.

LIST OF NOTATIONS

Figures in parentheses refer to definitive or explanatory equations for the particular symbol appearing to the left.

Symbol	
a	an arbitrary constant; (37).
b	an arbitrary exponent; (61).
c	the total area under the $R_k(\xi)$ curve; (19).
c_p	the specific heat of air at constant pressure.
c_v	the specific heat of air at constant volume.
C_k	the generalized diffusion coefficients of Sutton; (15).
d	the diameter of a component bar of the grid; also used as the representative size of a decay-corrected turbulent fluctuation.
Fi	the internal Froude number; (62).
$F(n)$	the amplitude density function in the power spectrum $nF(n)$; (47).
g	the acceleration of gravity.
i	subscript designating the "i-th particle."
j	subscript designating the "j-th time."
k	subscript designating the "k-th component"; $k = x,y,z$.
K	a diffusion coefficient defined for Fickian theory; (28).
K_k^*	a virtual diffusion coefficient based upon scales of velocity and length defined by the statistical theory of turbulence; (25).
ℓ_k	the Lagrangian length scale; (24).
L_k	the Eulerian scale of turbulence; (26).
L^*	a characteristic length scale of turbulence; (33).

Symbol	
u_k	the total velocity in the k direction.
u',v',w'	turbulent velocity fluctuations in the x,y, or z direction.
u'_{ij}	the turbulent velocity fluctuation exhibited by the i-th particle at the j-th time, or the matrix of all such fluctuations.
u''_{ij}	the decay-corrected turbulent velocity fluctuation exhibited by the i-th particle at the j-th time, or the matrix of all such decay-corrected flucuations.
$\underline{u},\underline{v},\underline{w}$	root-mean-square turbulent velocity fluctuations in the x, y, or z direction; e.g., $\underline{u} = \overline{(u'^2)}^{1/2}$.
$\underline{u}_k$	the root-mean-square turbulent velocity fluctuation in the k direction; $\underline{u}_k = \overline{(u_k'^2)}^{1/2}$.
$\overline{U}$	the mean horizontal velocity, or its towing-channel equivalent, the speed of the carriage and grid.
U/	designates the unstably stratified cases.
V*	a characteristic velocity scale of turbulence; (33).
VS/	designates the "very stably stratified" cases.
VU/	designates the "very unstably stratified" cases.
WS/	designates the "weak, stably stratified" cases.
x_y	designates an x component viewed simultaneously with a y component, i.e., viewed from above.
γ	the ratio of the specific heats, c_p/c_v.
δ	the displacement factor in the compound, exponential representation of $R_k(\xi)$; (38).
η	a decay-dependent length devised by Taylor for use as an autocorrelation lag in decaying turbulence; (31).
θ	a temperature.
θ*	the potential temperature; (55).
ν	the kinematic viscosity.
λ_k	the pseudomicroscale; (45) or (46).

ABSTRACT

An experimental investigation of turbulent diffusion in a towing channel is described. Measurements of consecutive displacements of tracer particles suspended within grid-produced fields of homogeneous turbulence were corrected for decay and used to compute Lagrangian autocorrelation functions. Results in the form of correlograms and a number of turbulence characteristics obtained under conditions of three different initial turbulence intensities (i.e., three grid Reynolds numbers) in fluid stratifications ranging from weak instability to strong stability are compared.

By introducing a Richardson number of turbulence, the model is shown to be similar to prototype atmospheric motions of the order of small-scale eddy-diffusive circulations at stack height in conditions of slight to moderate stability. The results obtained demonstrate the feasibility of employing decay-corrected observations of homogeneous turbulence produced in the lee of rectangular grids for model studies of diffusion; they further suggest the usefulness of the Richardson number of turbulence and the Brunt-Vaisala stability parameter (N^2) for this purpose. More specifically, the present investigation finds that:

a) the horizontal components of the Lagrangian time scale either increase slowly or remain relatively stationary with increasing stability while the vertical component steadily decreases, a behaviour in marked contrast to that of the several components of the Eulerian scales which, in similar circumstances, are observed to uniformly decrease;

b) in most cases, Lagrangian autocorrelation functions can be accurately represented by modified, negative exponential functions,

Symbol	
μ	the dynamic viscosity.
κ	the thermometric conductivity.
ξ	the autocorrelation lag time; (12).
$\xi_{R=O}$	the time to zero, i.e., the value of ξ for which $R_k(\xi) = 0$.
ρ	a density.
ρ^*	the potential density; (55).
σ_k^2	variance of cross-wind distributions of dispersing tracer in the k direction (cf. Table 19).
τ	a decay-corrected time interval; (34)
χ	the concentration of pollutant at a point downstream; (15).

namely, $R_k(\xi) = 1$ for $\xi < \delta$ and $R_k(\xi) = \exp - \left(\frac{\xi - \delta}{a}\right)$ for $\xi \geq \delta$; however, in the specific instance of the vertical component in stable stratifications of sufficient strength ($N^2 > 10^{-2}$ sec^{-2} in the model), Gaussian normal error functions are more appropriate; thus, $R_z(\xi) = \exp -(\xi/a)^2$;

c) the foregoing results may be taken to indicate that relations between Lagrangian and Eulerian turbulence statistics are 1) strongly dependent upon gravitational stability, and 2) more complex than the simple scale factors between independent variables sometimes assumed.

In addition, two-dimensional (x,z) jet profiles were observed to form under conditions of stable stratification in association with regimes of increased disappearance of turbulent energy within the levels of maximum mean velocity; this suggests that, in these circumstances, the turbulence field supplies energy directly to the mean circulation.

CHAPTER I

AN INTRODUCTION TO THE PROBLEM

The basic foundations of the statistical theory of turbulence were set forth in an extensive series of papers by G. I. Taylor in 1935 and 1936. However, the particular portion of the general theory that applies to the diffusion problem, namely, the concept of "diffusion by continuous movements," was given by the same author some fifteen years earlier (Taylor, 1921). Thus, historically, eddy diffusion was the first aspect of turbulence to be treated by statistical methods

In the statistical approach, fields of turbulent motion are described in terms of functional relationships among the component turbulent fluctuations. The analysis is "statistical" in the sense that large numbers of instantaneous values of these rapidly changing fluctuations become involved, their aggregate contributions to a particular system being assessed through the estimation of collective expressions or "statistics" such as mean-square distributions, correlation functions, or power spectra. In general, such functions can only be estimated, since the data at hand in the form of some finite number of measurements do not ordinarily consist of more than a relatively small sample extracted from a much larger population.

In practice, accurate estimation of the statistical characteristics of turbulence presents unusual difficulties; data of extraordinarily fine resolution in time or space are required, and therefore highly specialized techniques of observation must be employed. This is especially true in the atmospheric boundary layer, where a significant fraction of the turbulence spectrum includes eddies of high frequency and small wavelength. More particularly, the acquisition of Lagrangian data suitable to the Taylor diffusion theory poses unique problems

unlike any in ordinary meteorology, since the Lagrangian formulation requires that observations be referred to individual, dispersing particles moving with the fluid rather than to a more convenient origin fixed in space. Consequently, it has seldom been found feasible to apply the statistical theory of turbulent diffusion directly to an atmospheric problem. However, the principles of the Taylor theory are very often employed indirectly in the form of certain semi-empirical diffusion relations derived from them by Sutton (1947).

At the present time Sutton's equations (e.g., equation [15] below) are widely employed in air-pollution surveys. Indeed, these relations have been shown to be capable of determining acceptable estimates of the distribution of pollutant concentrations downstream when the atmospheric lapse rate is approximately adiabatic The difficulty arises from the fact that, except during relatively infrequent periods of overcast skies and sustained high wind velocities, the adiabatic condition primarily occurs only as a transient state in the atmospheric boundary layer. Ordinarily, neutral stratification exactly occurs but twice daily in the lowest 100 m during transition between prevailing day-time regimes of positive and night-time regimes of negative stability. At Argonne National Laboratory, for example, three years of temperature differences observed between 2 and 42 m indicate that mean hourly lapse rates within 25 per cent of the adiabatic (i.e., $d\theta/dz = -1.0 \pm 0.25$ deg per 100 m) characterize only one hour out of eight (cf. Moses and Willett, 1955). Unstable stratifications with lapse rates in excess of the adiabatic were recorded during 26 per cent of the time, while definitely stable conditions in which the temperature actually increased with height were observed to comprise a surprising 46 per cent of the data.

Thus, as much as 80 per cent of the time, the neutrally stratified conditions necessary for the adequate performance of existing diffusion formulae simply are not present in the regions of primary interest to air-pollution surveys. It is therefore of considerable

practical interest to assess the influence exerted upon the turbulent diffusion process by conditions of fluid stability other than those of neutral stratification; and it is with this aspect of the atmospheric diffusion problem that the current investigation is concerned.

The Purpose of the Experiment

The investigation described in this report has been based upon the premise that the statistical representation of the turbulent diffusive mechanism contained in the Taylor diffusion equation is a fundamental kinematic statement that applies equally to fluids of stable and unstable, as well as neutral, density stratification. This fact is evident in the nature of the Taylor relation itself, for it contains no dynamic terms sensitive to the presence of external buoyancy forces (cf. equation [11], below). Rather, the dispersion achieved by a set of diffusing particles at any time in a fluid of any stability condition is expressed solely as a function of the intensity of turbulence and of a characteristic statistical description of the fluctuation velocity field known as the Lagrangian autocorrelation function.

Now it is well known that the presence of positive or negative buoyancy forces in a stratified fluid profoundly affects the rate of turbulent diffusion. One experimental procedure frequently employed in the field, as well as in the laboratory, directly evaluates this effect by measuring diffusion rates in fluids of different stabilities. But more fundamentally, the Lagrangian autocorrelation function itself must also be affected by these forces since, as the Taylor expression shows, this statistical expression is intimately connected with the rate of dispersion. In fact, since it does lie so close to the heart of the problem, it is reasonable to expect that an alternative experimental procedure which investigates the influence of fluid stability upon this correlation function should grant greater insight into the influence of density stratification upon the mechanism of turbulent diffusion.

With these considerations a laboratory model was designed in which the Lagrangian autocorrelation function could be evaluated by observing the motions of particles in turbulent fields generated in fluids of several gravitational stabilities. Results obtained from the subsequent experimental program are presented in this report in the form of autocorrelograms and a number of characteristic quantities derived from them. These results are compared with similar measurements obtained by others in meteorological field studies. In addition, there is discussed the similarity range within which circulations in the laboratory model and in the prototype atmosphere can be compared.

At the very outset it should be noted that although the fluctuation velocities utilized in these calculations do indeed derive from actual measurements, the steady-state fields of turbulence capable of supplying stationary time series data necessary for autocorrelation analysis never truly existed. The real fields of turbulence created within the experimental apparatus by the single passage of a rectangular grid inevitably underwent rapid decay, since the model contained no continuing source of turbulent energy. However, with the aid of certain well-founded assumptions upon the nature of this decay process, the motions of tracer particles observed in these fields were corrected for decreasing turbulent energy and increasing eddy scale. In the language of fluid-models research, the laboratory model employed in this study was a "distorted" one.[1] Consequently, before its representation could be compared with the reality of a prototype, the effects of that distortion had to be removed. The decay-correction procedures employed do impose certain limitations upon the experiment, as will be discussed

---

[1] A familiar example of the use of distorted hydraulic models can be found in studies of river systems for which, in order to minimize capillarity effects that tend to dominate thin sheets of water, the depth dimensions of river models are exaggerated; correction for distortion in this case is achieved by increasing the bottom roughness of the models to generate deeper turbulent boundary layers.

below; on the other hand, without them this program of Lagrangian measurement under the controlled conditions of the laboratory would not have been possible.

The Taylor Diffusion Equation

Because it is fundamental to the interpretation of the results of this investigation, it is useful to discuss both the derivation and the implications of the Taylor diffusion relation in some detail. This representation of turbulent diffusion bears a closely analogous relationship to a well-known analysis of dispersive motion on the molecular scale. The description of Brownian motion known as "the random walk" concerns the one-dimensional dispersion that results after a large number of particles undergo a series of equally probable, forward or backward displacements of constant magnitude from a common origin (cf. Sutton, 1953, p. 89-91). Taylor (1921) extended this concept to conditions more representative of fluid motion on the macroscale by providing for "continuous movements"; in his analysis, both the magnitude and probability of occurrence of the particle displacements were allowed to vary continuously in a manner prescribed by the character of the turbulent field.

The Taylor relation can be derived by considering a one-dimensional system of particles (or marked fluid parcels) which issue from a continuous point source but are constrained to move back and forth in only one direction. This is equivalent to limiting consideration of a three-dimensional system to the normal projections upon the x-axis of the positions of all particles in a diffusing cloud. From either point of view, the instantaneous position of each particle relative to the location of a common source at $x = 0$ can be designated by a single coordinate, $\pm x_i(t)$.

At any time t, the net displacement $x_i(t)$ that any one particle (say the i-th) has attained is the result of the integrated displacement increments contributed by all velocity fluctuations that particular

particle has experienced since leaving the source. Thus, we may write

$$x_i(t) = \int_0^t u_i'(\tau)\, d\tau, \tag{1}$$

where $u_i'(\tau)$ represents the instantaneous turbulent velocity fluctuation exhibited by the i-th particle at any time. Evidently the mean square of all such net displacements shown by all particles of a system at some particular time constitutes a statistical measure of the degree of dispersion achieved by the diffusive mechanism in the direction of x. Hence, we have

$$\overline{x^2(t)} = \frac{1}{N} \sum_{i=1}^{N} [x_i(t)]^2 = \frac{1}{N} \sum_{i=1}^{N} \left[\int_0^t u_i'(\tau)\, d\tau\right]^2. \tag{2}$$

Here the summation notation serves to emphasize that the foregoing is an instantaneous average over all N particles of the system.

In order to examine the time variation of the dispersion, we take the first derivative of the above:

$$\frac{d}{dt}[\overline{x^2(t)}] = \frac{2}{N} \sum_{i=1}^{N} \left\{\left[\int_0^t u_i'(\tau)\, d\tau\right] u_i'(t)\right\}. \tag{3}$$

With regard to the integral remaining within the brackets on the right, it is convenient to make the transformation

$$\tau = t - \xi \tag{4}$$

(cf. Haltiner and Martin, 1957, pp. 276-7). Thus $d\tau$ becomes $-d\xi$ and, with appropriate changes in limits, the integral becomes

$$-\int_t^0 u_i'(t - \xi)\, d\xi = \int_0^t u_i'(t - \xi)\, d\xi. \tag{5}$$

Since $u_i'(t)$ is not a function of ξ, it can be brought inside the integral, and the entire expression (3) can be rewritten as

$$\frac{d}{dt}\left[\overline{x^2(t)}\right] = \frac{2}{N}\sum_{i=1}^{N}\left[\int_0^t u_i'(t-\xi)u_i'(t)\,d\xi\right]. \tag{6}$$

Interchanging the operations of summation and integration, we obtain

$$\frac{d}{dt}\left[\overline{x^2(t)}\right] = 2\int_0^t \frac{1}{N}\sum_{i=1}^{N}\left[u_i'(t-\xi)u_i'(t)\right]\,d\xi \tag{7}$$

or, upon adopting the superposed bar for the instantaneous average over the system designated by the summation notation, we have

$$\frac{d}{dt}\left[\overline{x^2(t)}\right] = 2\int_0^t \overline{u'(t-\xi)u'(t)}\,d\xi. \tag{8}$$

From the definition of the Lagrangian autocorrelation function $R_x(\xi)$ we may write

$$\overline{u'^2}\,R_x(\xi) = \overline{u'(t-\xi)u'(t)}, \tag{9}$$

where the subscript x denotes the component of the diffusive mechanism under consideration.

Substituting this expression in (8), we obtain

$$\frac{d}{dt}\left[\overline{x^2(t)}\right] = 2\overline{u'^2}\int_0^t R_x(\xi)\,d\xi, \tag{10}$$

in which the term $\overline{u'^2}$ has been moved outside the integral with the understanding that thereby the analysis becomes limited to consideration of a turbulence field whose average intensity remains approximately stationary in time. This is not an entirely unreasonable restriction, at least insofar as small-scale diffusion of brief duration in the atmospheric boundary layer is concerned. However, it is a requirement that must receive special consideration before the Taylor theory can be applied to the decaying turbulence fields of the laboratory experiments described in this report.

Finally, by integrating equation (10) over a period of diffusion T, one obtains the Taylor diffusion equation:

$$\overline{x^2(T)} = \overline{2u'^2} \int_0^T \int_0^t R_x(\xi)\, d\xi\, dt. \tag{11}$$

Similar expressions for $\overline{y^2}$ and $\overline{z^2}$, respectively involving $R_y(\xi)$ and $R_z(\xi)$, extend the analyses to three dimensions.

As many writers have pointed out, this expression is especially remarkable in that it reduces the problem of diffusion in fields of quasi-stationary turbulence intensity to consideration of the properties of a single set of statistical relations, namely, the three components of the Lagrangian autocorrelation function:[1]

$$R_k(\xi) \equiv \frac{\overline{u_k'(t)u_k'(t+\xi)}}{\overline{u_k'^2}}. \tag{12}$$

Surprisingly, especially in view of the length of time this result has been known, comparatively little quantitative information on the behaviour of these functions has been obtained.

Applications; Sutton's Equations

Practical utilization of the principles set forth in the Taylor diffusion theory has been accomplished by Sutton (1947), who derived a set of expressions for diffusion from a point source from equation (11) by making certain assumptions upon the nature of the autocorrelation function. Using dimensional arguments, Sutton showed that, in a layer

---

[1] The notation $R_k(\xi)$ here and in the general discussions to follow refers equally to any one of the three components of the Lagrangian autocorrelation function, i.e., k = x, y, or z. Further, x_k will represent all three displacements while $u_k = dx_k/dt$ will represent the three components of velocity.

In (12) we have adopted the more familiar convention of positive lag time ξ; evidently, this form and that which appears in (9) are equivalent, for when t_2 is written for $t_1 - \xi$, then $t_2 + \xi$ corresponds to t_1.

of air flowing over a smooth surface, $R_k(\xi)$ could be approximated by expressions of the form

$$R_k(\xi) = \left[\frac{\nu}{\nu + \overline{(u_k'^2)}\xi}\right]^n. \tag{13}$$

Here ν is the kinematic viscosity, and the exponent n is a stability parameter varying between 0 and 1 in accordance with the horizontal wind-profile expression

$$\overline{u(z)} = \overline{u_1}\,(z/z_1)^{\frac{n}{2-n}}. \tag{14}$$

For flow over rough surfaces, Sutton suggested that ν be replaced by the macroviscosity, $N = u_* z_0$, in which the friction velocity u_* is a measure of the surface stress, and z_0 is a roughness length descriptive of the underlying surface.

Upon substituting these approximations for the components $R_k(\xi)$ in the Taylor equations and integrating, Sutton obtained a combined expression for the three-dimensional distribution of pollutant concentration that would result at a point at any time after an instantaneous emission from a point source of strength Q:

$$\chi(x,y,z,t) = \frac{Q}{\pi^{3/2} C_x C_y C_z (\bar{u}t)^{3(2-n)/2}} \exp\left[-(\bar{u}t)^{n-2}\left(\frac{x^2}{C_x^2} + \frac{y^2}{C_y^2} + \frac{z^2}{C_z^2}\right)\right] \tag{15}$$

Along with a number of related expressions extending this analysis to continuous sources, line sources, elevated sources, etc., equation (15) introduced the so-called "generalized diffusion coefficients," C_x, C_y, and C_z, as well as the stability factor n; taken together, these have come to be known as "Sutton's parameters." For diffusion in near-adiabatic conditions with moderate wind flow over level grass land, Sutton cites the following values obtained from field measurements (Sutton 1953, p. 292):

$n = 1/4$; $C_y = 0.4\ cm^{1/8}$, $C_z = 0.2\ cm^{1/8}$.

These are appropriate to the continuous point-source version of Sutton's equations in which the influence of C_x is considered negligible in comparison with the much larger contributions to longitudinal transfer made by the mean flow, hence, a C_x value does not appear. Note that the recommended value $n = 1/4$ in equation (14) exactly corresponds to the "seventh-root profile" which wind-tunnel studies have found to characterize the turbulent boundary layer of a smooth, flat plate.

Sutton's equations are widely employed in air-pollution surveys such as those associated with the evaluation of potential nuclear reactor hazards. Their application to engineering problems of this kind has, in fact, been reduced to the reading of a series of nomograms (cf. Meteorology and Atomic Energy, 1955); and new evaluations of Sutton's parameters for atmospheric conditions other than adiabatic periodically appear in the literature. However, such procedures have on occasion been decried on the grounds that they tend to encourage the view that these relations represent a kind of physical law which need only be mapped over the entire range of appropriate meteorological variables in order to be able to predict pollutant concentration distributions to be expected under any and all atmospheric conditions. Too often Sutton's equations are accepted without their critical dependence upon semi-empirical approximations of $R_k(\xi)$ being fully appreciated. Rather than continuing to evaluate C's and n's, a more profitable line of research would seem to lie in the investigation of the nature of the Lagrangian autocorrelation function itself.

CHAPTER II

THE LAGRANGIAN AUTOCORRELATION FUNCTION

The Lagrangian autocorrelation function $R_k(\xi)$ expresses the dependence of the correlation between the k^{th} component of the velocity of an "average particle" and its own values at later times upon the lag time allowed to elapse between the velocity observations correlated. Here the use of the term "average particle" emphasizes that, as in the preceding discussion of the diffusion equation, the superposed bar notation in (12) designates an average taken over all or (as usually must be the case in practice) a large sample of the particles in a system The function $R_k(\xi)$ is also averaged over all t, for each autocorrelation lag ξ refers to any and all base times. Statistically speaking, estimates of any particular $R_k(\xi_1)$, determined from any number of representative sets of particles selected from a given system and based upon any number of similarly representative sets of times along the trajectories of these particles, will necessarily converge to a single value, provided only that the samples are sufficiently large and that the turbulent velocity fluctuations constitute a stationary time series.

From the continuous nature of fluid motion, it is apparent that components of the velocity of individual diffusing particles will tend to remain highly correlated with their own previous values for some short period of time; speeds and directions will not be subject to sudden, discontinuous change. In other words, $R_k(\xi)$ will tend to preserve a value near unity so long as ξ remains small. On the other hand, velocities of particles moving in the more or less random manner characteristic of turbulence eventually must, on the average, become

entirely unrelated to their magnitudes and directions at some earlier reference time. In terms of an autocorrelation function truly representative of the behaviour of an infinitely large population of particles in random motion, $R_k(\xi)$ falls to zero when ξ becomes sufficiently large. Of course, in the random motion of a limited number of particles, chance alone will dictate that a significant fraction of their number will repeat earlier velocities from time to time. Therefore, estimates of $R_k(\xi)$ based upon limited samples drawn from a larger population cannot be expected to maintain a value of exactly zero for all large ξ; rather, they will be observed to oscillate around zero as a mean.

These considerations enable one to estimate a priori that the Lagrangian autocorrelation function will in general, behave in the manner sketched in Figure 1, at least during the early and late periods. Details characteristic of the intermediate period ($\xi_1 < \xi < \xi_2$ in the figure) cannot be anticipated, for in this region the rate at which $R_k(\xi)$ decreases depends upon the specific properties of the particular field of turbulence for which the function has been evaluated As the results of this experimental study show, one of the factors which can influence the shape of the $R_k(\xi)$ curve in this intermediate region is the gravitational stability of the fluid medium. The effect is most pronounced in the case of the vertical component $R_z(\xi)$ which under stably stratified conditions, for example falls to zero significantly earlier than it does otherwise.

Two Regimes of Diffusion

Taylor demonstrated the control exerted by the autocorrelation function upon the diffusion process by describing two limiting solutions of equation (11). With the dependence of $R_z(\xi)$ upon fluid stability in mind, an examination of these solutions clarifies the role played by stability in the determination of turbulent diffusion rates in the atmosphere.

Consider, first, the consequences of a diffusion time so short, and hence a maximum lag time ξ so limited, that the vertical component of the autocorrelation function, $R_z(\xi)$, remains very nearly unity for all ξ. With reference to Figure 1, this obtains when $T < \xi_1$. The inner integral of equation (11) then becomes simply

$$\int_0^t R_z(\xi)\, d\xi = \int_0^t 1\, d\xi = t, \tag{16}$$

and the solution of the entire expression reduces to

$$\overline{z^2} = 2\overline{w'^2} \int_0^T t\, dt = \overline{w'^2}\, T^2 \tag{17}$$

or

$$\overline{(z^2)}^{1/2} \propto T \quad \text{when} \quad T < \xi_1. \tag{18}$$

Consider this result in relation to vertical dispersion from the horizontal axis exhibited by particles simultaneously transported by a uniform horizontal flow, neglecting longitudinal diffusion in comparison to the much larger displacements contributed in this direction by the mean current. Equation (18) indicates that the dispersing particles will initially occupy a conical plume as shown schematically in Figure 2, for the envelope expands linearly with time. For the purpose of these illustrations, the volume occupied by diffusing particles in a plume can be delineated by assuming they are distributed normally along any section perpendicular to the horizontal axis of the plume, and that the radius to the visible edge can be identified with some constant multiple of the root-mean-square displacement. Theoretical outlines do not correspond to the instantaneous outlines of smoke plumes seen in the atmosphere; rather, they are more properly compared with composite envelopes of instantaneous plumes determined, for example, by multiple-exposure photographs.

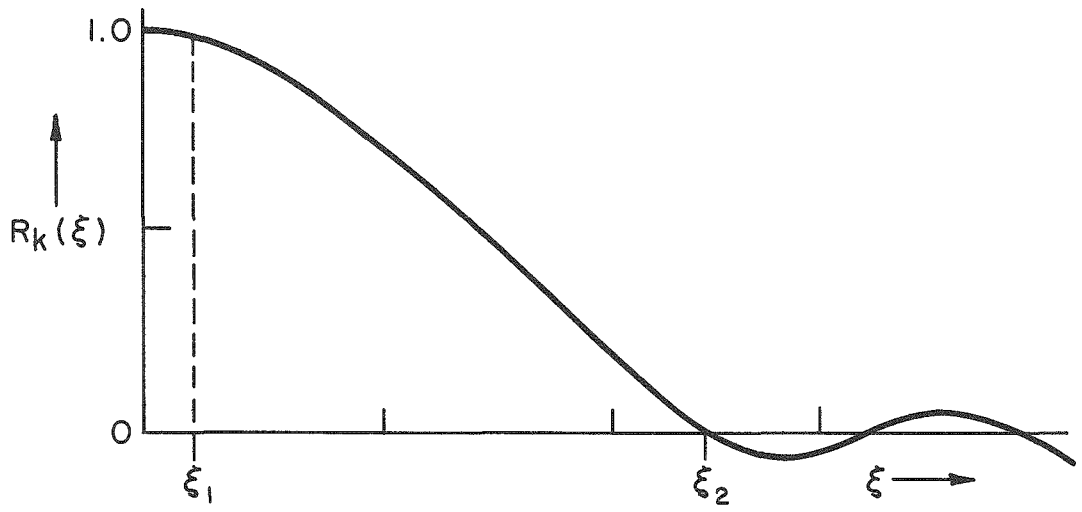

Fig. 1.--The nature of the Lagrangian autocorrelation function; $R_k(\xi) \approx 1$ for $\xi < \xi_1$; $\overline{R_k(\xi)} = 0$ for $\xi > \xi_2$.

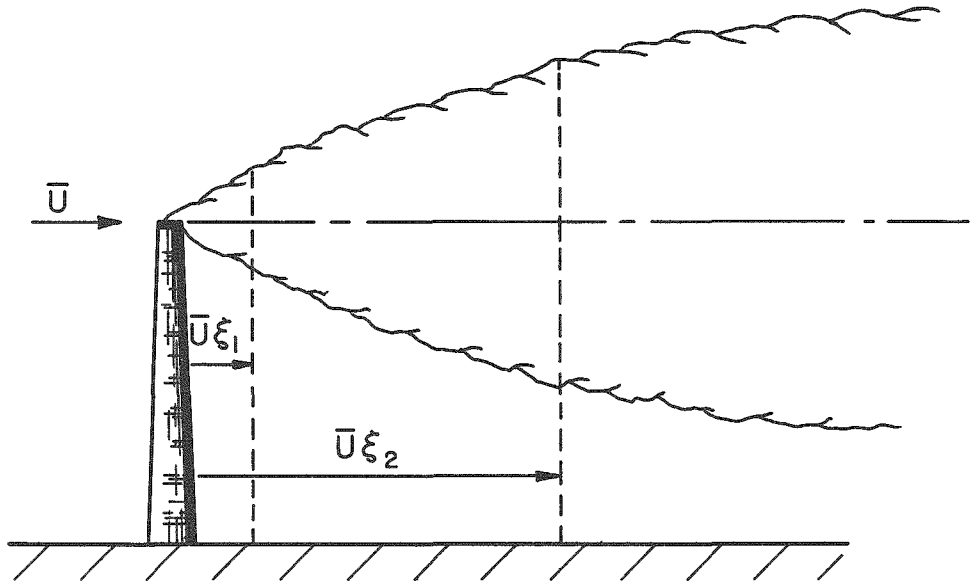

Fig. 2.--Theoretical average plume outline predicted by Taylor diffusion equation; plume approximately conical over initial length, $x < \overline{U}\xi_1$, but becomes approximately parabolic when $x > \overline{U}\xi_2$.

After the diffusion process has continued for a sufficiently long period (more particularly, until $T > \xi_2$ in Figure 1), the inner integral of (11) attains a constant value c equal to the total area under the $R_z(\xi)$ curve. This follows from the fact that the average value of $R_z(\xi)$

is zero after ξ_2, and no further net contribution to the integral is made after that time. In this second example, the diffusion equation becomes

$$\overline{z^2} = 2\overline{w'^2}\int_0^T c\,dt = 2c\overline{w'^2}T \tag{19}$$

or

$$\overline{(z^2)}^{1/2} \propto T^{1/2} \quad \text{when} \quad T \gg \xi_2. \tag{20}$$

Thus, the volume occupied by the plume eventually assumes the shape of a paraboloid as shown in Figure 2.

These two envelopes of diffusion can be seen to succeed one another under atmospheric conditions in the initial and final <u>average</u> outlines of smoke plumes issuing from stacks. The phenomenon has been used to estimate the time required for $R_Z(\cdot)$ to fall to zero from composites of photographs taken from the side of smoke issuing from factory chimneys by noting the horizontal distance from the source to the point where transition from the linear to the parabolic regime has been completed (Inoue, 1960).

In stably stratified atmospheres, transition from the rapidly thickening, conical plume shape to the more slowly divergent parabolic one occurs earlier than it does when the lapse rate either equals or exceeds the dry adiabatic. As a result, the vertical dimensions of plumes in stable air remain relatively shallow, and proportionately higher concentrations of the contaminant that a particular stack has been designed to disperse are maintained for longer distances downstream. At the other extreme, final attainment of the parabolic regime tends to be delayed in unstable atmospheres, a phenomenon which may also be inferred from the results of the current laboratory studies. Consequently, diffusing plumes grow to greater diameters at comparable distances; hence, their constituents undergo more rapid dilution.

The growth of a diffusing plume downstream does not depend solely upon the behaviour of $R_k(\xi)$; the intensity of the turbulent field, $\overline{u'^2_k}$, is also involved. In fact, as may be seen from the first derivative of (17), the constant rate of plume growth characteristic of the early, linear regime depends upon $\overline{u'^2_k}$ alone:

$$\frac{d}{dt}(\overline{x_k^2})^{1/2} = \frac{d}{dt}[(\overline{u_k'^2})^{1/2}T] = (\overline{u_k'^2})^{1/2}. \tag{21}$$

In the region of transition, the influence of $R_k(\xi)$ gradually makes itself felt as its value falls from unity. Plume growth rate decreases with decreasing $R_k(\xi)$ until, upon reaching the parabolic regime as the average value of $R_k(\xi)$ attains zero, it becomes

$$\frac{d}{dt}(\overline{x_k^2})^{1/2} = \frac{d}{dt}[(2c\overline{u_k'^2}T)^{1/2}] = (2c\overline{u_k'^2})^{1/2}T^{-1/2}, \tag{22}$$

which follows from equation (19).

Lagrangian Turbulence Parameters

It is useful at this point to note that equations of the form of (22) above (as well as equation [19] earlier) contain, either explicitly or implicitly, the following characteristic expressions descriptive of turbulence in Lagrangian coordinates:

$$c = \int_0^\infty R_k(\xi)\, d\xi \equiv \mathcal{t}_k; \tag{23}$$

$$c(\overline{u_k'^2})^{1/2} = (\overline{u_k'^2})^{1/2} \int_0^\infty R_k(\xi)\, d\xi \equiv \ell_k; \tag{24}$$

$$c(\overline{u_k'^2}) = \overline{u_k'^2} \int_0^\infty R_k(\xi)\, d\xi \equiv K_k^*. \tag{25}$$

The first of these, $\mathcal{t}_k$, is termed the Lagrangian scale time; the second, ℓ_k, differing from the first only by the velocity factor $(\overline{u_k'^2})^{1/2}$, is known as the Lagrangian scale length. Both parameters are at least

homologous, if not entirely analogous, to the more familiar Eulerian scale of turbulence:

$$L_k = \int R(x_k)\, dx_k, \tag{26}$$

in which $R(x_k)$ represents the Eulerian space correlation. The Eulerian scale L_k is commonly accepted as a measure of the "average turbulent eddy size" in the Eulerian spectrum (Taylor, 1935, p. 426); similarly, ℓ_k can be considered an equivalent measure for the Lagrangian spectrum. Interestingly enough, the Lagrangian length scale can also be compared with the early concept of a "mixing-length," since it represents, in a sense, the average distance a particle must move before it completely loses its original momentum to its surroundings, i.e., the distance traveled while the velocity correlation falls to zero (ibid., p. 425).

The Lagrangian scale time, on the other hand, has been identified with "the lifetime of the largest tourbillon" by Inoue (1960), who uses this term to characterize the fundamental element of turbulent motion. Frenkiel (1948) has used the $\mathcal{T}_k$ scale parameter to characterize the time required for the onset of the final, parabolic regime of diffusion, since it is numerically equal to the area under the $R_k(\xi)$ curve and thus depends fairly closely upon the time required for $R_k(\xi)$ to fall to zero. This particular application of $\mathcal{T}_k$ will be employed in the interpretation of the results of the current experiments; for, as it turns out, decay-correction errors in the computation of $R_k(\xi)$ for longer lag times (i.e., those for values of ξ which require data taken early in the experiments to be correlated with data taken toward completion) tend to make the intersection of the $R_k(\xi)$ curves with the ξ axis uncertain. The area under the curve, however, is less sensitive to this ambiguity.

The third quantity, K_k^*, has the dimensions of a diffusion coefficient, an interpretation that is justified under certain special circumstances. Frenkiel (1953) has derived the following expression for

three-dimensional diffusion from an instantaneous point source from the standpoint of statistical theory, basing his treatment upon the Taylor equation:

$$\chi(x, y, z, t) = \frac{Q}{2\pi(\overline{x^2})^{3/2}} \exp\left(-\frac{x^2+y^2+z^2}{2\overline{x^2}}\right). \tag{27}$$

Here the variance of the displacements of the diffusing particles $(\overline{x^2})$ is a function of t determined by Taylor's diffusion equation. Comparing this result with the K-theory solution for the same problem given by Roberts (1923),

$$\chi(x, y, z, t) = \frac{Q}{(4\pi KT)^{3/2}} \exp\left(-\frac{x^2+y^2+z^2}{4KT}\right) \tag{28}$$

it can be seen that the two expressions are identical when $(\overline{x^2}) = 2KT$. Further, we have from the general form of equations (19) and (25),

$$\overline{x_k^2} = 2K_k^*T. \tag{29}$$

Thus, for $T > \xi_2$ (cf. Figures 1 and 2), the parameter K_k^* is the equivalent of the constant coefficient of diffusion assumed by Roberts in his Fickian analysis, a result which demonstrates that the statistical theory of turbulent diffusion converges to a form of the K theory once the parabolic regime has been established.

Atmospheric Measurements of $R_k(\xi)$

Although the direct evaluation of $R_k(\xi)$ in the atmosphere entails considerable practical difficulty, such procedures have been successfully carried out on a number of occasions. For example, Edinger (1951), photographed soap bubbles released from a balloon tethered at an elevation of 1000 ft. Successive one-second displacements of bubbles were used to compute the estimate

$$R_x(\xi) = 1 - 0.068\xi.$$

The Lagrangian time scale appeared to be about 7 sec, but since a relatively narrow field of view restricted the duration of observations, values of $R_x(\xi)$ less than 0.5 were not observed. In another field

experiment, Gifford (1955) obtained Lagrangian data within the atmospheric boundary layer through double-theodolite observations of neutral-buoyancy balloons released from a 300-ft tower.

More recently, a program of experiments at Wallops Island, Va., has used radar to record the successive positions of constant-level "tetroons"[1] at intervals of from 10 sec to one minute as they moved along extended trajectories several thousand feet above the ocean (Angell and Pack, 1962). Here again the $R_x(\xi)$ and $R_y(\xi)$ functions obtained appeared to approximate linear functions of the form $1 - a(\xi)$; but in this case of medium-scale diffusion, Lagrangian time scales between 3 and 12 minutes were found rather than those of only a few seconds obtained by Edinger in soap-bubble experiments. In even larger-scale studies, Angell (1960) used the positions of horizontal sounding balloons determined by radio-direction-finding techniques every 2 hr as they drifted at the 300-mb level across the Pacific to compute the autocorrelation functions

$$R_x(\xi) = \exp - [(7\xi + 1)/6]$$

and

$$R_y(\xi) = e^{-\xi}\cos\pi\xi,$$

where ξ is in days. The periodic term in $R_y(\xi)$ was considered to have been associated with the passage of the balloons through long waves in the westerlies. Measured over periods of from several days to an entire week, these "transosonde" trajectories gave Lagrangian scale estimates six or more hours long. Evidently the continuous involvement of progressively larger and slower eddies in the diffusive motions of air parcels on long trajectories in the free atmosphere results in the association of larger $\mathcal{L}_k$ scales with longer observation times.

---

[1]Helium-filled, super-pressure, aluminized Mylar balloons whose near-tetrahedral shape provides corner reflectors designed to maximize the return signals.

Atmospheric studies have sometimes employed an indirect method of estimating the Lagrangian autocorrelation function suggested by Taylor (1921) in his original treatment of the statistical theory. He pointed out that $R_k(\xi)$ could be determined from more readily obtainable pollution-concentration data by substituting measurements of the variance of the displacements of dispersing particles downstream into a doubly differentiated form of his basic equation. Taking the derivative of equation (10) and solving for R, one obtains

$$R_k(\xi) = \frac{1}{2\,\overline{u_k'^2}} \frac{d^2(\overline{x_k^2})}{dt^2} \tag{30}$$

Measurements of cross-stream distributions of concentration at a number of locations along a plume originating from a source of known strength, along with the assumption that these distributions are approximately Gaussian in character, are then used to estimate the second derivative appearing as the last term in (30).

Hay and Pasquill (1957) used this method to obtain estimates of $R_z(\xi)$ by measuring relative concentrations of microscopic particles (Lycopodium spores) collected at several elevations by sampling devices mounted on balloon cables tethered at several distances downstream from a continuous point source. A somewhat similar technique was employed by Hilst (1957) in a program of experiments that concentrated upon the stably stratified atmospheric condition. As one further example of the indirect method, estimates of the transverse component $R_y(\xi)$ have been obtained through equation (30) by Barad (1959); he utilized distributions of sulfur dioxide concentration sampled at many points along arcs of several radii downstream from a continuous point source during the 1956 Prairie Grass Project at O'Neill, Nebraska.

Unfortunately, indirect determinations of $R_k(\xi)$ that result from diffusion experiments of the foregoing type are subject to considerable uncertainty, for they rely upon the computation of second derivatives of

distributions of empirical data that are generally limited in quantity (and often to some degree in quality) by the practical difficulties inherent in meteorological experimentation in the field. Barad (ibid.) has noted that the graphical methods frequently employed for the determination of $d^2(\overline{x_k^2})/dt^2$ often give results which vary from one analyst to another. As a partial remedy, he introduced an objective, numerical method of evaluation that, within the limitations of the data, minimizes this effect.

Laboratory Measurements of $R_k(\xi)$

Many laboratory studies of diffusion to be found in the literature were principally designed to investigate specialized problems of engineering or physical chemistry, but a number are of more general interest, since they have utilized the indirect method to obtain estimates of the $R_k(\xi)$ function as well. For example, Kalinski and Pien (1944) indirectly computed the transverse component $R_y(\xi)$ from measurements of the cross-stream variation of chloride concentration at a number of distances downstream of a point source in the fully developed turbulent flow of an open water channel. In another study, by Mickelsen (1955), data obtained from the diffusion of helium in the fully developed turbulent flow of an air duct were used to compute a form of the Lagrangian autocorrelation. Mickelsen was able to compare these results with Eulerian data simultaneously determined in the same experiments. Interestingly, this study avoided the questionable step of deriving Lagrangian data from doubly-differentiated diffusion measurements by calculating an intermediate "turbulent spreading coefficient" just short of the differentiation, and comparing this in turn to a doubly-integrated form of the Eulerian correlation.

Recently, the interesting point of comparison between the Lagrangian coefficients peculiarly appropriate to diffusion and their more easily obtainable Eulerian counterparts has also been studied by Baldwin and Walsh (1961). In their investigation, the Lagrangian autocorrelation function was inferred from measurements of the radial

distribution of heat determined at intervals downstream from a source located on the axis of a long cylindrical pipe containing fully developed turbulent air flow; Eulerian data were simultaneously obtained through standard hot-wire anemometer measurements.

Experimental evaluations of Lagrangian autocorrelation functions of a special kind have occasionally been indirectly computed from diffusion data measured in homogeneous, decaying fields of turbulence produced in the lee of grids mounted in wind tunnels or water channels (Collis, 1948; Uberoi and Corrsin, 1953). These studies were based upon a modified diffusion equation proposed by Taylor (1935, pp. 428-29), a variation on his basic equation in which the energy of the turbulence field was allowed to decay with time. The analysis resulted in a new form of the correlation function $R_k(\eta)$ for which the independent variable η was defined as

$$\eta \equiv \int_{t_1}^{t_2} (\overline{u_k'^2})^{1/2} \, dt. \tag{31}$$

In the modified diffusion expression, $R_k(\eta)$ serves in much the same way $R_k(\xi)$ does in the original equation. Note that since the turbulence intensity $\overline{u_k'^2}$ decays with increasing distance from the grid, for a particular, constant value of η equation (31) specifies a variable time lag $(t_2 - t_1)$ which increases with increasing distance from the grid. As will be seen below, one of the decay corrections employed in the current experiments defines an autocorrelation lag with similar properties. In this latter case, however, the viewpoint differs somewhat from that taken by Taylor. Where his modification sought to produce a diffusion equation which could be specifically employed in decaying turbulence fields, the treatment of the present experimental measurements attempts to correct numerically for turbulent decay in such a way as to restore to the data the properties of a stationary time series. The analysis then proceeds from the point of view of Taylor's original, unmodified theory.

The author is aware of only one previous experimental study in which estimates of the Lagrangian autocorrelation function were directly computed from decay-corrected turbulent-velocity fluctuations originally obtained by the actual measurement of successive displacements of particles moving along trajectories through fields of homogeneous, decaying turbulence. Vanoni and Brooks (1955) carried out this procedure in the lee of a grid mounted in continuous, neutrally stratified flow through a water tunnel. Although in their apparatus tracer particles were swept through the field of observation in a matter of a few seconds, trajectory data sufficiently long to determine autocorrelation estimates nearing or reaching zero were recorded in about half the cases. $R_x(\xi)$ and $R_z(\xi)$ being found to attain zero in from 0.5 to 1.5 sec. Since these results are to a degree comparable with those obtained in the current investigation they are discussed in further detail in a later section (cf. Chapter V).

Vanoni and Brooks allowed for the influence of turbulent decay in correlation computations by using a centered difference technique, whereas the analysis of the current experimental results employs certain velocity- and time-scale corrections suggested by Batchelor (see Chapter IV, below). For any particular estimate $R_k(\xi_1)$ Vanoni and Brooks used only one velocity product from each of a number of trajectories; velocity factors were taken at $+\xi_1/2$ and $-\xi_1/2$, these being measured from a central time approximately the same for all trajectories and for all $R_k(\xi)$ determinations. In the authors' words, this method was designed "to keep the effects of decay reasonably uniform." In contrast, the corrections used in the current study attempt to fully compensate for the effects of turbulent decay.

Departures from Ideal Conditions

There are distorting influences present within the friction layer of the earth's atmosphere (approximately the lowest kilometer) which complicate the determination of the Lagrangian autocorrelation function.

and hence the application of the principles of the statistical theory of turbulent diffusion. Near the earth's surface, for example, the average turbulent eddy size regularly increases with height. In Taylor's statistical theory, this organized vertical variation in the eddy spectrum means that $R_k(\xi)$ itself varies with height; thus, no single estimate of the autocorrelation function can be expected to apply over more than a relatively narrow range of heights within these layers.

In addition, the presence of organized circulations on the scale of convective clouds or cloud systems contributes larger-scale eddy motions which, although they can often be treated as parts of the mean flow in short-range diffusion, must be included as integral members of the diffusive mechanism in medium- and long-range diffusion problems. Then, too, the normal variations in both the speed and direction of the mean flow throughout the depth of the friction layer contribute further complications.

As one example of an effort to accommodate the lack of atmospheric homogeneity in statistical theory, Gifford (1959) developed a "fluctuating plume model" to describe plumes which meander from side to side as a result of relatively slow oscillations in the direction of the mean wind. The model treats dispersion due to smaller-scale turbulent eddies separately from that due to the simultaneous influence of larger-scale fluctuations that cause the plume to meander, the latter including slow fluctuations such as those caused by the presence of convective eddies.

In general, a single determination of a Lagrangian autocorrelation function can represent the characteristics of only a selected portion of the diffusive circulations present in the broad spectrum of atmospheric motions. A relatively narrow spectral band is essentially selected through filtering effects imposed by the methods of observation. Thus, the interval over which individual observations are averaged (normally the time elapsed between observations of the positions

of a moving tracer particle) determines the highest frequency of the turbulent field to which the autocorrelation estimates can be considered to correspond, whereas the total duration of the trajectory observations determines the lowest frequency. For N observations ΔT seconds apart, this spectral range is approximately

$$\frac{1}{2N\Delta T} < f < \frac{1}{2\Delta T} \tag{32}$$

where f is the frequency in cycles per second. Note that these values are determined by the ability of the observations to resolve one-half cycle of the upper and lower limiting frequencies.

From (32) it can be seen that the spectral band viewed by Edinger with soap bubbles (1-sec samples from 7-sec long trajectories) lay between 0.5 and 0.07 cps, whereas that observed by Angell and Pack in tetroon flights (10-min samples from 100-min trajectories) lay between 3.0 and 0.3 cps. Thus, different averaging intervals and total observation times employed by various experimenters largely explain the widely divergent results. This points out the difficulties involved in comparing estimates of $R_k(\xi)$ determined in one investigation with those obtained in another.

CHAPTER III

THE THEORETICAL BASIS FOR THE EXPERIMENT

The particular form of turbulent circulation for which the most comprehensive body of experimental and valid theoretical knowledge has been gathered is that found in the lee of a rectangular grid of bars placed normal to uniform flow in a wind tunnel. These approximately isotropic fields decrease in intensity in the direction of the mean flow, that is, $\overline{u_k'^2}$ decays with time within a given volume of fluid as it moves with the mean flow. Relative to the grid, however, the gradients of turbulence intensity are stationary and local departures from homogeneity are small. For this reason these fields are generally termed homogeneous, decaying turbulence. Their relative simplicity and the ease with which they can be produced in the laboratory have led to their extensive study. It is not surprising, therefore, that Taylor suggested grid-produced turbulence be utilized to investigate diffusion, as noted in the previous chapter. But perhaps because the modified diffusion analysis for the decaying turbulence condition accompanying this suggestion did not appear to have any direct practical application, only a few investigations along these lines were carried out.

More recently G. K. Batchelor (1952) suggested that dimensional and temporal scales of velocity fluctuations measured in homogeneous, decaying fields could be adjusted in such a way that data approximating the characteristics of stationary, random turbulence would result. Batchelor used this concept in an analysis of the properties of diffusion in a system of decaying turbulence, as Taylor had earlier from his, somewhat different, viewpoint. In the present study, however, it is the decay-corrected turbulence field itself that is the chief point of interest; for the subject of this investigation is not the

response under various experimental conditions of the diffusion symptom, as it were, but rather the behaviour of the more fundamental characteristic of the turbulence field, the Lagrangian autocorrelation function.

Homogeneous Turbulent Decay

The decay-compensation method suggested by Batchelor is based upon several well-established characteristics of grid-produced, homogeneous turbulence. In wind tunnels, the decay phenomenon has been observed to be divided into at least two well-marked regimes differentiated from one another by characteristic rates of turbulent energy decay. During the initial period, the decreasing intensity of turbulence follows the linear law $\overline{u_k^2} \propto t^{-1}$ throughout a region that extends from about 10 to about 150 mesh lengths[1] downstream of the grid. Here t is measured from t_0, the time of occurrence of the "virtual origin," a point located some distance behind the grid where extrapolation backward in time via the linear decay law implies the turbulent decay process would have begun with infinite energy. The displacement of this point downstream has been described as representing the period of time required for the field of motion to settle down into the high rate of energy dissipation characteristic of turbulence.[2] Beyond 500 mesh lengths, a final or "viscous" stage of decay becomes

---

[1]The mesh length M, the distance between the component bars of a wind-tunnel grid, is a representative measure of distance commonly employed to specify relative positions downstream and, as it turns out, relative states of decay in homogeneous turbulence experiments; it is frequently used to specify the "grid Reynolds number," $Re_g \equiv \overline{U}M/\nu$, where $\overline{U}$ is the mean flow and ν is the kinematic viscosity.

[2]Throughout this report, a distinction is made between two measures of real time in the experiment: the "grid time" T which is measured from the time of grid passage, and the "decay time" t which is measured from the virtual origin of the linear decay.

established at a slightly faster rate. $\overline{u_k'^2} \propto t^{-5/4}$. There is some evidence for an even more rapid intermediate rate. $\overline{u_k'^2} \propto t^{-10/7}$, somewhere in the intervening region between 150 and 500 mesh lengths, but the conditions for the existence of this regime have not been firmly established (cf. Lin, 1961, pp. 230-36).

These separate regimes of energy decay are supported by theory in that the several rates have been derived by combining the effects, in different relative strengths, of the two principal energy-modifying processes. (a) the transfer of energy from larger to smaller wavelengths across the turbulence spectrum, and (b) the final disappearance of kinetic energy through viscous dissipation. Thus, the linear law for the initial period has been obtained by assuming that the transfer term is equal in importance to the viscous dissipation, whereas in the determination of the decay rate characteristic of the final period, the transfer term is considered negligible. The intermediate regime has been termed a "nonviscous" stage since in this case, the rate of decay has been derived by assuming the viscous dissipation to be negligible in all but the highest frequencies. In addition, these theoretical treatments require certain assumptions to the effect that all or some portion of the turbulence spectrum remains "statistically similar" (see below) during the evolution of the decay process

For the first period of decay (the only region within which the Batchelor decay corrections can be employed as will be shown), Lin (loc. cit.) has obtained the linear decay law by assuming that similarity extends over all portions of the eddy spectrum except those containing the very lowest frequencies, this in addition to regarding the transfer and dissipative terms to be equally important; that is to say, decay during the initial period can be considered to proceed in such a way that a form of statistical equilibrium is maintained which enables the turbulence spectrum to preserve approximately the same shape, even though individual eddy components within the spectrum are decreasing in amplitude. In Lin's application of this, the so-called

similarity assumption, the lowest frequencies are specifically excepted, since there appears to be insufficient time for these largest eddies to adjust to the rapidly changing equilibrium condition. This last is borne out by observations of Stewart and Townsend (1951), who found that, at any one grid Reynolds number, "self-preservation[1] of the spectral shape is good for all but the smallest values of the wave number."

Finally, both experimental observation and theoretical analysis agree that the characteristic length scale of turbulence (i.e., the Eulerian scale L_k) increases as $t^{1/2}$ during the initial period of homogeneous decay. Successive spectra measured during this period show this effect as a monotonic shift of the spectral mode toward longer wavelengths with increasing time. In fact, all three of the characteristic features of the initial period important to the decay corrections are visibly evident in spectra successively recorded during the first period of decay: the turbulent energy (spectral amplitude) decreases as t^{-1}, the length scale (spectral mode) increases as $t^{1/2}$, and the spectral distributions retain more or less the same shape (cf. Townsend, 1956, Fig. 3.5). With regard to the similarity condition, those departures from self-preservation that do appear during the initial period of decay can be largely attributed to the inability of larger eddies to maintain the equilibrium distribution required for complete similarity (Stewart and Townsend, loc. cit.).

The Decay Corrections

The Batchelor corrections are readily deduced from the foregoing characteristics of the initial period of turbulent decay. First,

---

[1] A somewhat less restrictive version of the general similarity hypothesis which requires that similarity need only be maintained within a single system characterized by a particular value of the grid Reynolds number, rather than in all systems with the same (high) Reynolds number.

from the fact that the velocity scale of turbulence, V*, say, decays as $t^{-1/2}$ while the length scale L* increases as $t^{1/2}$, a time scale T* characteristic of the decaying field can be defined which is itself a linear function of time. Thus:

$$T^* = \frac{L^*}{V^*} \propto \frac{t^{1/2}}{t^{-1/2}} = t \quad \text{or} \quad T^* \propto t. \tag{33}$$

Under the assumption that the portion of the turbulence spectrum in which one is primarily interested remains approximately self-preserving, it then becomes possible to apply suitable scale factors in such a way that the decaying, shifting spectral distributions characteristic of successively later times are continuously corrected to a statistically stationary state approximately representative of the conditions of the uncorrected field of turbulence at time t = 1. This is accomplished by:

(a) compensating for velocity decay by multiplying the observed turbulent fluctuations by the square root of their times of observation;

(b) compensating for increasing time scale by dividing characteristic time intervals measured in the experiment by the central time of their occurrence.

Note that in consequence of the time-scale correction in (b) a consecutive series of infinitesimal, normalized time intervals dt_i/t_i becomes a new "corrected time period" when integrated over a real period of time in the experiment, say $t_2 - t_1$:

$$\tau = \int_{t_1}^{t_2} \frac{dt}{t} = \ell n\, t_2 - \ell n\, t_1 = \ell n \frac{t_2}{t_1}. \tag{34}$$

The units of τ can be considered to be seconds, or, more properly, "corrected-seconds"; for in view of the correction of the turbulent fluctuations observed at any time to the characteristics of a stationary field whose velocity and length scales are similar to those which

prevail in the decaying field at time t = 1, it follows that the scale of corrected time can be expected to preserve the properties of that particular epoch as well.

As noted in Chapter II, this definition of the corrected time interval exhibits a qualitative property in common with Taylor's η given in equation (31). Constant values of both η and τ derive from real time intervals which increase with increasing distance from the grid. Thus, where $\tau = \ell n\, 2 = 0.69$ corrected seconds corresponds to a time interval measured from decay time t = 1 to t = 2 real seconds early in the experiment, the same corrected time requires a real time interval measured from t = 10 to t = 20 late in the same experiment (cf. Table 2 below).

Both the need for and the effects of the velocity-decay correction are self-explanatory, but the same cannot be said of the time-scale adjustment. However, by examining the results of autocorrelation computations derived from homogeneous turbulence experiments and comparing those results upon scales of both real and corrected time, the effectiveness achieved by this adjustment in converting the observed data to the characteristics of a stationary time series can be demonstrated.

Table 1 displays results obtained from one of the experiments in the current series, a set of data frankly selected for the purposes of this demonstration because of their excellent adherence to the characteristics of the first period of decay. The nature of the experiment itself is described in detail in the next chapter; at this point it will suffice to note that the turbulent-velocity data utilized to compute the autocorrelation estimates in the table were derived from 17 successive one-second displacements measured along the trajectories of 50 different tracer particles. The trajectories were photographed in one "experiment" consisting of ten independent realizations of homogeneous fields of turbulence. These were generated in a towing channel by ten separate "runs," each involving a single passage of the rectangular

grid of bars through the fluid. The notation S/25/y for this case specifies that the experimental data consisted of transverse (y) particle displacements in a stably stratified (S) fluid observed in the lee of a grid moving with a speed of 25 cm/sec.

TABLE 1.--Autocorrelation estimates corresponding to a constant real time interval of one sec; data from experiment S/25/y (see Figure 26)

t_1, t_2	$t_2 - t_1$	$R(\xi)$	$\ell n(t_2/t_1) = \xi$
2, 3	1	0.652	0.405
3, 4	1	0.756	0.287
4, 5	1	0.764	0.223
5, 6	1	0.817	0.182
6, 7	1	0.915	0.154
7, 8	1	0.899	0.133
8, 9	1	0.949	0.117
9, 10	1	0.950	0.105
10, 11	1	0.961	0.095
11, 12	1	0.961	0.087
12, 13	1	0.940	0.080
13, 14	1	0.965	0.074
14, 15	1	0.973	0.069
15, 16	1	0.983	0.064
16, 17	1	0.977	0.060
17, 18	1	0.983	0.057

TABLE 2.--Autocorrelation estimates corresponding to a constant interval of 0.693 corrected sec; data from experiment S/25/y (see Figure 26)

t_1, t_2	$t_2 - t_1$	$R(\xi)$	$\ell n(t_2/t_1) = \xi$
2, 4	2	0.328	0.693
3, 6	3	0.414	0.693
4, 8	4	0.238	0.693
5, 10	5	0.440	0.693
6, 12	6	0.410	0.693
7, 14	7	0.341	0.693
8, 16	8	0.349	0.693
9, 18	9	0.386	0.693
		0.363	

In the first column of the tables, the times of observation of the two factors in the mean velocity product which appears in the numerator of $R_y(\xi)$ are listed, the times being measured from the virtual origin of the turbulent-decay process. The second column notes the constant real time interval between these observations; the third column lists the autocorrelation estimates obtained from these data. Note that even though the first Batchelor correction for velocity decay has already been applied to the observed turbulent fluctuations, the autocorrelation estimates still exhibit a steady trend toward higher values at later times; $R_y(\xi)$ increases from 0.65, when data at times 2 and 3 are correlated, to 0.98, when the calculation employed data at times 17 and 18. The correlation estimates behave as though lag times between successive velocities along the trajectories were shrinking; evidently the constant real time lag of column 2 is not appropriate. Further, as may be seen in column four, the time-scale adjustment defined by equation (34) defines just such a shrinking time interval.

If Table 1 shows the necessity for a time-scale adjustment, the results presented in Table 2 demonstrate that the second Batchelor correction is sufficient to the task. In this table the columns are classified as before, but here a selection of data which have a constant corrected time lag is listed. Note that while the real time lags $t_2 - t_1$ systematically increase from 2 to 9 sec. the corrected intervals for the same data maintain a constant value of $\xi = \ell n\, 2 = 0.69$ corrected second. What is more, this constant, adjusted lag time can be seen to be more suitable than the real intervals when considered in relation to the autocorrelation estimates, for the $R_y(\xi)$ entries in column 3 do not exhibit any significant trend at all. Rather, they are distributed in a more or less random manner about a mean value near 0.36. The observed variance of the $R_y(\xi)$ estimates in this case is, in fact, surprisingly small and should probably be considered largely fortuitous; the upper and lower 95 per cent confidence limits on a correlation estimate of 0.36 determined from a sample of only 50 velocity pairs

are 0.57 and 0.09, respectively, a range considerably larger than that shown by the estimates of column 3.

The preceding discussion demonstrates that the Batchelor corrections can approximately restore stationary time series characteristics to turbulent fluctuations measured in grid-produced fields of turbulence during the initial period of decay. This procedure, in turn, makes available a laboratory model in which $R_k(\xi)$ can be evaluated by the direct method, provided that the conditions of the experiment do not unduly distort the behaviour of the first period of decay.

CHAPTER IV

THE EXPERIMENTAL PROCEDURE

One of the conclusions appended by Vanoni and Brooks to their study of the motions of tracer particles in a water tunnel was in the form of a recommendation that Lagrangian measurements of this kind be extended to longer observation times and, hence, to longer trajectories. Unfortunately, this soon becomes quite difficult in a continuously flowing tunnel, for in order to generate turbulence of significant intensity, the mean flow must be kept fairly high. Unless the experimenter has at his disposal a tunnel with an unusually long test section and, perhaps, a point of observation that moves with the mean flow, the tracer particles are soon swept out of view. An alternative approach (that, in fact, used in the current investigation) employs a towing channel in which fluid initially at rest is set into turbulent motion by the passage of a moving grid. In this way, homogeneous turbulent fields very nearly at rest relative to a fixed observer are generated, and it becomes possible to keep particles moving along turbulent trajectories within the field of view of a camera for periods of significant duration

An additional advantage of considerable importance to this particular investigation is afforded by the fact that the fluid in a towing channel is essentially at rest most of the time, since the motions induced by the passage of the grid are relatively short-lived as compared with the intervals allowed to elapse between experimental runs In the continuous flow of a tunnel it would be extremely difficult, if not impossible, to maintain the vertical density gradients employed in this series of experiments. The preconditioning section of such an apparatus, the region within which differential heating and cooling would be required to set up the desired lapse rates, would have to be quite long,

to say nothing of the severe heat transfer problems that would arise. In the towing channel, on the other hand, it is a relatively simple matter to generate a given lapse rate since the fluid volume involved is both limited and at rest. As to maintaining the density gradient from one experimental run to the next, the small amount of mixing generated by the grid during a single passage through the fluid at designed speed, plus the almost negligible amount caused by its slow return to the starting position, can be readily corrected between runs.

The Argonne Towing Channel

The towing channel shown in Figure 3 was specifically designed and constructed for this investigation. It is 30 ft long, 26 in. wide, and was operated in these experiments with an effective fluid depth of $12\frac{7}{8}$ in. The sides of the channel are $\frac{1}{2}$-in. plate glass mounted in steel frames; the end bulkheads and the bottom are $\frac{1}{2}$-in. aluminum plate. The bottom, constructed of a number of aluminum sections welded into a single piece, forms the active side of the lower heat exchanger

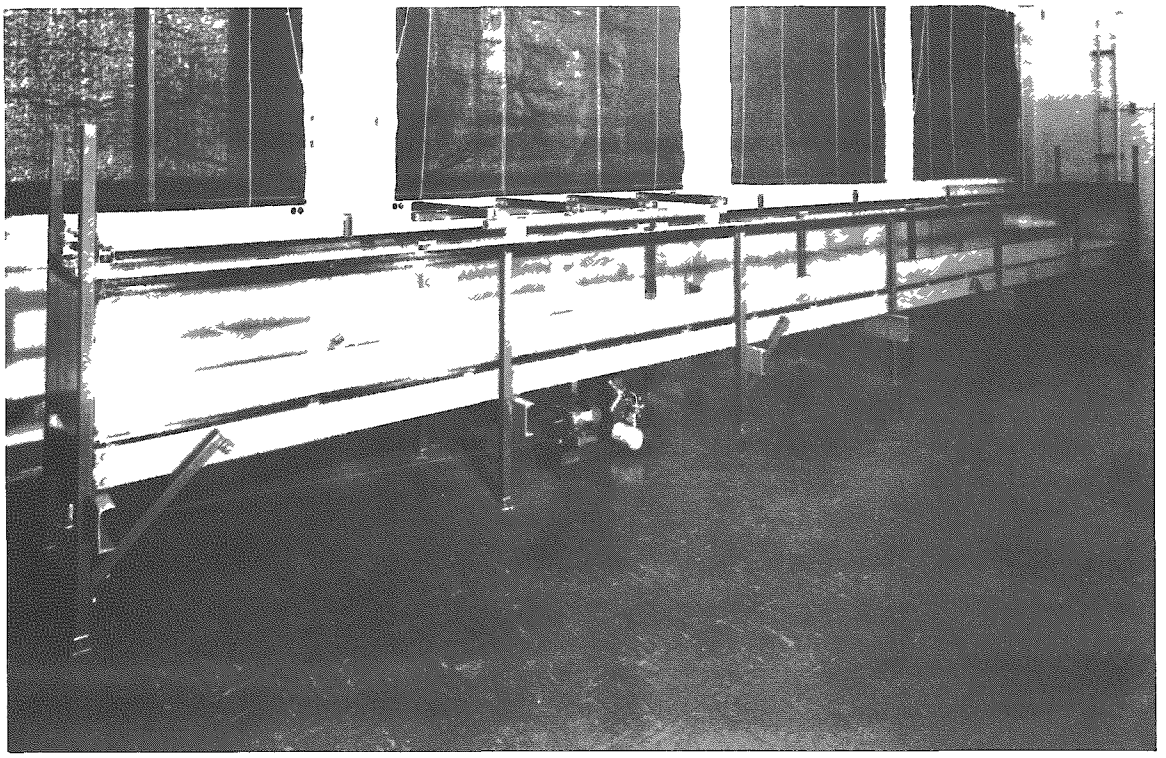

Fig. 3.--The Argonne meteorological model towing tank; note overhead carriage, endless driving cable, and hydraulic transmission.

(see below). Joints in the water-bearing portion of the assembly were caulked with a synthetic Thiokol rubber compound (3M, EC-801) which insures that the tank remains water-tight, yet allows for differential expansion during temperature changes. Although it weighs more than 2 tons when filled, the channel is mounted with its base 2 ft above floor level on a frame constructed of 6 x 2-in. steel channel supported by the adjustable legs visible in the figure. This elevated design allows for a considerable degree of flexibility, both in auxiliary experimental arrangements, and in the operation and maintenance of the channel itself.

During operation, all but the wave motions of longer periods set up by the moving grid were damped by a semirigid upper boundary. A lid consisting of a number of 24-in.-wide, 5- and 10-ft-long aluminum trays, firmly clamped to one another as well as to the ends of the tank, was floated on the water. The bottoms of these trays form the active surface of an upper heat exchanger, and one of them contains a glass window through which the interior of the test section can be either viewed or illuminated. The lid assembly occupies all of the free surface save for two $\frac{3}{4}$-in.-wide slits adjacent to either wall, which allow the unrestricted passage of two thin struts which carry the grid through the fluid.

The struts extend downward from an overhead carriage that runs on parallel rails mounted along the top of each sidewall (see Figure 3). Carriage speeds up to 40 cm/sec were supplied by an electrically driven, hydraulic transmission which pulled the carriage along the tank on an endless cable. The drive system could reproduce the same preset carriage speed for a series of ten runs within ±1 per cent. Acceleration from rest was accomplished smoothly and reproducibly by means of a speed control operated by a synchronous electric motor; the carriage was brought to 12.5 cm/sec in 3 sec, to 25 cm/sec in 6 sec, and to 40 cm/sec in 3 sec, the more rapid acceleration being required in the last case in order to bring the carriage up to full speed

within a maximum allotted distance of 75 cm. Smooth deceleration at the far end of the tank was carried out by a mechanical limit-cam arrangement connected to the output shaft of the transmission; this returned the speed control to neutral when the carriage reached a predetermined position.

Attached to the underside of the tank is an assembly of corrugated aluminum that forms the 9 ducts that make up the lower heat exchanger. Water continuously circulated through this assembly was kept within ±0.1 °C of a selected temperature by a thermostatically operated mixing valve (Powers Regulator Co.). Each duct also contains a 30-ft length of lead-covered, electrical heating cable rated to dissipate up to 7 w/ft. The more uniformly distributed electrical heaters were employed in the unstably stratified experiments when it was found that the nonrecirculating design of the lower heat exchanger tended to set up longitudinal temperature gradients which led to undesirable, large-scale thermal convective circulations.

The upper heat exchanger was incorporated in the floating trays that make up the semirigid lid of the channel. A system of copper tubes, here arranged in a counterflow pattern to eliminate gradients along the tank, circulated water of a temperature again controlled by a thermostatic valve as in the lower heat exchanger. In operation, the lids were filled with water to a depth of $\frac{1}{4}$ in. to improve the heat transfer between the aluminum trays and the copper tubes. Above the tubes an insulating layer consisting of $\frac{1}{4}$ in. of transite and 2 in. of Styrofoam virtually filled the remaining volume of the lids. This insulation, plus the fact that both the rate of flow and the difference between the input and output temperatures of the water circulating through the lids could be measured, made it possible to employ the upper heat exchanger as a device to estimate the vertical heat flux through the tank.

With both heat exchangers operating, lapse rates from +0.30 to -0.02 deg/cm were maintained in the tank for periods in excess of

24 hr without appreciably changing the mean temperature of the fluid. The equipment is capable of generating considerably stronger stable gradients, but the unstable lapse rate listed represents the maximum gradient that the electrical heaters could maintain against vertical convective transfer.

Vertical temperature gradients were measured with mercury-in-glass thermometers graduated in 0 1-deg divisions, readings being further estimated to the nearest 0.01 deg with the aid of a small hand lens. Four thermometers were mounted in a Lucite bracket that held them in horizontal orientations, 5 cm above one another, across the central levels of the tank. This assembly, placed 1 m downstream of the test section and 2 cm from the glass sidewall, was read immediately prior to each run and then removed in order not to interfere with the passage of the grid. In view of the spacing between thermometers and the known accuracy of the instruments themselves, lapse-rate measurements taken just prior to each run are considered to have been accurate within ±0.01 deg/cm.

Ambient air temperatures during the experiments were kept within ±0.5 deg of the mean tank temperature by auxiliary air-conditioning equipment. This environmental condition was of some importance (especially to the neutrally stratified cases), since each series of runs occupied a period of 8 to 10 hr.

Water as a Model Atmosphere

As a convenient and readily available fluid, water offers an advantage over air in hydrodynamic models in that its kinematic viscosity is smaller by more than an order of magnitude. At 20 °C, $\nu = 0.15$ cm^2/sec in air, whereas at the same temperature it is only 0.01 cm^2/sec in water. This property makes it possible to attain a given Reynolds number in a water channel with less than one-tenth the mean flow velocity required in a wind tunnel equipped with a grid of similar mesh length

Lack of compressibility does not raise significant problems when comparing experimental results obtained in water models to prototype circulations observed in the gaseous atmosphere, for two reasons discussed in some detail by Batchelor (1953). First, there is the more familiar argument to the effect that Mach numbers appropriate to natural atmospheric motions are in general small; that is to say, atmospheric velocities involved in turbulent mixing do not ordinarily approach the speed of sound; therefore dynamic compressibility effects need not be considered. But secondly, and more importantly, in the eddy motions of the atmospheric boundary layer the distances over which fluid elements experience appreciable changes in velocity are quite small in comparison with the distances over which the densities undergo significant variation. Batchelor shows, in fact, that for atmospheric motions of a scale less than 100 m, changes in density are so small that air behaves essentially as if it were incompressible. As a result, he shows that for this class of relatively small-scale motion, the Richardson number can be considered the sole criterion for similarity between two flow fields, a point discussed further in Chapter VII below.

One further consideration with regard to the use of water as a modelling medium for prototype motions in air concerns the relative effectiveness of the transports of heat and momentum in the two media. On the scale of molecular exchange, this may be expressed in terms of a nondimensional ratio characteristic of the fluid, the so-called Prandtl number:

$$\mathrm{Pr} = \nu/\kappa \,, \tag{35}$$

where ν is the kinematic viscosity and κ is the thermometric conductivity. In water at 20 °C, Pr = 7.15, whereas in air at the same temperature, Pr = 0.74, only about one tenth as large; therefore, the relative molecular transfer of heat to or from a fluid parcel moving

vertically through a stratified environment (as compared with that of momentum) is smaller by an order of magnitude in water than it is in air. Conceivably, this effect could be of importance to very small scales of eddy motion, since it might cause variations in the temperature of vertically displaced fluid parcels, which would make it inappropriate to compare quasi-adiabatic vertical motions in air with quasi-isothermal vertical motions in water. However, in consideration of the relatively large scale of eddy motion observed in these experiments (from several mm to 1 cm) and the relatively long period over which the velocity measurements were averaged (1 sec), effects due to molecular exchange may be considered to have been small. Moreover, since the "eddy Prandtl number" (the ratio of the eddy transfer coefficients) depends upon the properties of the field of motion and not upon those of the fluid medium, to a first approximation eddy transfers of heat and momentum can be considered essentially identical in the two media.

The Location of the Test Section

In experiments involving homogeneous turbulent decay in a towing channel, virtually any portion of the tank through which the grid has passed at proper speed can be considered a suitable test section. The average lapse rate is essentially the same in all portions of the tank, and sooner or later the fluid in any region, save where the grid has been accelerated or decelerated, will exhibit the characteristics of the initial period of decay. Specifically, first-period decay will be observed to occur roughly between $10/\overline{U}$ and $150/\overline{U}$ seconds after the grid has passed through the selected region at a speed of $\overline{U}$ mesh lengths per second. However, the occurrence of longitudinal surging motions generated by starting and stopping the grid makes it desirable to place the test section as close to the starting position of the grid as possible. In the first place, the surge components are of smallest amplitude near the ends of the tank, both because of the presence of the rigid end

plates and because here vertical excursions of the semirigid lid are effectively restricted by the end clamps. Secondly, when turbulence measurements are made close to the starting point of the grid, one need only consider the disturbance to the mean flow contributed by the initial surge generated during acceleration and its subsequent reflection from the far end of the tank approximately 10 sec later, provided the rarefaction wave caused by decelerating the grid can be delayed so as not to reach the test area upstream until after the observations have been completed.

This last requirement taken along with the usable length of the channel effectively determines the maximum dimensions of a grid for an experiment concerned with the first period of turbulent decay. In order to prevent interference by the rarefaction wave, the carriage should have an uninterrupted run of at least 150 mesh lengths beyond the test section to the region of deceleration, this to allow sufficient time for the first period of decay to be completed before the rarefaction wave begins. With the test section located between 1.0 and 1.3 m from the starting position of the grid, the 9.1-m Argonne channel allows a maximum constant speed run of 6.0 m, the first meter upstream being provided for acceleration from rest while 2 m are required to decelerate and accommodate the carriage after it stops at the far end. Thus, a grid with a mesh length of 4 cm would allow sufficient time to observe homogeneous turbulent decay over a full 150 mesh lengths with only the starting surge to contend with in the mean flow.

In the present experiments, however, the levels of turbulence produced by the relatively low grid Reynolds numbers used tended to become too weak in the final stages of decay. Therefore a somewhat coarser grid, with a 5-cm mesh length, was employed in all runs. Although this grid generated slightly stronger turbulence fields, observations could only be made during runs of 120 mesh lengths before the grid decelerated. The grid was of so-called "standard" design, a

biplanar array of cylindrical bars placed at right angles to one another and spaced with a ratio of mesh length M to bar diameter d between 4 and 6 (cf Townsend, 1956, p. 35) Constructed of $\frac{3}{8}$-in aluminum bars mounted 2 in apart, as shown in Figure 4, the grid had a solidity ratio M/d = 5 3

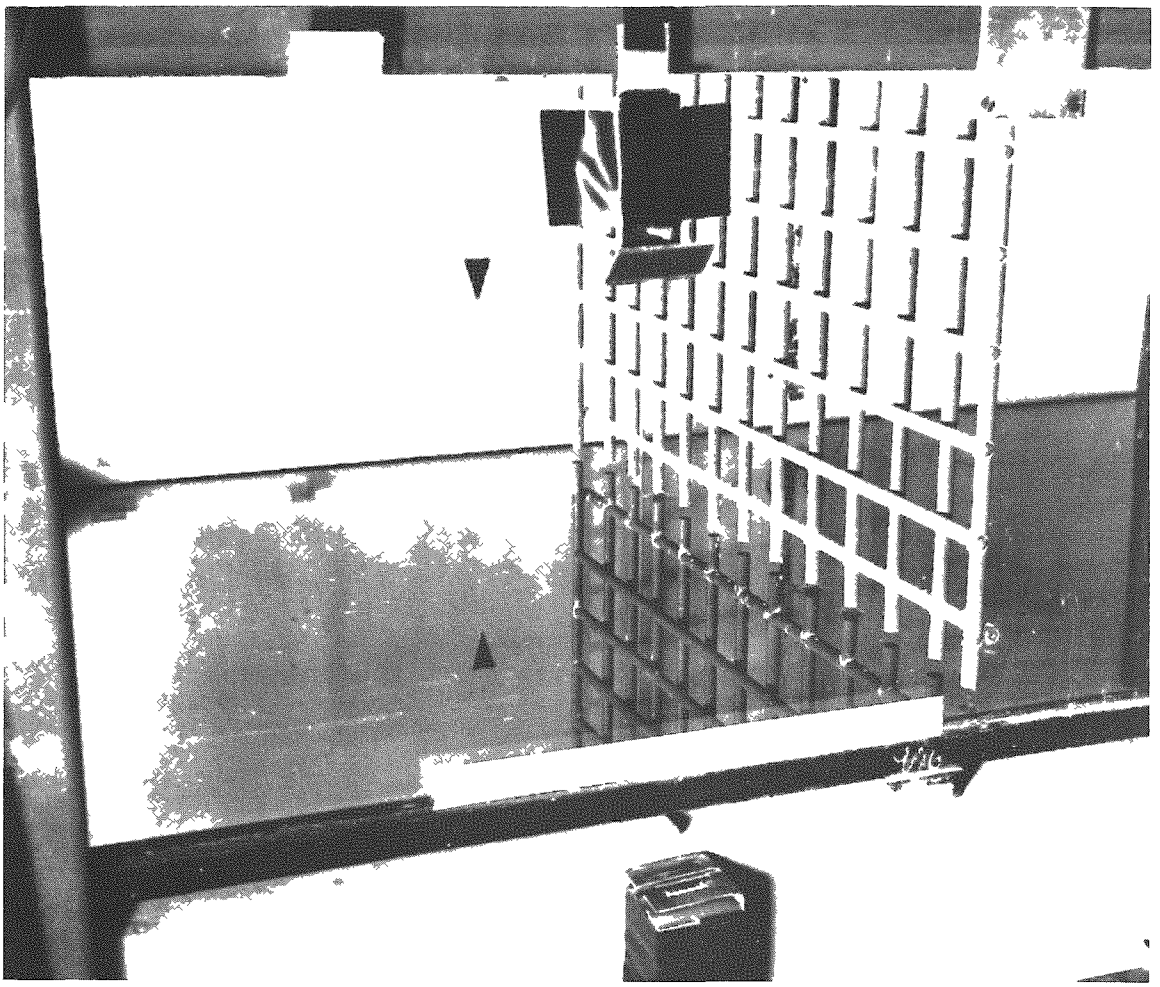

Fig. 4 --View of the interior of the test section with grid approaching from the right; note arrows which locate center of the camera field

Tracer Materials and Tracer Response

Lagrangian observations following the dispersive motions of the fluid were obtained by photographing the successive positions of neutral-density tracer droplets as they moved along turbulent trajectories in the wake of the moving grid The tracer material employed

was a mixture of nitrobenzene and olive oil, two compounds which are miscible with each other but immiscible with water. In the ratio of about 48 parts of nitrobenzene to 100 of olive oil, the mixture has a specific gravity very nearly equal to that of water at 25 °C. In addition, the refractive index of the mixture is such that droplets illuminated from a position at nearly right angles (~88°) to the line of sight are seen as bright points of light, since by refraction and internal reflection, each drop reproduces a tiny image of the source of illumination.

Droplets approximately one mm in diameter were introduced into the test section a few minutes prior to each run by means of a hypodermic syringe equipped with a long, 10-mil-diameter needle, the short delay being sufficient for the extraneous motion introduced into the fluid by this operation to decay to an insignificant level. Since the density of the tracer mixture was very nearly identical to that of the water within which the droplets were suspended, and since the interfacial tension between the mixture and water was sufficiently high for the droplets to behave in the manner of rigid particles, such tracer can be expected to respond to all motions of the fluid except those of a scale smaller than the droplet diameter. In these experiments, this high-frequency filtering effect becomes relatively unimportant, since the turbulent fluctuations were determined from tracer motions averaged over an interval of one second, a procedure that imposed an additional high-frequency filter with an even lower cutoff.

One possible source of spurious tracer response could arise under certain experimental conditions from the fact that the nitrobenzene-olive oil mixture expands more rapidly with temperature than does water (see Table 3). In stably stratified experiments tracer droplets whose densities exactly equal that of the surrounding water at a particular level become subject to unbalanced buoyancy forces that force them further away from their original equilibrium positions once they have been displaced either upward into warmer regions or

downward into cooler regions. In unstably stratified conditions, the net forces resulting from such displacements are reversed, that is, they are stabilizing instead of destabilizing; but in these cases the average vertical temperature gradients are so small that the effect is negligible. Of course, in the isothermal condition tracer droplets retain the same relative buoyancy at all levels.

TABLE 3.--Thermometric conductivities and expansion coefficients for olive oil, nitrobenzene, and water; tracer component values are only approximate since basic data for a range of temperatures from 6 to 25°C were used[a]

Material	κ ($cm^2/sec \times 10^3$)	$d\rho/d\theta$ (gm/cm^3-deg $\times 10^3$)
Olive Oil	0.92	-0.68
Nibrobenzene	1.09	-1.04
Water at 25°C	1.43	-0.26

[a]International Critical Tables; Handbook of Chemistry and Physics.

It can be shown that the droplets adjust very rapidly to changes in the temperature of their surroundings. Using the value $\kappa = 10^{-3}\ cm^2/sec$ for the tracer mixture (quite reasonable in view of the values shown in Table 3), a solution of the heat equation for a sphere one mm in diameter indicates that the average temperature of droplets so small will attain 99 per cent of the change to a new environmental temperature only one second after the change has occurred (cf. Carslaw and Jaeger, 1959, Figure 12). If one therefore assumes that the temperatures of the tracer droplets are always virtually identical with that of their surroundings, the differential volume-expansion effect will be overestimated, but probably not by a very large amount.

Consider this effect as it acts in the maximum stably stratified condition used in the experiments, namely, in the conditions of case VS/25/x,z where $d\theta/dz = +0.30$ deg/cm. When a tracer droplet,

initially in equilibrium with its surroundings at some particular level, is displaced vertically 3.3 cm, its temperature will very quickly change by 1°. Such a displacement, it is to be noted, is large even in comparison with the total vertical distances traversed by the tracer droplets of this experiment during the entire 16 sec of observation; in the 50 trajectories of case VS/25/x,z it is equalled only 6 times and is significantly exceeded only twice. If $d\rho/d\theta$ of the mixture is taken to be approximately 10^{-3} gm/cm^3-deg (also reasonable in view of Table 3, but, again, an overestimate), one obtains a density change of 10^{-3} gm/cm^3. Substituting this into Stokes' solution for the slow motion of a sphere of radius r and density ρ_1 through a medium of density ρ_2 and dynamic viscosity μ, we obtain for the terminal velocity

$$v = \frac{\frac{4}{3}\pi r^3(\rho_1 - \rho_2)\, g}{6\pi\mu r} \approx \frac{2(0.05)^2(10^{-3})(10^3)}{9 \times 10^{-2}} \approx 0.05 \text{ cm/sec.} \qquad (36)$$

Again this can be considered an overestimate, since the assumed conditions of maximum density difference are not likely to persist sufficiently long for terminal velocity to be attained.

Actual measurements of the magnitude of the differential expansion effect in fair agreement with the foregoing result were obtained from photographs of the initial tracer distribution taken just prior to each run of the VS/25/x,z series (using a streak-flash technique similar to that illustrated in Figure 7, but with a time interval of 10 sec rather than one). These show tracer droplets approximately in balance a few centimeters below the center of the field; at the same time, tracer at the top of the 15-cm field of view is rising at an average rate of 1.1 mm/sec, while that near the bottom sinks at the average rate of 0.3 mm/sec. Thus, the rate of vertical drift due to excess tracer expansion is observed to increase somewhat less than 0.1 mm/sec with each 1.0-cm change in depth, just two-thirds of that obtained in the theoretical estimate (0.5 mm/sec after a 3.3-cm displacement).

Since the selection of trajectories for measurement was restricted to the central 10 cm of the test section, and since individual trajectories were seldom observed to move through more than one-quarter of this vertical distance, the maximum change in vertical speed experienced by any tracer droplet as a result of this buoyancy effect was of the order of ±0.25 mm/sec. Comparing this with the magnitude of the root-mean-square vertical speeds actually observed in experiment VS/25/x,z (ranging from 5.3 mm/sec down to 2.3 mm/sec at the termination of the observations), we find that in the least-favorable temperature distribution, the observed vertical velocity fluctuations exceed the contributions of the differential expansion effect by an order of magnitude or more in all but the final stages of the experiment. In the remaining experiments with smaller temperature gradients, the effect can be considered to have been of proportionally smaller importance.

Photographic Techniques

Tracer droplets were illuminated by a multiple light source that simultaneously supplied continuous and pulsed illumination. Depending upon the position of the camera in the particular experiment, this assembly was either suspended above the test section or mounted at the side. Continuous light from a pair of 250-W mercury-vapor lamps (GE model H-250-A5) was briefly supplemented at intervals of one second by four, closely grouped electronic flash tubes (Kemlite 23-ST-Q). These ordinarily supplied an additional 110 W-sec of illumination of very short duration, but every fifth flash was automatically increased to 175 W-sec. A cam-operated microswitch operated once each second by a synchronous timing motor both triggered the electronic flash and supplied a pulse to drive a stepping switch that momentarily added a supplementary charged capacitor to the electronic flash power supply every 5 sec. The interval between flash-trigger pulses was quite constant, varying at most only ±1 ms from the nominal

period of one second between observations, this resulting from minor irregularities in the closing of the microswitch.

Tracer droplets were photographed with a 35-mm camera (Robot) equipped with a 15-in., f-4.5 telephoto lens (Graflex Tele-Optar) and a solenoid-operated shutter release (see Figure 5). During each experimental run, the shutter was held open for the entire period of observation; as a result, each negative recorded complex, intersecting patterns of long trajectories similar to those shown in Figure 6. With the aid of the more intense images appearing every fifth second, plus the fact that turbulent decay insured that displacements at the beginnings of trajectories were markedly larger and more irregular than those toward their ends, it became relatively simple to identify

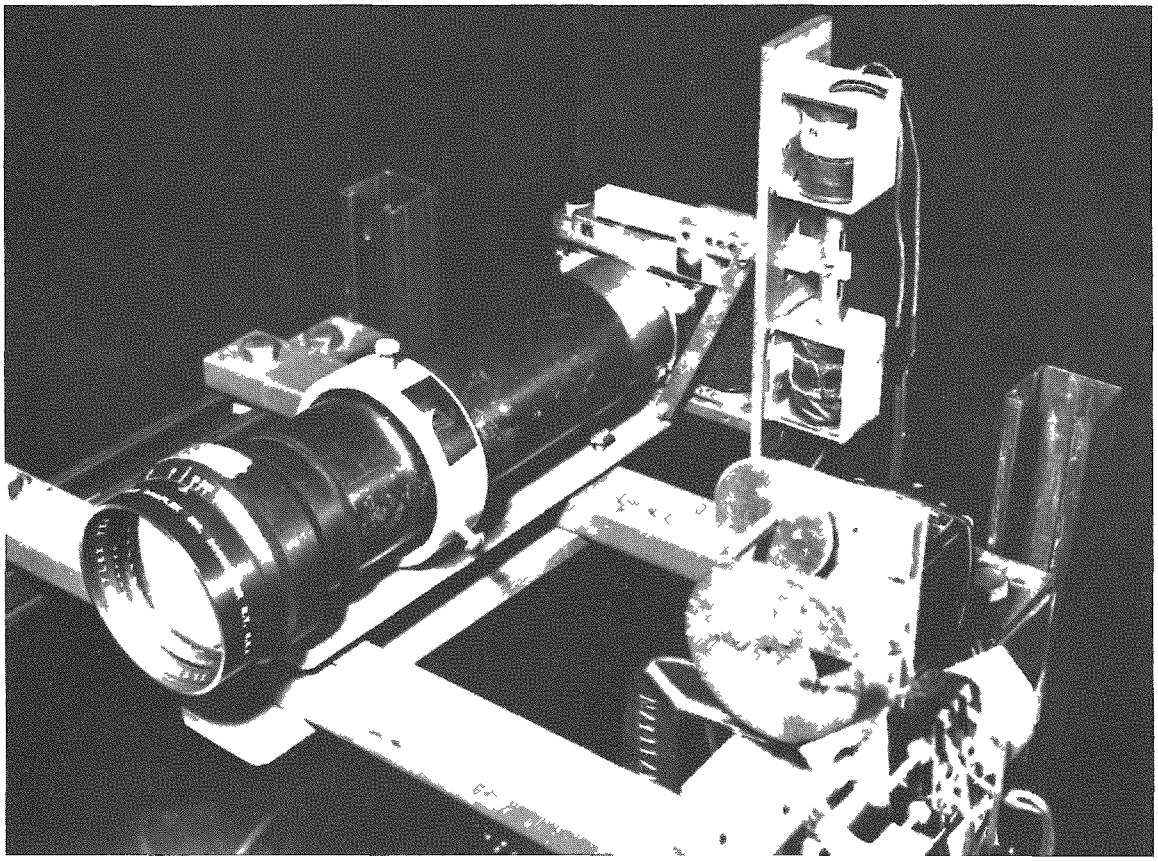

Fig. 5.--Robot 35-mm camera with 15-in. telephoto lens attached; note solenoid shutter release and pulse timer in right foreground.

Fig. 6.--Positive reversal of 17-sec long turbulent trajectories photographed from above in experiment S/25/y; horizontal line is the drive cable; droplets are moving in direction of the arrow.

the consecutive positions of individual tracer droplets. Figure 7 shows another type of photograph, a short time exposure taken with the electronic flash programmed to fire in an asymmetrical sequence (** *) designed to label both the average speed and direction of the droplets during a single second; this technique was used in a series of preliminary studies (cf. Appendix, below) to map the distribution of mean circulations within the test section.

Fig. 7.--Positive reversal of 1-sec long droplet displacements photographed from the side for the determination of the drift profile; droplets are moving in direction of the single dot.

Parallax errors in apparent particle displacement were reduced by placing the camera 5.5 m from the tank, necessarily viewing the test section through a front-surface mirror in order to accommodate this extended optical path within the space available. At that distance, the 2.5° field of view of the telephoto lens includes only a 25-cm length of the test section. When droplets are located in a position for maximum parallax error at the very edge of the field, less than 3 per cent of their movement toward the camera is recorded as spurious longitudinal or vertical displacement.

In each experimental run, the photographic sequence (that is, the opening of the camera shutter and the starting in correct phase of the timed electronic flash mechanism) was automatically initiated when the moving carriage tripped a microswitch 3.5 sec after the grid had passed through the midpoint of the test section. This fixed delay assigns to the first one-second displacement of each trajectory recorded a central grid time T = 4 sec measured from the time the passage of the grid set the droplets into motion. Some unavoidable uncertainty arises in this determination since the tracer droplets do not all start from the same longitudinal position relative to the grid; consequently, turbulent trajectories may begin at slightly different times. However, among those droplets for which complete trajectories were recorded and analyzed, none were ever separated by more than half the width of the test section at the start. At the slowest grid speed employed (12.5 cm/sec), this corresponds to a maximum relative timing uncertainty distributed among the trajectories of ±0.5 sec, but it falls to ±0.25 sec in runs at 25 cm/sec and to ±0.15 sec in those at 40 cm/sec. During the run down the tank, the carriage also tripped two microswitches placed 100 cm apart that started and stopped a 0.01-sec electric timer, this device determining the carriage speed for each run.

Data Reduction

As the first step in the conversion of the Lagrangian turbulent fluctuations from photographic analogue form to digital data for statistical analysis, the 35-mm negatives were enlarged to 11 x 14-in. prints. This was done on plasticized, shrink-resistant photographic paper (Eastman Kodak, Resisto-Rapid) with the use of a non-diffusing-type, precision, 35-mm enlarger (Leitz Focomat). An average of 5 trajectories were selected from each print, to make in most cases a total sample of 50 drawn from 10 realizations of the homogeneous turbulence field produced by as many grid runs under each set of experimental conditions.

After the points along each selected trajectory had been serially numbered for ready identification during measurement, the x and then the z components of the distances between consecutive images of the tracer droplets were measured with a Benson-Lehner Oscillograph Analyzer and Reader (OSCAR). This device, although principally designed to evaluate amplitudes of selected points on curves traced on continuous strip charts, readily adapts to this type of measurement. Observed displacement magnitudes were converted to digital data with a standard scale factor of 300 OSCAR counts per one cm of real displacement in the experiment. Normal scatter in the machine's digital output was ±1 count, while random errors on the part of the operator in setting the cross hairs upon the centers of the droplet images were somewhat larger, but not more than ±3 counts. Thus maximum errors in measurement were of the order of ±4 OSCAR counts; in the case of a median one-second droplet movement of the order of 5 mm (150 OSCAR counts), this is equivalent to determining the particle displacement (and hence the average velocity for that second) within ±3 per cent.

With the Flexowriter output of the OSCAR set to print all measurements of each trajectory on a single line, the operator measured the successive displacements along each trajectory in their order of occurrence, from the trajectory beginning to its end. When similarly measured displacements from each succeeding trajectory were printed on succeeding lines, the OSCAR print-out of all data from one experiment took the form of an u_{ij} matrix of the observed displacements of i particles over j identical grid-times. This matrix of raw observations was then transferred to punched tape, the input format required by the Argonne digital computer, GEORGE.[1]

---

[1] An automatic, high-speed digital computer designed and constructed by the Applied Mathematics Division of Argonne National Laboratory featuring a two-address system and a 4096-word magnetic core memory.

CHAPTER V

THE ANALYSIS OF THE OBSERVATIONS

Determination of one component of the Lagrangian autocorrelation function from the results of one experiment (i.e., from data derived from ten photographs similar to Figure 6) typically involved the calculation of more than one hundred mean products of 50 terms each, in addition to the computation of the variances of some 15 to 20 sets of 50 numbers each for the decay plots. Though the solution of one such problem is not a very large task by digital computer standards, a computer program was prepared because of the large number of times this procedure was to be repeated. As it turned out, the program was used more than one hundred times in the analysis of the set of 26 experiments described in this report, since each of the two components of $R_k(\xi)$ determined from each experiment required a minimum of two computer runs apiece.

The Computer Program

Before computing estimates of $R_k(\xi)$, it was necessary to carry out the following preliminary steps:

(a) to convert observed displacements to turbulent fluctuations by removing contributions of the mean flow;

(b) to determine the virtual origin of the decay process to provide a valid time base for the decay corrections;

(c) to convert the decaying fluctuations to a stationary time series through application of the decay correction.

These preliminary steps as well as the calculation of $R_k(\xi)$ estimates for all possible values of ξ were carried out through the following program. The computer:

(1) accepts as input the u_{ij} matrix of measured one-second displacements, i.e., the observed droplet velocities of i particles at j times;

(2) averages all velocities with the same observation time as an estimate of the mean flow;

(3) subtracts these means from the u_{ij} matrix of displacements to obtain a u'_{ij} matrix of observed turbulent fluctuations;

(4) determines the variance of the 50 fluctuations observed at similar times j in all ten experiments and prints out these turbulent-energy estimates for a separate, manual determination of the virtual origin and the rate of decay;

(5) subtracts the time of the virtual origin from the times of observation to determine the decay time t;

(6) multiplies each entry in the observed fluctuation matrix u'_{ij} by the square root of the appropriate decay time $t^{1/2}$ to obtain a decay-corrected, fluctuation matrix u''_{ij};

(7) calculates autocorrelation estimates (equation [12]) for all possible time lags $t_2 - t_1$, etc., and averages those obtained with data of identical decay times over all trajectories;

(8) prints out the averaged correlation estimates $R_k(\xi)$ along with the redefined lag intervals of corrected time ($\xi = \ell n\, t_2/t_1$) to which they correspond.

The first computer run for each set of observations was automatically interrupted between operations (4) and (5), and the intermediate print-out of decay data was plotted in order to determine the virtual origin (see decay plots Figures 11 through 40). These plots also revealed those data which for one reason or another systematically departed from the first-period decay law. Since the decay corrections could not be expected to apply to such data, these points

were deleted from the input tape,[1] and the remainder, along with the additional information on the value of the virtual origin, were resubmitted to the computer in step (5). Reasons for this failure of the turbulent decay to adhere to the characteristics of the initial period are discussed in the Appendix.

Block-averaging Correlation Estimates

For convenience in plotting and fitting curves to the large number of scattered autocorrelation estimates obtained from the computer, values of $R_k(\xi)$ which lay within narrow blocks of corrected time ($\xi_1 \pm 0.05$ sec or less) were collected in simple averages. The need for this simplification can be seen in Figure 8, where all correlation estimates computed for one case are plotted along with the curve determined by their "block-averaged" values.

In general, correlation estimates calculated from data samples differing in size cannot be collected in simple averages, even though all samples have been drawn from a single population for which just one true correlation exists. However, when, as in this case, the samples are all approximately of the same relatively large size (i.e., between 48 and 50, but nearly always the latter), the correlation estimates are all very nearly equally weighted; and on this ground averaging might seem permissible. But in this case the populations from which the samples are drawn are all slightly different, for they derive

---

[1] At first glance it may appear that this operation constitutes omitting observations which fail to satisfy some preconceived notion of the results of an experiment. But this is not the case; rather, these data are deleted because they systematically fail to satisfy the critical assumption that the input data to the correlation computation for decay-corrected fields follows the linear law of the first period of homogeneous turbulent decay. It cannot be emphasized too strongly that failure upon the part of any portion of the data in this regard invalidates the application of the Batchelor decay corrections to those data. Therefore, when excessive departures from linear decay appeared, the data involved were deleted.

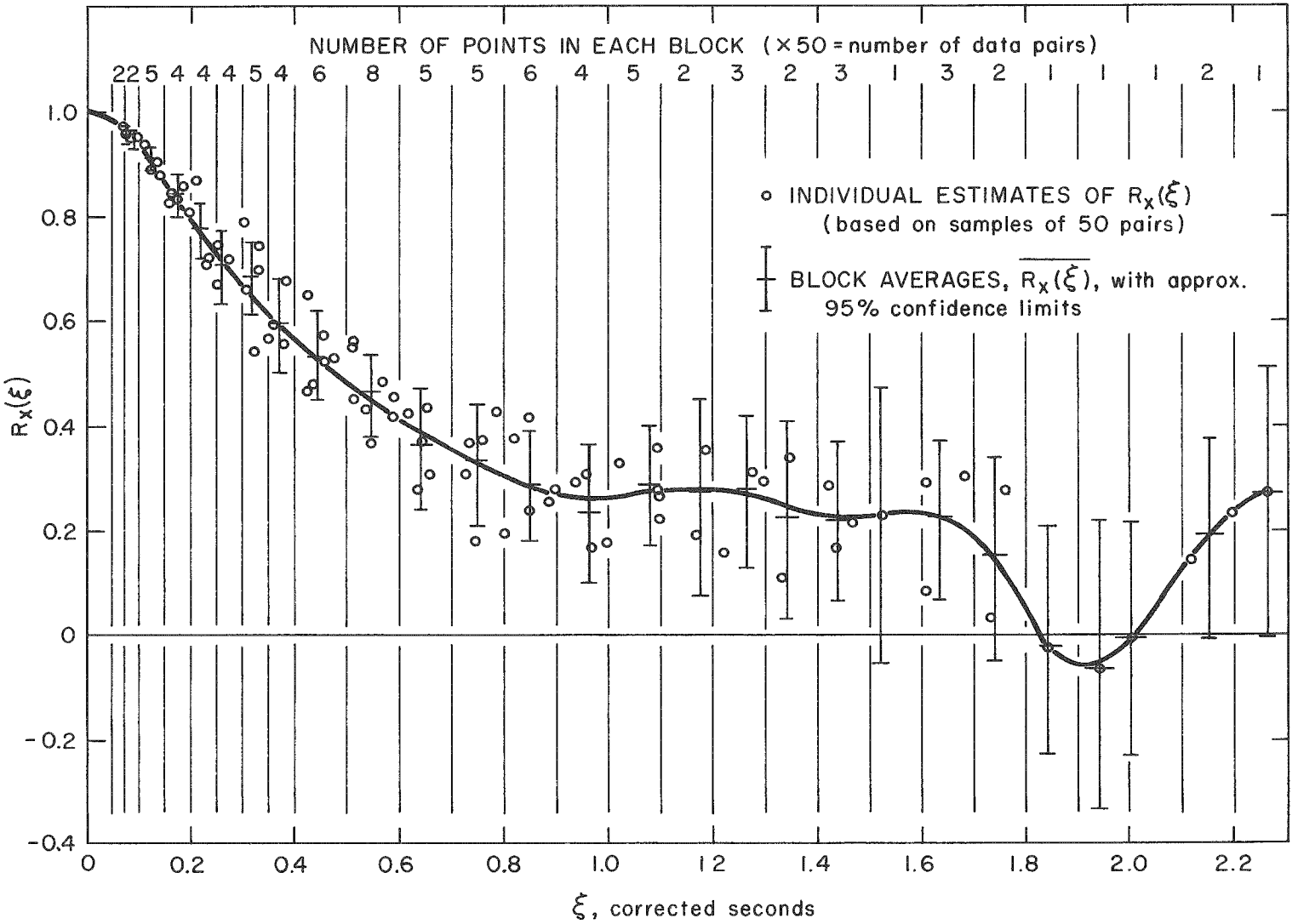

Fig. 8.--Complete plot of all correlation estimates obtained for experiment S/25/x_y.

from lag times which vary over the range $\xi_1 \pm 0.05$ corrected seconds. However, $R_k(\xi)$ is observed to be a comparatively smooth, continuous function which over a small interval can be approximated quite well by a straight line (cf. Figures 11 through 40). Further, although sets of nonzero correlation estimates based upon random samples drawn from a single large population in general exhibit skewed distributions around their true values, this skewness decreases with increasing sample size as well as with decreasing values of R, as may be seen in the distribution of 95 per cent confidence intervals shown in Table 4.

Table 4.--95 per cent confidence intervals on correlation estimates R as a function of sample size and correlation magnitudes[a]

R	Number of data pairs in sample			
	5	10	50	400
0.95	+0.04, -0.57	+0.03, -0.17	+0.03, -0.04	+0.01, -0.01
0.90	+0.08, -0.80	+0.07, -0.40	+0.04, -0.07	+0.02, -0.02
0.70	+0.26, -1.09	+0.21, -0.58	+0.12, -0.17	+0.05, -0.05
0.50	+0.42, -1.04	+0.34, -0.68	+0.18, -0.23	+0.07, -0.08
0.25	+0.62, -0.98	+0.48, -0.68	+0.24, -0.28	+0.09, -0.09
0.00	+0.82, -0.82	+0.61, -0.61	+0.28, -0.28	+0.09, -0.09

[a]David, 1938, Chart II.

To illustrate this mode of presentation, given an estimate R = 0.70 derived from a sample of 50 data pairs, the table indicates that there is only one chance in twenty that the true correlation of the population from which the sample has been drawn (assuming that population to be a bivariate normal distribution) will be greater than R + 0.12 = 0.82 or less than R - 0.17 = 0.53.

Although distributions of nonzero correlations based upon small samples are evidently badly skewed, increasing the number of data pairs to as much as 400 sufficiently narrows the confidence intervals that one may consider the correlation estimates to be distributed essentially symmetrically about R, over the entire range of R.

In fact, as may be seen in the table, this is only slightly less true for 50 data pairs, the sample size used in the present experiments. Therefore, it may be reasonably expected that the distribution of a number of estimates of $R_k(\xi)$, corresponding to closely spaced values of ξ over a maximum range of ± 0.05 corrected second, will be approximately symmetrical about the virtually linear descending trend of the true correlation value over that interval. It follows that the simple "block-average" of a number of such closely spaced estimates, say $\overline{R_k(\xi)}$, when assigned a mean lag time $\overline{\xi}$ equal to the average of the individual lag times, can be expected to determine an improved estimate of a single point on the Lagrangian autocorrelation curve.

The Mean Flow Problem

As is often the case in experimental studies of turbulence, the results obtained in this investigation were found to be strongly dependent upon procedures adopted to remove the mean flow. In the fields produced in the lee of a moving grid, the problem becomes not so much one of distinguishing between the mean and turbulent flows, since the rapid rate of decay exhibited by the latter clearly separated it from the remainder of the circulation; rather, it becomes one of insuring that the mean flow remains essentially the same in each run of a given experimental series and, in so far as possible, at each level in the test section during each run. If this ideal could have been realized, then the average of all tracer displacements observed at similar times in the ten separate runs of each set would have indeed constituted an adequate estimate of the mean flow characteristic of each particular time in the experiment.

However, as is discussed in some detail in the Appendix, the mean flow was found to exhibit velocity maxima centered about the middle levels of the tank. Moreover, these jetlike profiles in the general longitudinal drift periodically intensified when the surging

disturbance associated with starting the grid was reflected back through the test section from alternate ends of the tank. Unfortunately, the simple averaging procedure included in the computer program to estimate the mean flow, although able to accommodate the periodic surge, tacitly assumed the longitudinal drift to be independent of height. Consequently, in those experiments in which trajectories were, on the average, unfavourably distributed relative to the drift profiles, the averaging procedure became inadequate, and some portion of the mean flow remained in the matrix of observed fluctuations, u'_{ij}. Since these uncompensated fractions of the mean flow were subsequently magnified by the velocity-decay correction, a positive parabolic trend was imposed upon the data, a trend that eventually dominated the nominally decay-corrected fluctuation matrix u''_{ij}. Superposition of a monotonic trend upon the data in this manner gives the appearance of the presence of large-scale eddy components whose periods exceed the total observation times of the experiment. As a result, the autocorrelation functions for such cases were prevented from reaching zero, an effect similar to that which has been discussed by Webb (1955) for the case of linear trends superimposed upon otherwise stationary turbulence data.

Since it was of fundamental importance that such effects be minimized, a separate investigation of the nature of the mean flow in the towing tank was carried out. A description of these auxiliary experiments and a summary of their results is included in the Appendix.

Observed Distortions in Correlograms

In spite of all precautions adopted relative to the preservation of uniform mean flows and the deletion of data unduly affected by surge-induced departures from the first-period decay law, many of the autocorrelation functions evaluated in this study appear to have been adversely affected by uncompensated mean flows As may be seen in the plots of $R_k(\xi)$ or "correlograms" of Figures 11 through

40, the correlation fails to approach zero in many cases scattered over the entire range of the experiment. In such cases characteristic parameters, such as the time to zero, $\xi_{R=0}$, and the Lagrangian time scale $\mathcal{L}_k$, are more or less indeterminate. What is more, even in those cases where the $R_k(\xi)$ curve does intersect the ξ axis, it cannot be ascertained whether or not the presence of some uncompensated lesser fraction of the mean flow has not acted to delay the fall of $R_k(\xi)$ and thus artificially increased both these parameters. In case N/12.5/z, for example, cutting off the data at T = 15 results in the curve shown in Figure 12, $R_k(\xi)$ falling to zero near $\xi = 1.22$. But when later data to T = 20 are included (adding points which systematically depart from the first-period decay slope), the intercept is delayed until $\xi = 1.38$.

The distorting influence that mean-flow effects exert upon autocorrelation estimates increases with increasing lag time due to the positive parabolic trend imposed by the decay corrections upon these more slowly decaying fractions of the total velocity field. It follows, then, that the earlier portions of correlograms can be expected to be less subject to this source of error than are the later portions.

This expectation is borne out by two separate determinations of $R_x(\xi)$ made under identical experimental conditions of neutral stratification and grid Reynolds number. The first correlogram (case N/25/x, Figure 13) is based upon longitudinal displacements photographed from the side, while the second (case $N/25/x_y$, Figure 15) derives from longitudinal displacements photographed from above in an entirely different set of experimental runs. Note that the two correlation curves are essentially identical for $\xi < 0.6$; but from that point on, the curve determined by data photographed from the side appears to level out around R = 0.25, while that derived from data photographed from above very nearly reaches zero. The difference between these two results can probably be attributed to improved lighting and initial

tracer distribution achieved in the later experiments, factors which favoured the selection of trajectories from narrower ranges of depths than had previously been possible. As a result, tracer droplets selected from vertical views probably experienced significantly more uniform mean flows than those selected over wider ranges of depths in earlier side-view experiments. Of course, this also tended to place tracer nearer the jet maxima and, hence, in regions of less homogeneous decay (see Appendix); note that larger and somewhat earlier departures from linear decay appear in Figure 15 as compared with those shown in Figure 13. However, average displacements measured at similar times in the vertical-view case very probably constituted superior estimates of the actual mean flow; therefore, since data exhibiting disturbed decay were deleted from both computations, $R_x(\xi)$ determined from the vertical view still gave the better result.

It is evident from these two figures that for $\xi \lesssim 0.6$, these two independent autocorrelation determinations are nearly identical. This suggests that significantly more representative estimates of characteristic parameters such as λ_k would result if they were based solely upon the first portions of the correlograms. Indeed, by fitting adequate functional representations to the autocorrelation functions, this procedure can be followed.

The Exponential Approximation

The reader will recall that several determinations of $R_k(\xi)$ in the field described in Chapter II approximated simple linear expressions of the form

$$R_k(\xi) = 1 - a\xi.$$

Functions of higher order have also been used for this purpose; Frenkiel (1948) has suggested that forms of the normal error function or combinations of exponential and trigonometric or algebraic functions might be used. On the other hand, from considerations of the

general similarity theory, Inoue (1951) has shown that the Lagrangian autocorrelation function can be expected to approximate the form

$$R_k(\xi) = \exp - (\xi/a) \tag{37}$$

except where $R_k(\xi)$ approaches unity or zero. Physical considerations to the effect that turbulent eddies cannot continuously decrease at the small end of the spectrum to infinitesimally small sizes require that the slope of the $R_k(\xi)$ curve at $\xi = 0$ must be zero, a property not exhibited by a simple negative exponential; similarly, the negative exponential is unsuitable for large ξ since it asymptotically approaches zero as ξ becomes infinite, whereas correlograms derived from turbulent fields with a finite range of eddy sizes intersect the ξ axis at finite values of ξ.

The resemblance to decaying exponentials borne by the earlier portions of the majority of the correlograms obtained in these experiments is quite striking. This can be seen by comparing the observed $R_k(\xi)$ data points shown in the figures with the dashed exponential curves that appear with them. In most cases these curves represent functions similar to (37) displaced by a small increment of time δ in order to better fit the observed departure of $R_k(\xi)$ from a true exponential near $\xi = 0$ as shown in Figure 9. Expressing this in a compound functional form, we have

$$R_k(\xi) \equiv 1 \quad \text{for } 0 < \xi < \delta; \quad R_k(\xi) = \exp - \left(\frac{\xi - \delta}{a} \right) \quad \text{for } \xi \geq \delta. \tag{38}$$

The displacement factor δ is readily determined as the intercept of the exponential with $R = 1$ on a semilogarithmic plot of the correlogram, as shown in Figure 10. Note that since δ is a measure of the time $R_k(\xi)$ remains very nearly unity, it can be considered a measure of the duration of the initial, linear period of dispersion to be expected in the turbulent field that gives rise to a particular correlogram.

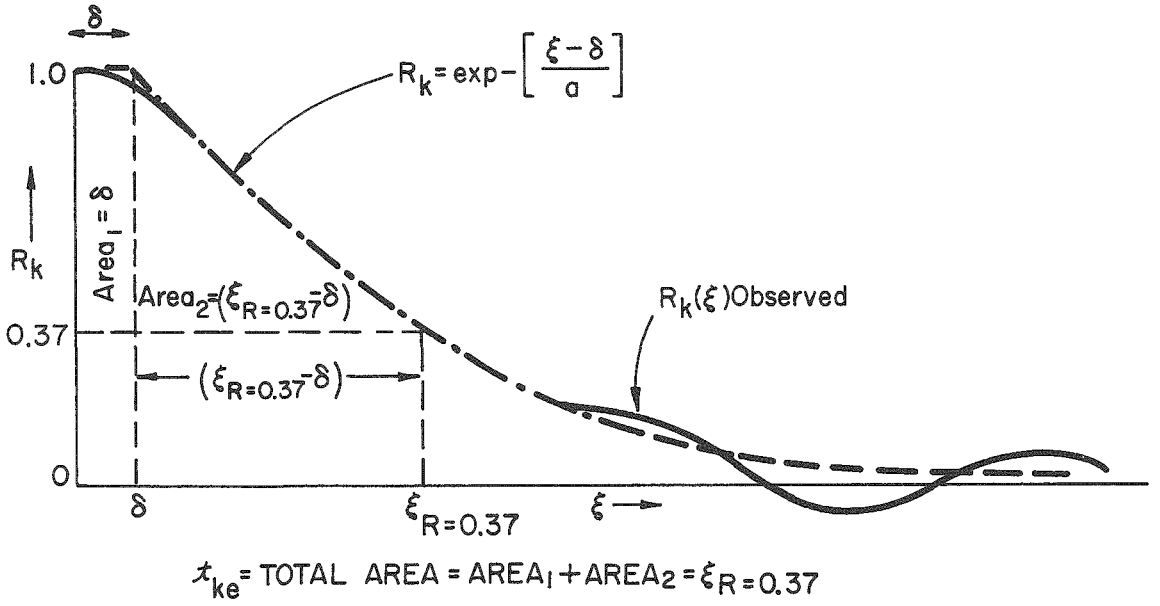

Fig. 9.--Sketch illustrating the method of determining the area under the compound functional representation of $R_k(\xi)$.

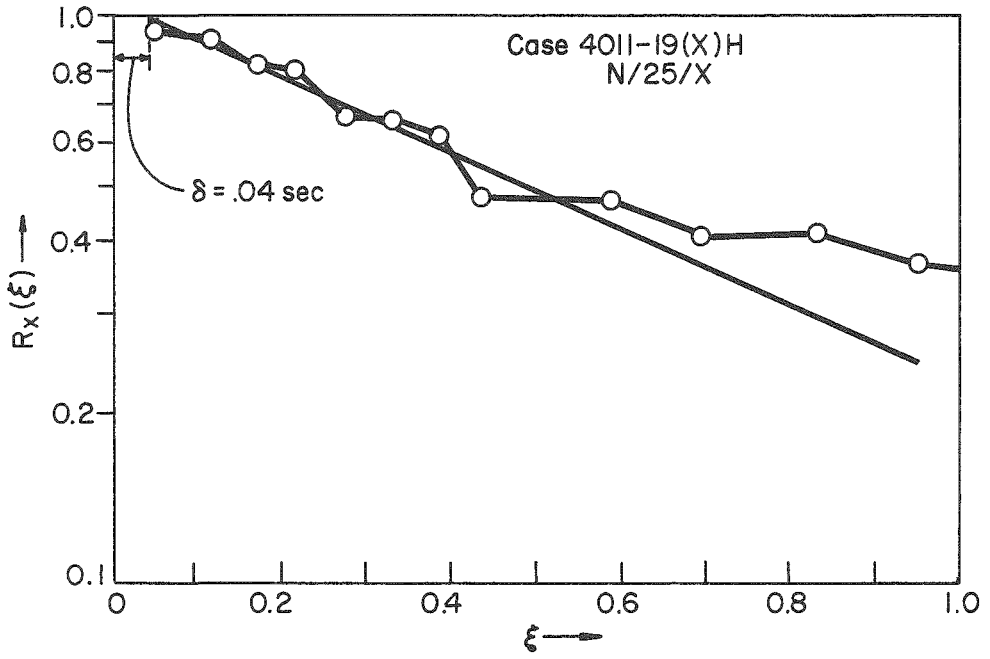

Fig. 10.--Sketch illustrating the method of determining the displacement factor δ for the compound functional representation of $R_k(\xi)$.

The area under the exponential portion of the curve is simply

$$\int_{\delta}^{\infty} R_k(\xi)\, d\xi = \int_{\delta}^{\infty} \exp -\left(\frac{\xi - \delta}{a}\right) d\xi = a. \tag{39}$$

The value of the constant a can be determined directly from the exponential curve itself, for when $R = e^{-1} = 0.37$, then $\xi - \delta = a$. Since the additional area under the curve for $\xi < \delta$ is numerically equal to δ, we have for the total area, that is, for the estimated magnitude of the Lagrangian scale time based on the exponential approximation,

$$a + \delta = \xi_{R=0.37} \equiv \mathcal{L}_{ke}. \tag{40}$$

The details of this calculation are shown graphically in Figure 9.

The foregoing method contributes a negligible overestimate of $\mathcal{L}_k$ due to the introduction of the small additional area above the $R_k(\xi)$ curve in the vicinity of $\xi = \delta$. A somewhat larger, but still negligible, overestimate is contributed by use of a functional form that asymptotically approaches zero at infinity. For a = 0.5 sec and $\delta = 0.05$ sec, values which are close to those observed in the experiments, the exponential has fallen to R = 0.02 when $\xi = 2$ sec, whereas the additional area contributed beyond that point is a little less than 2 per cent of a. Beyond $\xi = 1.5$ sec, the error is still only 5 per cent of a. In the experimental correlograms obtained, Lagrangian scales for curves with times to zero less than 1.5 sec could be evaluated directly since these intersected the ξ axis.

The Pseudomicroscale

The observed shape of the correlogram near $\xi = 0$ determines an additional characteristic of the turbulent field, namely, a "microscale" or "dissipation length" which Taylor (1935) suggested might be considered a measure of the smallest eddies, i.e., those primarily responsible for the final conversion of turbulent energy into heat through the effects of viscosity. The concept is appropriate

to either Lagrangian or Eulerian coordinates, the definitions of the microscale from these two points of view being closely analogous to one another. Thus, one can define a Lagrangian microscale λ_k in terms of the initial curvature of the $R_k(\xi)$ function:

$$\frac{1}{\lambda_k^2} \equiv \lim_{\xi \to 0} \left[\frac{1 - R_k(\xi)}{\xi^2} \right]. \tag{41}$$

Taylor showed that the osculating parabola which just fits the correlogram near $\xi = 0$ intercepts the ξ axis at the value λ_k. In fact, Taylor used this graphical method to estimate a Lagrangian microscale from a correlogram derived from data obtained from a field of grid-produced turbulence in which allowance had been made for the influence of turbulent decay by means of the method described in equation (31) et seq. In this early estimate of a Lagrangian-Eulerian relationship for turbulent motions, he found that the microscales viewed in the two coordinate systems appeared to differ by only a constant scale factor.

Because of the limitations in sensitivity imposed both by the comparatively slow response of the relatively large tracer droplets and by the relatively long one-second displacements used to determine fluctuation velocities, data obtained in the current experiments are inherently deficient in higher frequencies. Therefore, an accurate estimate of the true microscale cannot be obtained. However, a "pseudomicroscale" based upon the early curvature of the observed correlograms can be used at least to compare the results of the several experiments of this investigation with one another. Since this procedure bases the osculation parabola on points of the $R_k(\xi)$ curve for values of ξ significantly larger than zero, whereas the definition of λ_k strictly applies only to the limiting case $\xi \to 0$, the pseudomicroscales can be expected to tend to overestimate the true value.

For the osculating parabola we may write

$$R_k(\xi) = 1 - (\xi^2/\lambda_k^2), \tag{42}$$

where the intercept with the ξ axis, λ_k, is the pseudomicroscale. Taking the logarithm of both sides of the expression in (38) for the exponential portion of the correlogram, we have

$$\ell n\, R = -\frac{\xi - \delta}{a} \approx R - 1, \tag{43}$$

where the approximation on the right is valid when $R > 0.85$. As may be judged from the correlograms, this last is generally true since $R \geq 0.9$ at the point of osculation in all cases. Solving (42) and (43) simultaneously, we obtain

$$\xi^2 - \frac{\lambda_k^2}{a}\xi + \frac{\delta\lambda_k^2}{a} = 0. \tag{44}$$

This quadratic expression has a double root appropriate to the point of tangency when the characteristic $(b^2 - 4ac) = 0$. Thus:

$$\frac{\lambda_k^4}{a^2} - \frac{4\delta\lambda_k^2}{a} = 0$$

or

$$\lambda_k = 2(a\delta)^{1/2} = 2[(\mathcal{t}_{ke} - \delta)\delta]^{1/2}, \tag{45}$$

since from equation (40) we have $a = \mathcal{t}_{ke} - \delta$.

As described in greater detail in a later section, the exponential approximation becomes less appropriate in the specific case of the vertical component $R_z(\xi)$ under conditions of moderate to strong stable stratification. In these cases, Gaussian normal error functions of the form $R = \exp -(\xi/a)^2$ are superior, as may be seen in Figures 20, 24, 28, and 32. A simultaneous solution for points of tangency of osculating parabolae to this form of $R_z(\xi)$ shows that the curves touch only at $\xi = 0$ and that the constant a used in the error

function for any particular correlogram is numerically equal to the intercept of the osculating parabola with the ξ axis, that is, for

$$R_z(\xi) = \exp - (\xi/a)^2, \quad \text{then } \lambda_z = a. \tag{46}$$

The Lagrangian Power Spectrum

The significance of Lagrangian scale time changes observed in the experiments can be interpreted in terms of changes in the relative distribution of energy among various turbulent eddy sizes, for the magnitude of the $\mathcal{L}_k$ scale can be shown to determine the frequency of a significant peak in the Lagrangian power spectrum. If one assumes the experimental correlograms can be represented with sufficient accuracy by the compound form given in equation (38), then corresponding Lagrangian power spectra can be obtained through the cosine transform (cf. Taylor, 1938). Thus

$$F(n) = 4 \int_0^\infty R(\xi) \cos n\xi \, d\xi, \tag{47}$$

where n is the frequency in radians per second and f(n) is an "amplitude density" that expresses the fraction F(n)dn of turbulent energy per unit frequency contained in the frequency band between n and n + dn. It follows that the power spectrum can be written nF(n). Substituting equation (38) for $R(\xi)$ in (47) and multiplying by n, we have

$$nF(n) = 4n \int_0^\delta (1) \cos n\xi \, d\xi + 4n \int_\delta^\infty \exp - \left(\frac{\xi - \delta}{a}\right) \cos n\xi \, d\xi.$$

After introducing the change of variable $z = \xi - \delta$ in the second integral above, integration gives

$$nF(n) = \frac{4}{1 + a^2n^2} [\sin n\delta + an \cos n\delta]. \tag{48}$$

Since the first derivative of the foregoing result is transcendental, a general expression for the frequency of the point of zero slope cannot readily be obtained. However, it can be shown that at $n = a/(a^2 + \delta^2)$ the slope of this spectrum function is positive, whereas at $n = 1/a$ the slope is negative; therefore, the frequency of the spectral peak lies between these limiting values. If we examine the width of the foregoing range relative to the magnitude of, say, the upper limit, we obtain

$$\left(\frac{1}{a} - \frac{a}{a^2 + \delta^2}\right) \Big/ \frac{1}{a} = \frac{\delta^2}{a^2 + \delta^2}.$$

For $a = 0.50$ and $\delta = 0.05$, values which are representative of those obtained in the experiments, the interval between limits can be seen to be slightly less than 1 per cent of the value of the upper limit. What is more, with even the largest displacement factor δ observed in all of the experiments (case N/12/z, $\delta = 0.09$, $a = 0.55$), the interval between limits is still less than 3 per cent of the upper value, $1/a$. Therefore, for the purpose of analyzing the results of the experiments, the upper limit itself provides an adequate estimate of the frequency n_k of the peak in the Lagrangian power spectrum. Converting the latter to cycles per second, we have

$$n_k = (2\pi a)^{-1} = [2\pi(\mathcal{t}_{ke} - \delta)]^{-1}, \tag{49}$$

where the last follows from equation (40). Actually, the lower limit $n = a/(a^2 + \delta^2)$ can be shown to provide a somewhat closer estimate of the location of the spectral peak, but in view of the narrow separation between upper and lower limits and in consideration of the uncertainties involved in the experimental data, little is to be gained by using the less convenient expression.

The Brunt-Vaisala Stability Parameter

In the discussions to follow, it will be convenient to express gravitational fluid stability in terms of the Brunt-Vaisala frequency N.

For an incompressible fluid (cf. Eckart, 1960)

$$N^2 \equiv \left(\frac{g}{\rho} \frac{d\rho}{dz} \right) = \left(\frac{g}{\rho} \frac{d\rho}{d\theta} \frac{d\theta}{dz} \right). \tag{50}$$

Substitution of suitable numerical values for water in the temperature range of the current experiments gives the approximate expression

$$N^2 \approx 0.23 \, (d\theta/dz) \, \text{sec}^{-2}.$$

The Brunt-Vaisala frequency is an appropriate stability parameter to introduce into an investigation of the influence of gravitational stability upon small-scale turbulent circulations, since it is a measure of the buoyancy forces that support or oppose vertical displacement of fluid elements in a stratified environment. When $d\theta/dz > 0$, as in stable stratifications, N is a real number that can be shown to represent the frequency of vertical oscillation about an equilibrium level exhibited by a fluid parcel after a small initial displacement. On the other hand, when $d\theta/dz < 0$, as in an unstable stratification, N becomes imaginary. In this case the frequency equation has an exponential solution that describes the monotonic passage of a disturbed parcel from an original position of unstable equilibrium; here N corresponds to the reciprocal of the "time of flight" required for the parcel to reach a level e units above or below the starting point.

A further advantage in the use of the Brunt-Vaisala parameter for these incompressible-model experiments arises from the fact that the definitions of N^2 for compressible and incompressible media are closely analogous. Allowance for adiabatic changes of density during vertical motion in the compressible, atmospheric prototype requires only that a potential density referred to a standard pressure level be substituted for ρ in (50), as will be discussed in a later section. Further support for the suitability of this parameter to the present investigation appears in the experimental results themselves; for, as

will be seen, several key parameters descriptive of the decay-corrected turbulence fields exhibit approximate linear variation with the absolute value of N.

CHAPTER VI

THE RESULTS OF THE EXPERIMENTS

The principal results obtained in this investigation are displayed in the energy-decay plots and Lagrangian autocorrelation curves of Figures 11 through 40. These have been derived from a large number of independent realizations of turbulent fields generated in the towing tank under several conditions of initial turbulence intensity and fluid stability. The $R_k(\xi)$ curves have also been used to derive a number of characteristic parameters that describe the properties of the decay-corrected turbulent fields; these are collected in tables which appear throughout the chapter.

Details of the neutral, stable, and unstable experiments are first presented below with only a minimum discussion of results. In later sections of this chapter, the results of the neutral experiments are compared with those obtained under similar conditions of stratification by Vanoni and Brooks; finally, the influences of initial turbulence intensity and fluid stability upon the Lagrangian autocorrelation function are discussed in some detail. Particular attention is paid to the behaviour of three key parameters, the average corrected turbulence intensity, the Lagrangian scale time, and the pseudomicroscale. Note that the remaining parameters depend upon one or more of these (see note appended to Table 7 below).

In each experiment the grid was driven at one of three standard carriage speeds: 12.5, 25, or 40 cm/sec. Since the mean water temperature remained in the narrow range $23 \pm 2°C$, these speeds effectively define three grid Reynolds numbers, namely 0.7×10^4, 1.4×10^4, and 2.2×10^4. In subsequent discussions, these will frequently be referred to simply as the slow, moderate, and fast cases. Coded notations such

as "N/25/x" are used to designate the "x component of the neutrally stratified experiment with a grid speed of 25 cm/sec." In these designators, VU/ means "very unstable," and WS/ means "weak stable"; the absolute strengths of the temperature gradients so designated will be clear in the context in which these notations appear.

The Neutrally Stratified Experiments

The difficulties involved in maintaining a near-zero vertical temperature gradient for long periods of time in a large quantity of fluid are probably not generally realized. Heat losses through evaporation plus conduction to or from the environment combine to generate lapse rates that are anything but isothermal. In these experiments, the success achieved in this regard resulted from several features built into the apparatus: (a) only 5 per cent of the water surface was open to the air; (b) the temperature of the environment was kept within ±0.5°C of the mean temperature of the tank; and (c) a rapid flow of thermostatically controlled water at a temperature equal to that of the tank was continuously circulated through the upper and lower heat exchangers connected in series. With these arrangements, the average of all lapse rates observed in the neutrally stratified experiments was +0.002°C/cm, whereas the maximum range of lapse rates observed in any one set of runs with the same grid Reynolds number was ±0.003°C/cm. The remaining experimental conditions of the neutral runs are summarized in Table 5.

The initial computer output for each experiment consisted of the means of the displacements observed at each time along with the standard deviations of the observations from these means. The latter (provided of course the simple averages do indeed represent the mean flow as explained in the previous chapter) represent the root-mean-square turbulent fluctuations, hereafter designated $\underline{u}_{ki}$. Thus, the variance $\underline{u}_{ki}^2$ represents the k component of the turbulent energy at any time i. Above each correlogram the reciprocals $1/\underline{u}_{ki}^2$ are plotted

(Text continues on page 81)

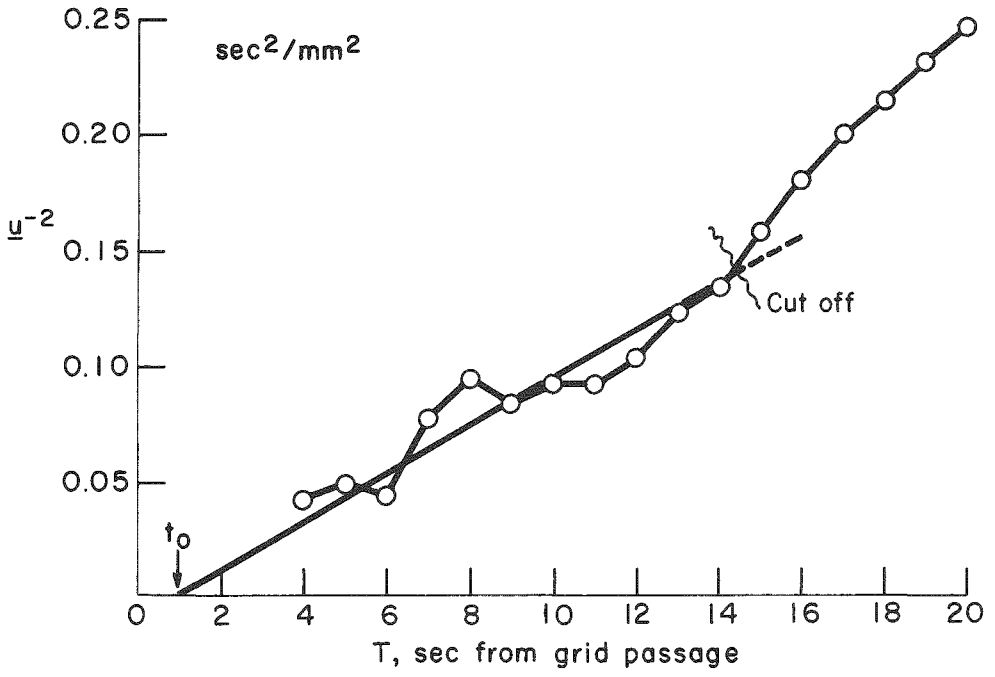

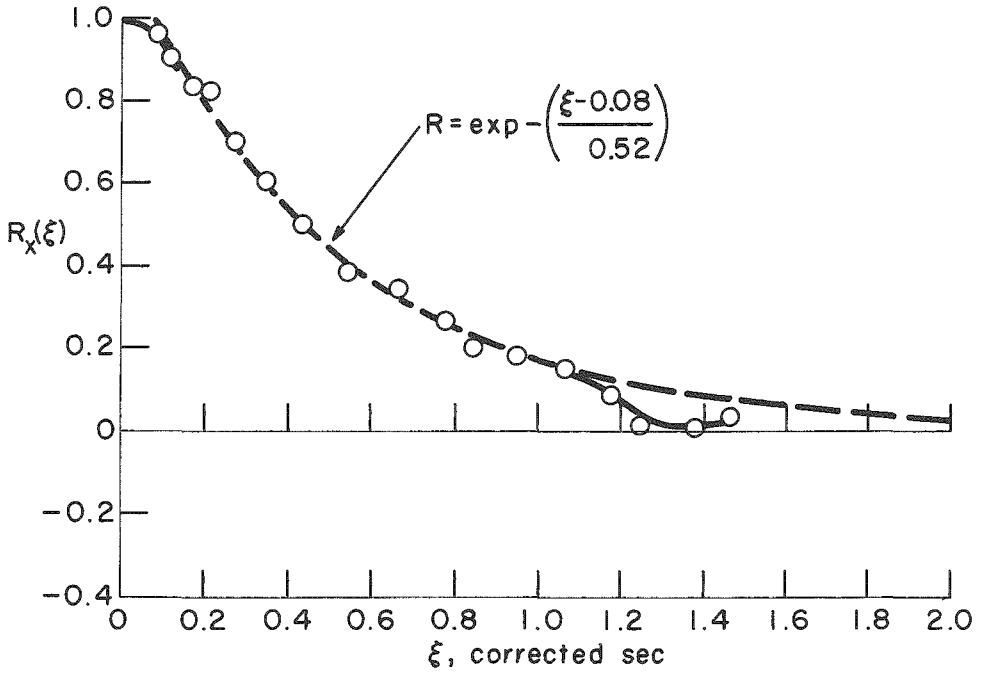

Fig. 11.--Decay curve and correlogram for experiment N/12.5/x.

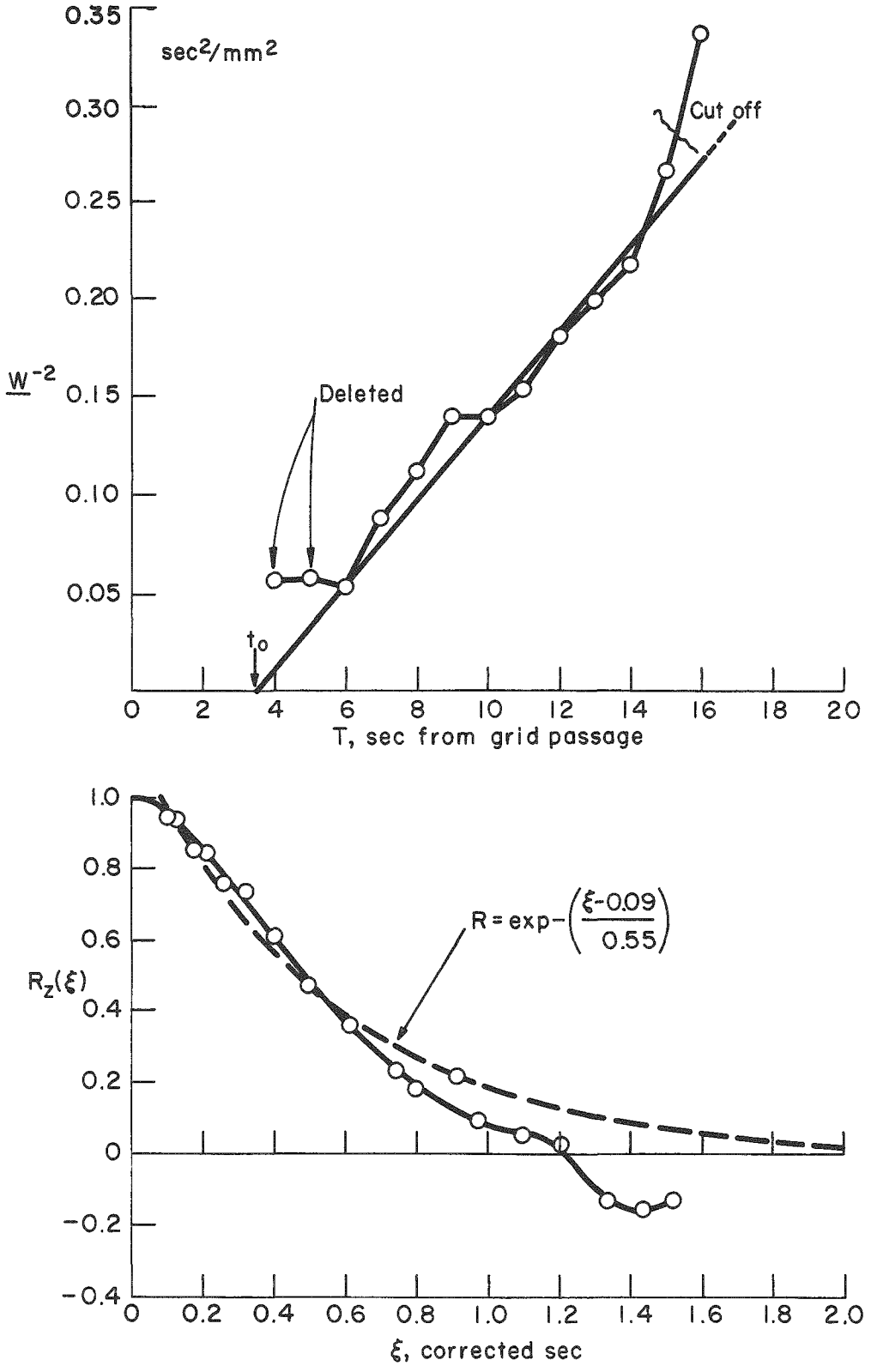

Fig. 12.--Decay curve and correlogram for experiment N/12.5/z.

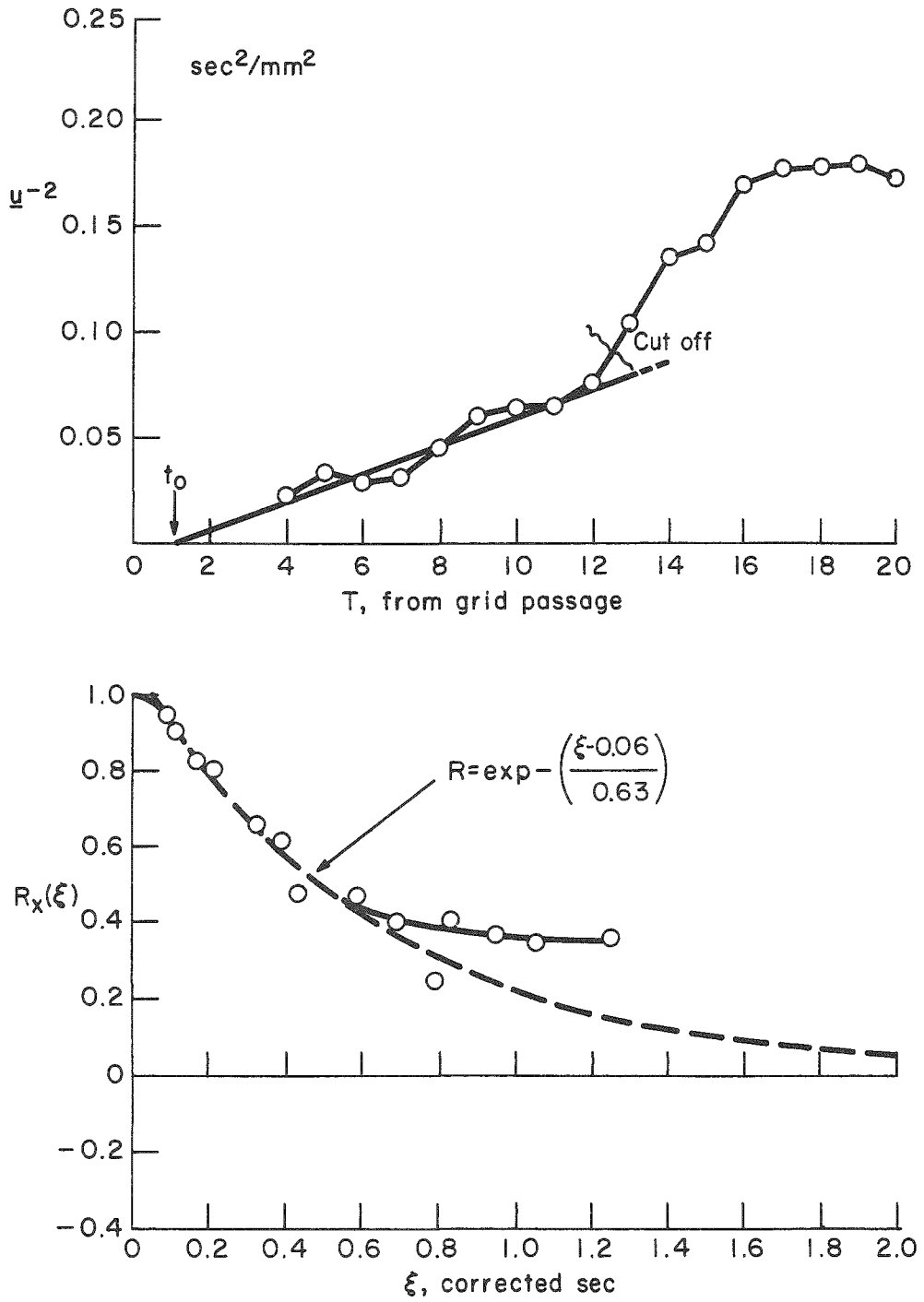

Fig. 13.--Decay curve and correlogram for experiment N/25/x.

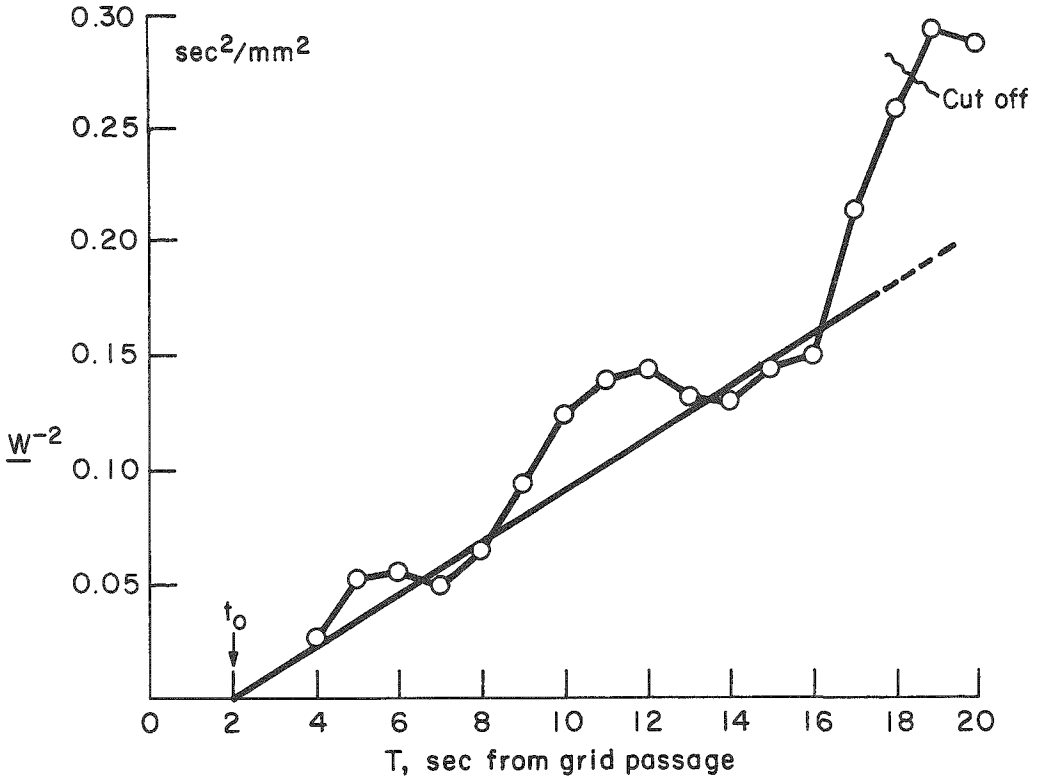

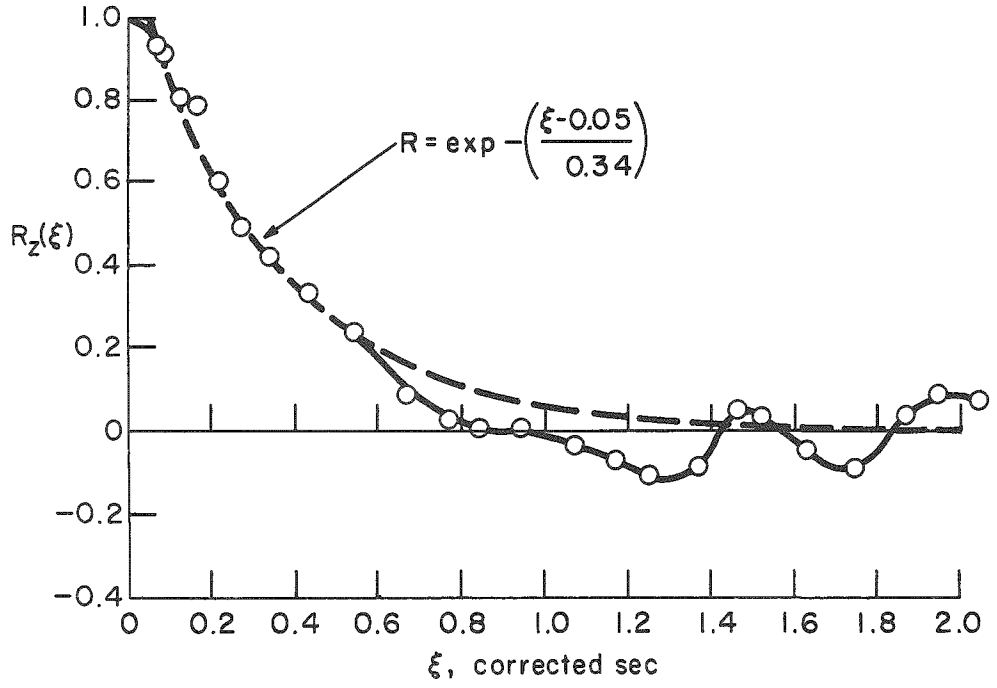

Fig. 14.--Decay curve and correlogram for experiment N/25/z.

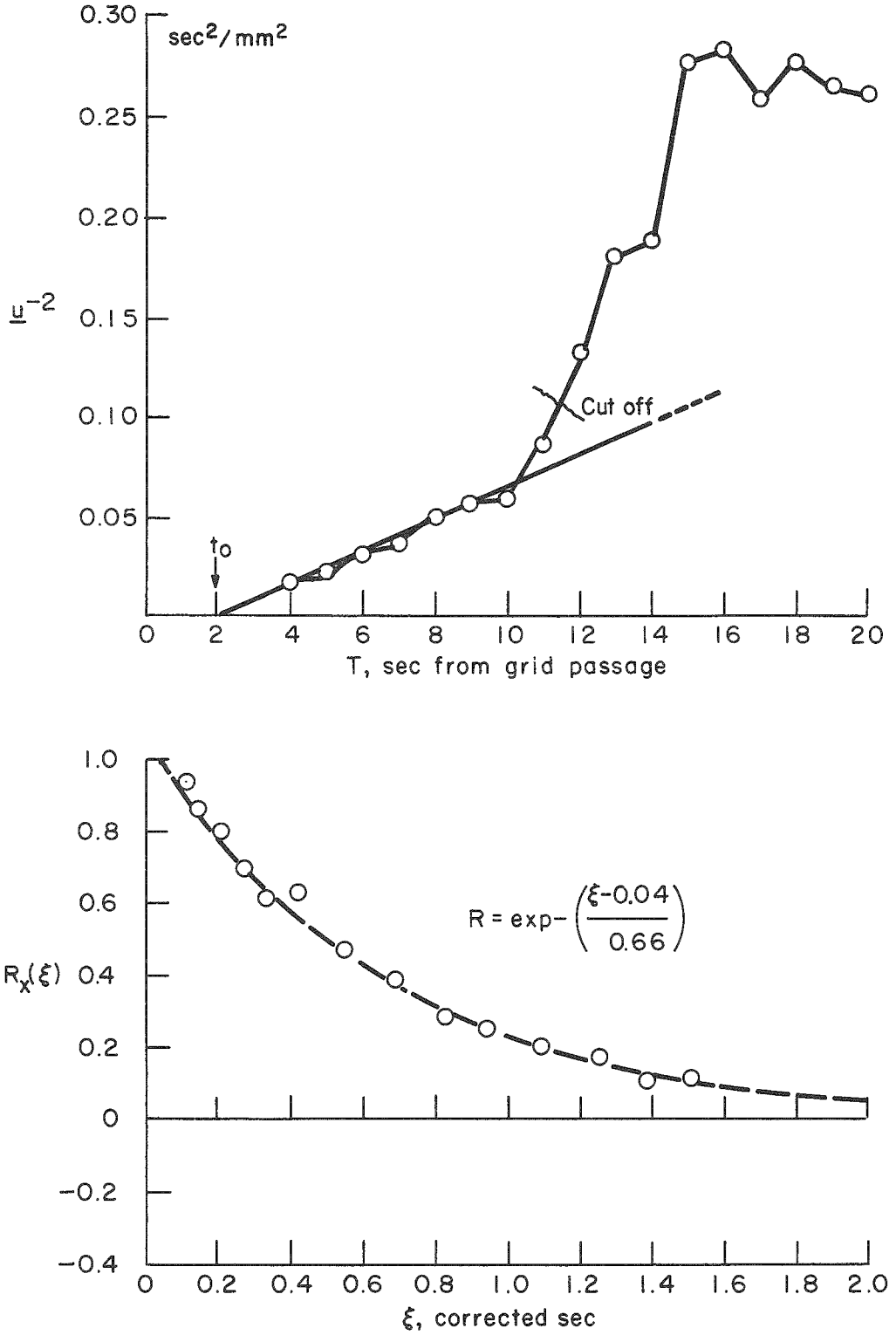

Fig. 15.--Decay curve and correlogram for experiment $N/25/x_y$.

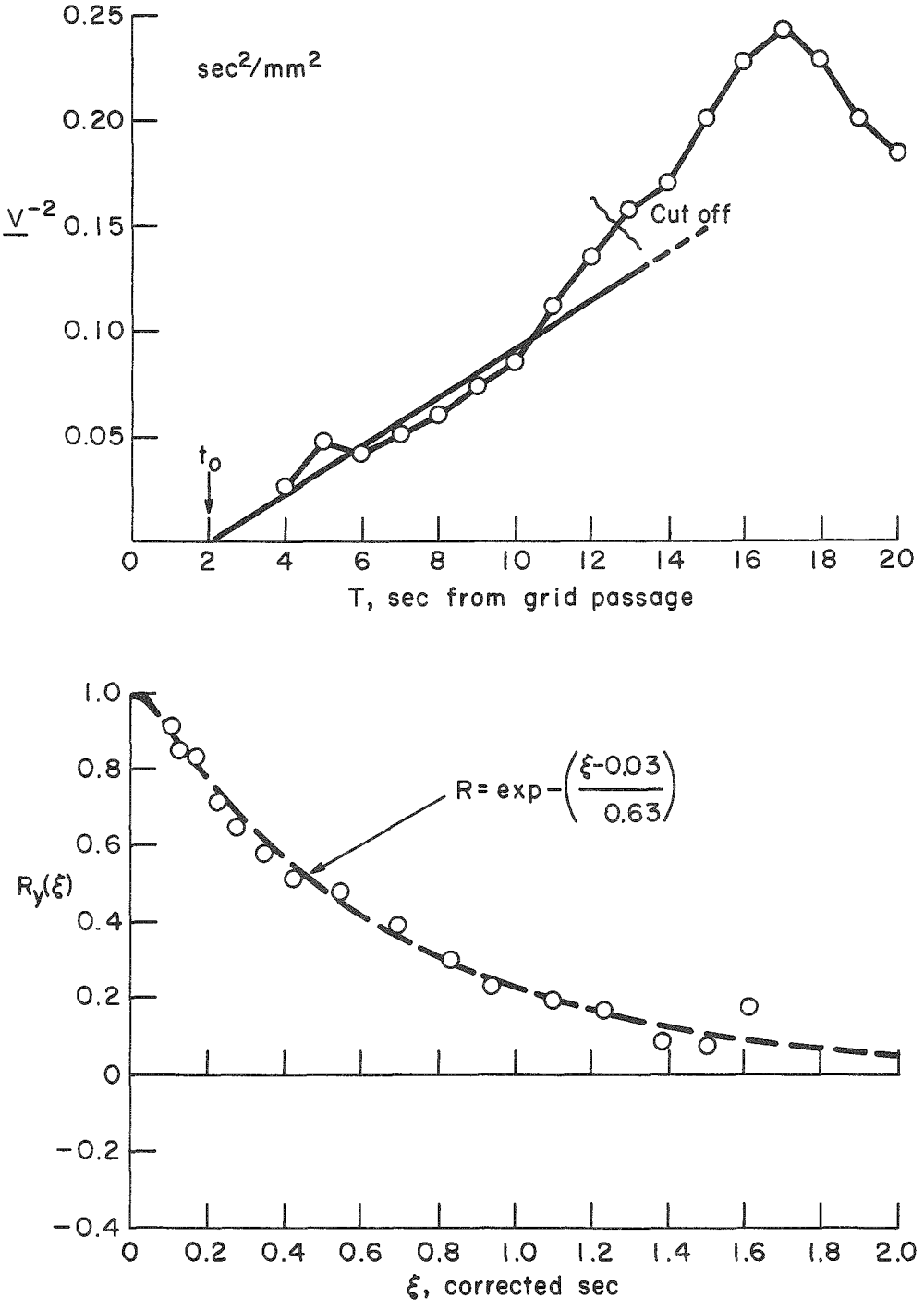

Fig. 16.--Decay curve and correlogram for experiment N/25/y.

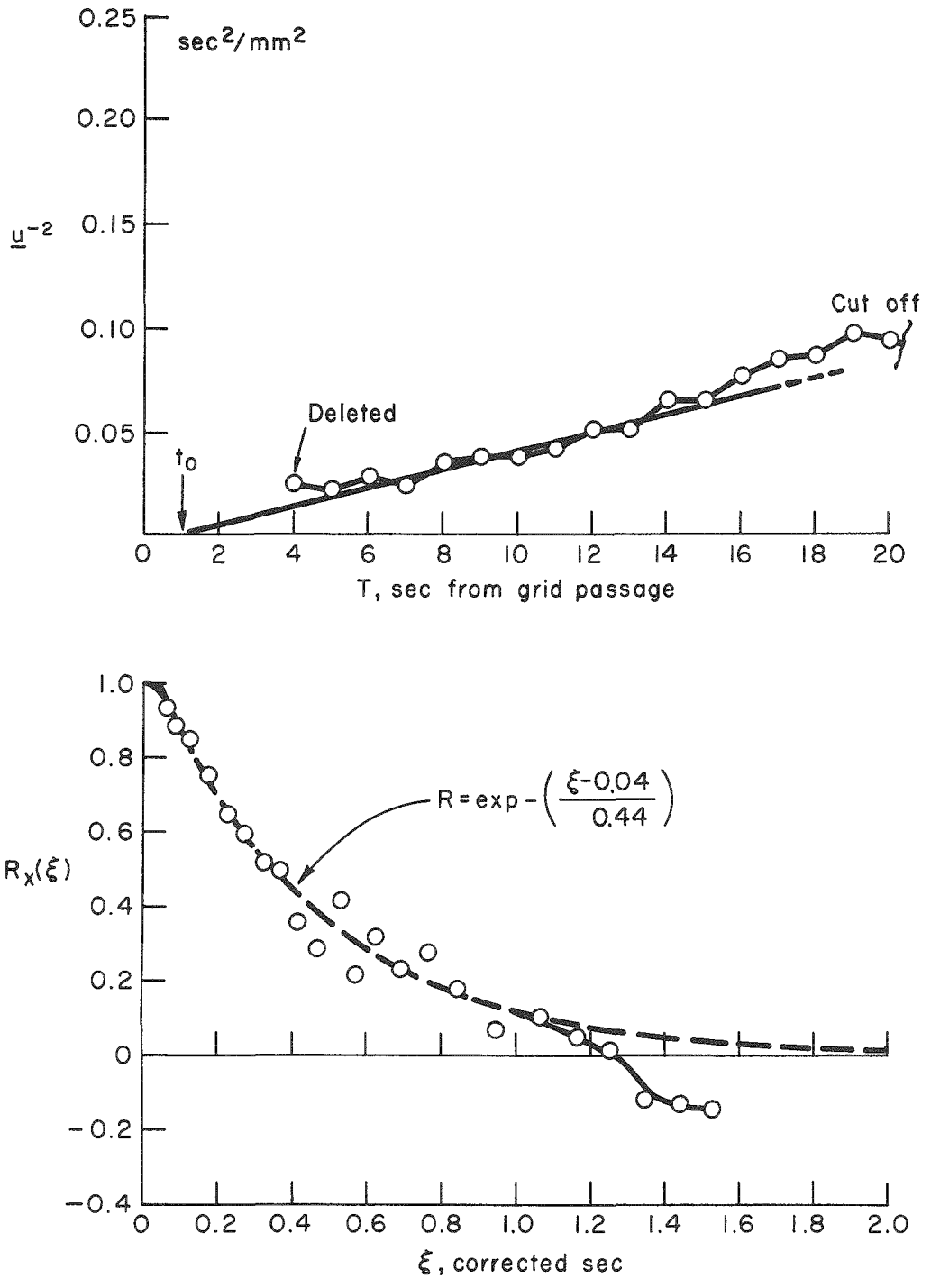

Fig. 17.--Decay curve and correlogram for experiment N/40/x.

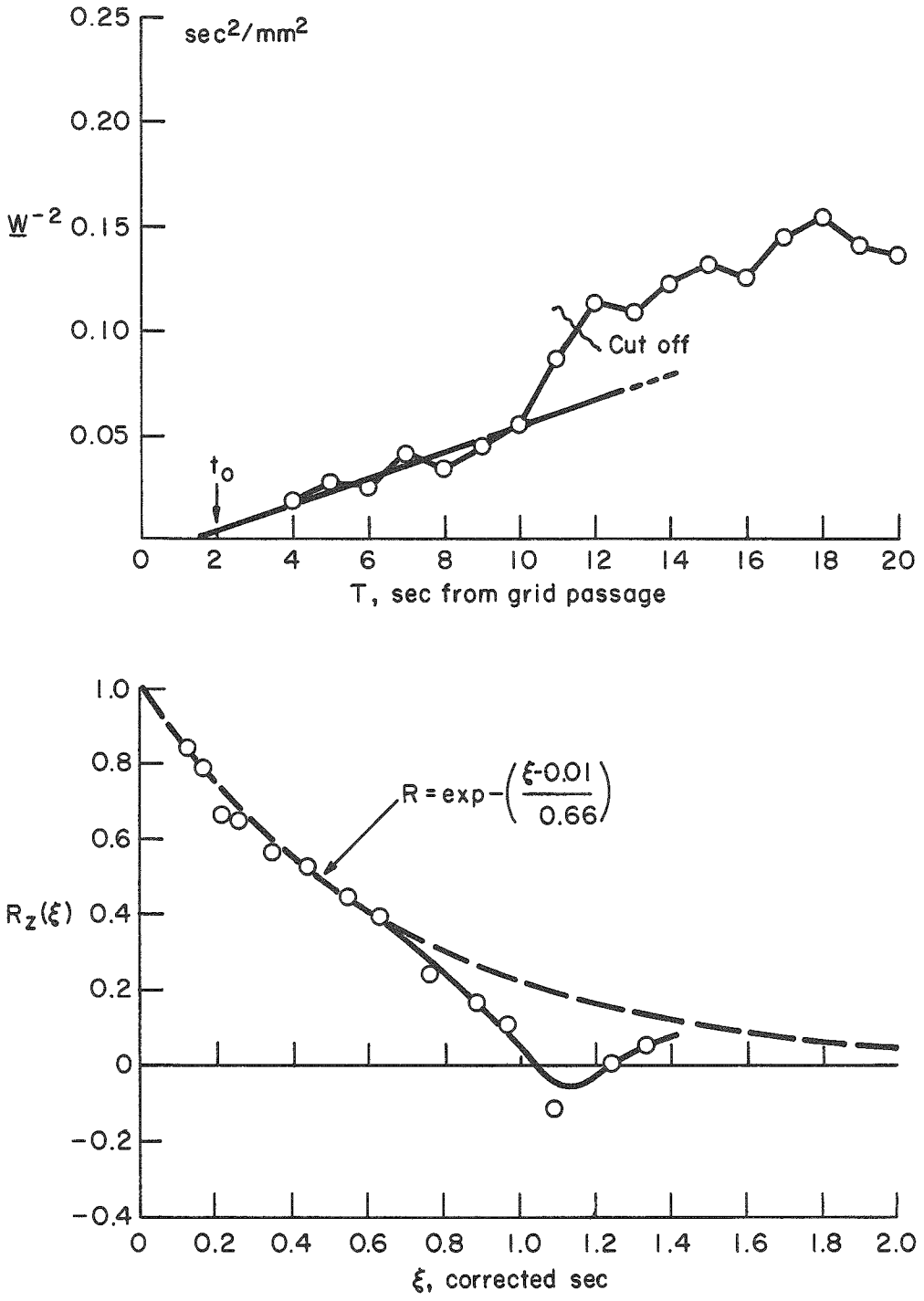

Fig. 18.--Decay curve and correlogram for experiment N/40/z.

TABLE 5.--A summary of the experimental conditions and key decay characteristics of the neutrally stratified experiments

Designator Code, (Fig.)	$Re_g \times 10^{-4}$	Virtual Origin		Data Cut off T(sec)
		T(sec)	M	
N/12/x, (11)	0.7	1.0	2.5	>14
N/12/z, (12)	0.7	3.5	8.8	<6, >15
N/25/x, (13)	1.4	1.0	5	>12
N/25/z, (14)	1.4	2.0	10	>17
$N/25/x_y$, (15)	1.4	2.0	10	>11
N/25/y, (16)	1.4	2.0	10	>12
N/40/x, (17)	2.2	1.0	8	<2
N/40/z, (18)	2.2	1.5	12	>11

against the grid time T = i. The intercept of the resulting linear slope with the abscissa determines the virtual origin (t_0) of the first-period decay, while subsequent deviations from the linear relation reveal observations which must be deleted since they violate the assumptions underlying the decay corrections.

Virtual origin times listed in Table 5 for the neutral experiments correspond to positions that range from 2.5 to 12 mesh lengths behind the grid. With the exception of the smallest of these values (which may be in error due to the very low level of turbulence in that particular, slow-speed case), these compare favorably with locations of t_0 between 10 and 20 mesh lengths observed in wind tunnels at higher grid Reynolds numbers. Since the position of t_0 has been observed to shift downstream with increasing Re_g, and since values of this ratio that obtain in these experiments are quite low by wind-tunnel standards, virtual origins located at less than 10 mesh lengths from the grid are not unreasonable. Note there is some evidence in the table to show t_0 tending toward greater distances from the grid as Re_g increases. It is interesting that in the case of the longitudinal (x) components of turbulence, the times of occurrence of t_0 tend to remain constant at 1.0 sec after grid passage for all three grid speeds, the

increasing mesh-length distance between the grid and t_0 largely resulting from the increase in speed.

Table 5 also reveals a marked tendency for the virtual origin of the vertical components of turbulence at any one value of Re_g under neutrally stratified conditions to be delayed in comparison to t_0 for either the longitudinal or transverse component. This indication of a departure from isotropy is confirmed when one compares the relative magnitudes of the average, corrected turbulence intensities of these components in Table 6. This effect may have resulted from the rectangular cross section of the towing tank; but, on the other hand, it may have a more general origin since it also appears to some degree in measurements obtained in a water tunnel of symmetrical section (see Table 14 et seq., below). The turbulence field becomes more isotropic as the grid Reynolds number increases, for whereas the time of ocurrence of t_0 for the longitudinal component remains constant in Table 5, that for the vertical turbulence component steadily decreases. In a similar manner, the vertical, longitudinal index of isotropy, $\underline{w}^2/\underline{u}^2$, steadily increases with increasing Re_g, an effect that can be attributed to increased mixing that results from increased turbulence levels at higher grid Reynolds numbers. As will be discussed in a later section, this tendency for anisotropy in the towing channel is greatly reduced by the introduction of either unstable or, surprisingly enough, weak stable gradients.

TABLE 6.--Average turbulence intensities and indices of isotropy observed in the neutrally stratified experiments

Designator Code	$Re_g \times 10^{-4}$	Turbulence Intensity (mm^2/sec)			Indices of Isotropy	
		$\underline{u}^2$	$\underline{v}^2$	$\underline{w}^2$	$\underline{v}^2/\underline{u}^2$	$\underline{w}^2/\underline{u}^2$
N/12/x,z	0.7	94		46		0.49
N/25/x,z	1.4	145		88		0.61
N/25/x,y	1.4	110	88		0.80	
N/40/x,z	2.2	222		159		0.72

Table 5 also lists the grid times of observations deleted from the autocorrelation computation as a result of departures from linear decay. In two of the cases (N/12/z, Figure 12, and N/40/x, Figure 17) data measured at the beginning of the observations were deleted since these points were clearly above the decay curve, an indication that the rapid rate of decay characteristic of fully established turbulence had not yet fully set in.

Case N/25/z, Figure 14, is particularly interesting since it shows a return to linear decay after a 6-sec disturbed period, probably associated with a surge-induced departure from homogeneity, as discussed in the Appendix. In this case, it was not found necessary to delete data during this period of evidently not too seriously disturbed decay, for the inclusion of mean products involving data observed at T = 10, 11, 12 and even 18, did not significantly alter the block-averaged correlation estimates.

These two examples of data deletion early and late in the experiment illustrate a fact that tends to be obscured in the decay curve due to its nature as a plot of the reciprocal of the energy. Note that what may appear to be only small departures from the decay law early in two of the neutral experiments were deleted when seemingly larger departures late in another were retained. However, the magnitude of such departures from the linear law must be considered in relation to the magnitude of the ordinate at the point of departure; an excess of one unit where the amplitude of the reciprocal decay curve is only one unit corresponds to a relative reduction in energy of 50 per cent, whereas a similar excess where the ordinate of the decay curve is larger represents a proportionately smaller percentage reduction in energy.

Table 7 summarizes the characteristic scales of turbulence and virtual diffusion coefficients derived from the correlograms of the neutral experiments. These are discussed in detail in a later section, particularly with regard to the influence of increasing grid Reynolds

number. For convenience, a brief description of the origin of the entries in the table is given below; it applies equally, of course, to the summaries of the stable and unstable results given in Tables 10 and 13.

TABLE 7.--Characteristic parameters derived from correlograms of the neutrally stratified experiments[a]

Designator Code, (Figs.)	Times to Zero (corrected sec)			Lagrangian Scales: Time (corrected sec)			Lagrangian Scales: Length (mm)			Virtual Diffusion Coefficients (mm^2/sec)					Pseudomicro-scales (corrected sec)		
	$\xi_{R_x=0}$	$\xi_{R_y=0}$	$\xi_{R_z=0}$	$\mathcal{t}_x$	$\mathcal{t}_y$	$\mathcal{t}_z$	ℓ_x	ℓ_y	ℓ_z	K_x^*	K_y^*	K_z^*	K_y^*/K_x^*	K_z^*/K_x^*	λ_x	λ_y	λ_z
N/12/x,z (11, 12)	1.4		1.22	0.55		0.54	5.3		3.7	51.7		24.8		0.48	0.42		0.45
N/25/x,z (13, 14)			0.90	0.69* av: 0.70		0.39*	8.3 av: 7.8		3.7	100.0 av: 88		34.3		0.34	0.39		0.26
N/25/x,y (15, 16)				0.70*	0.65*		7.4	6.1		77.0	57.1		0.74		0.33	0.28	
N/40/x,z (17, 18)	1.26		1.05	0.45		0.50	6.7		6.3	99.9		79.5		0.80	0.27		0.16

[a]Entries in Table 7 above and in Tables 10 and 13 to follow are derived in the following manner:

$\xi_{R=0}$ the intercept of the $R_k(\xi)$ curve with the ξ axis, when available.

$\mathcal{t}_k$ the area under the $R_k(\xi)$ curve when available, equation (23); values marked with asterisks derive from the exponential approximation, equations (39) and (40);

ℓ_k $\mathcal{t}_k$ multiplied by u_k, equation (24); u_k from Table 6;

K_k^* ℓ_k multiplied by u_k, equation (25);

λ_k derived from functional representation of correlogram through equation (45) or (46).

av average values obtained by combining entries immediately above and below.

The Stably Stratified Experiments

As described in Chapter IV, the fact that the water remained at rest the great majority of the time made it possible to maintain strong, stable temperature gradients in the towing tank. Gradients as large as +0.7°C/cm have been achieved, this corresponding to a top-to-bottom temperature difference of 20°C. But because of the tendency for two-dimensional jet-velocity profiles to appear under conditions of strong stable stratification, the Lagrangian trajectory experiments were limited to weaker stabilities in the range from 0.03 to 0.30°C/cm.

In six of the seven stably stratified experiments, lapse rates measured just prior to each of the ten runs remained constant within ±7 per cent. In the weak stable case, the lapse rates observed were within ±0.002°C/cm of +0.030°C/cm, whereas in the two very stable cases, lapse rates were (+0.280 ±0.020) °C/cm and (+0.300 ±0.012) °C/cm, respectively. In one moderately stable case, the lapse rates

(Text continues on page 99)

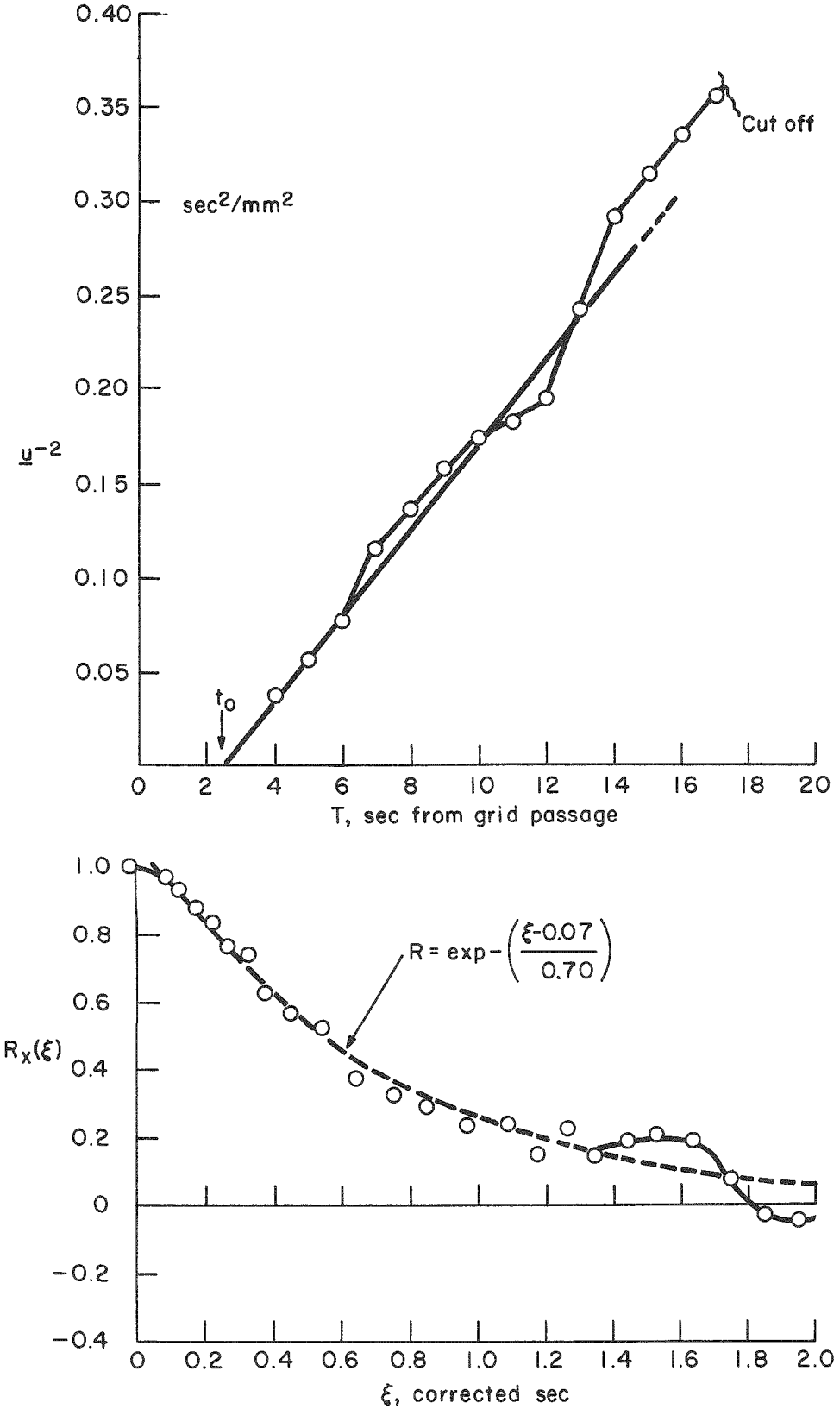

Fig. 19.--Decay curve and correlogram for experiment S/12.5/x.

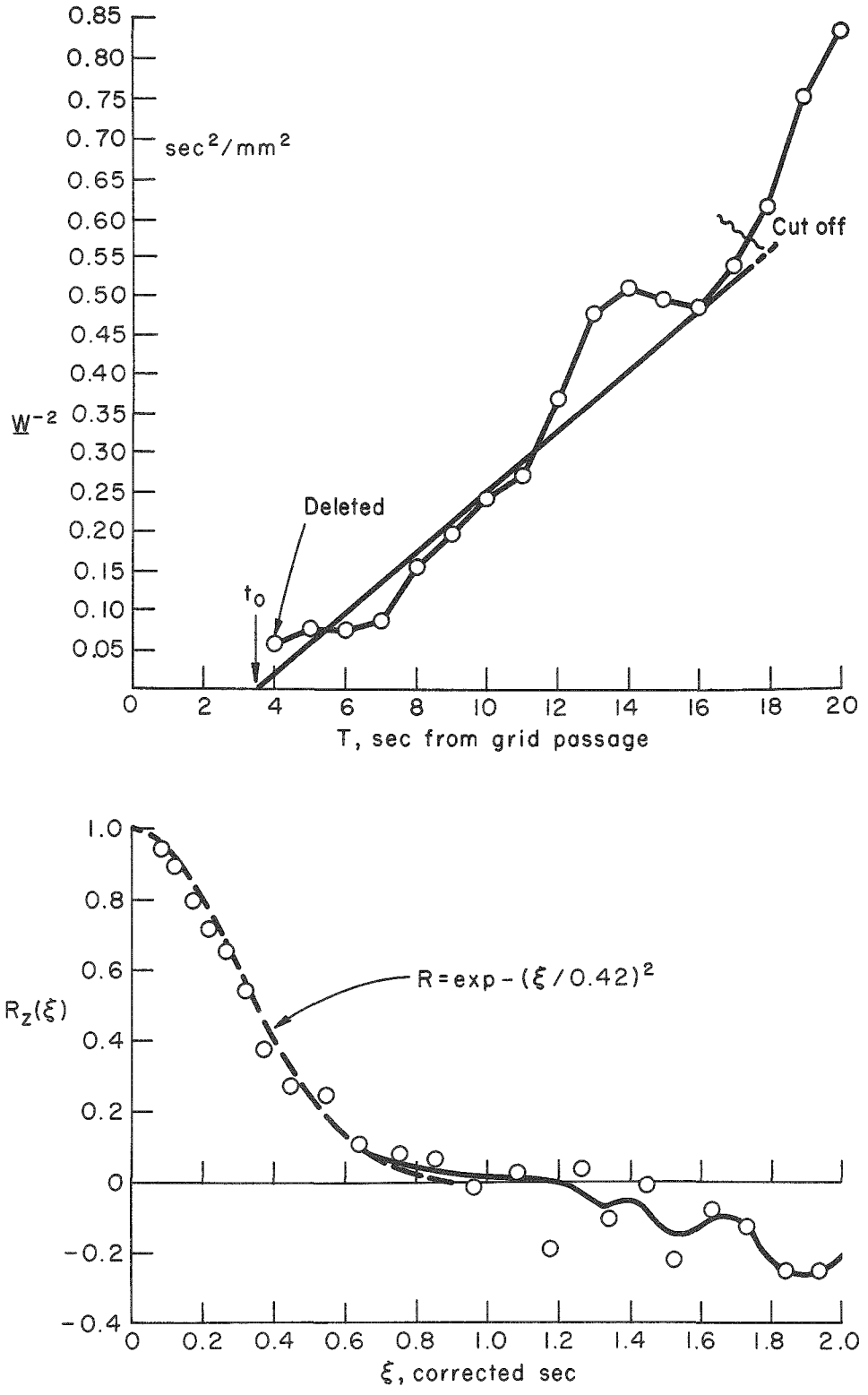

Fig. 20.--Decay curve and correlogram for experiment S/12.5/z.

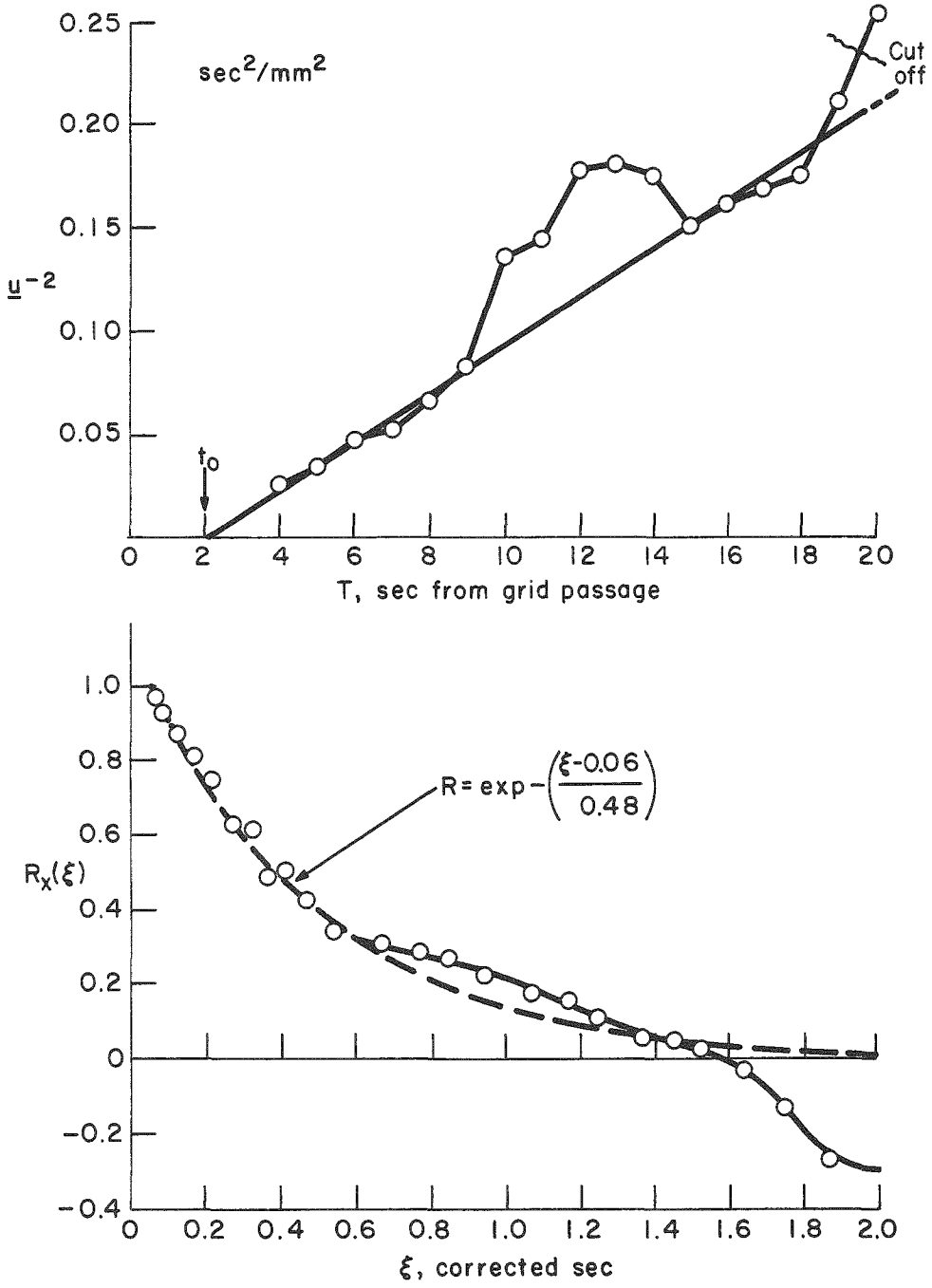

Fig. 21.--Decay curve and correlogram for experiment WS/25/x.

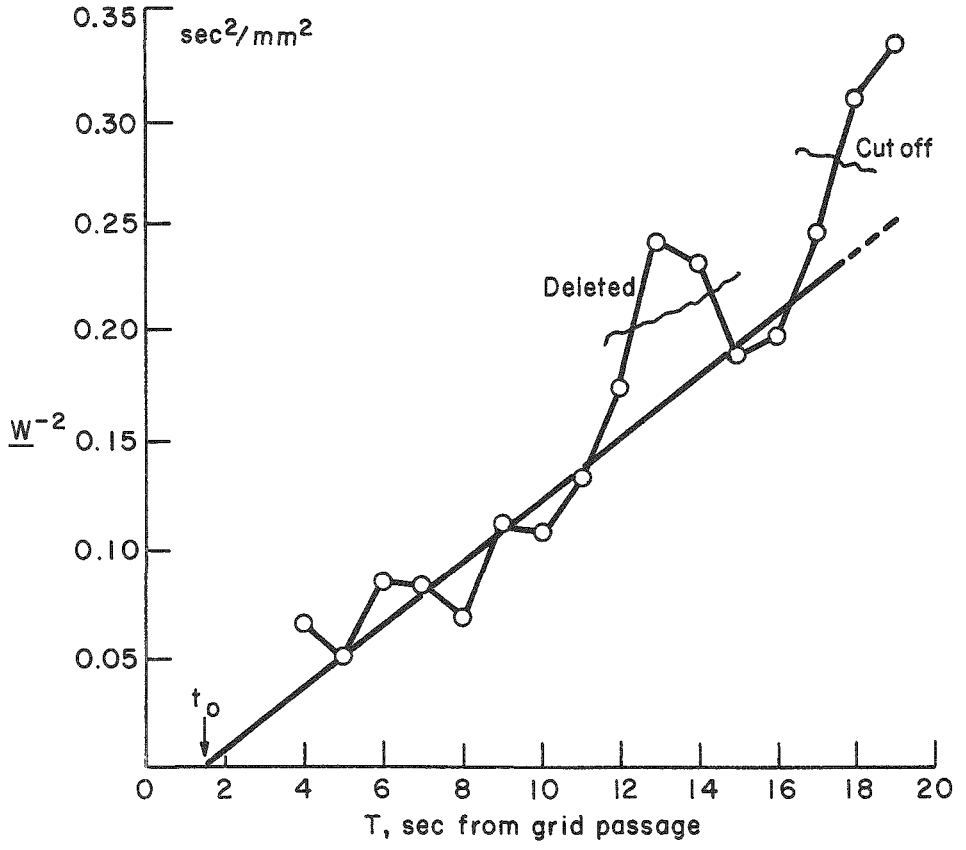

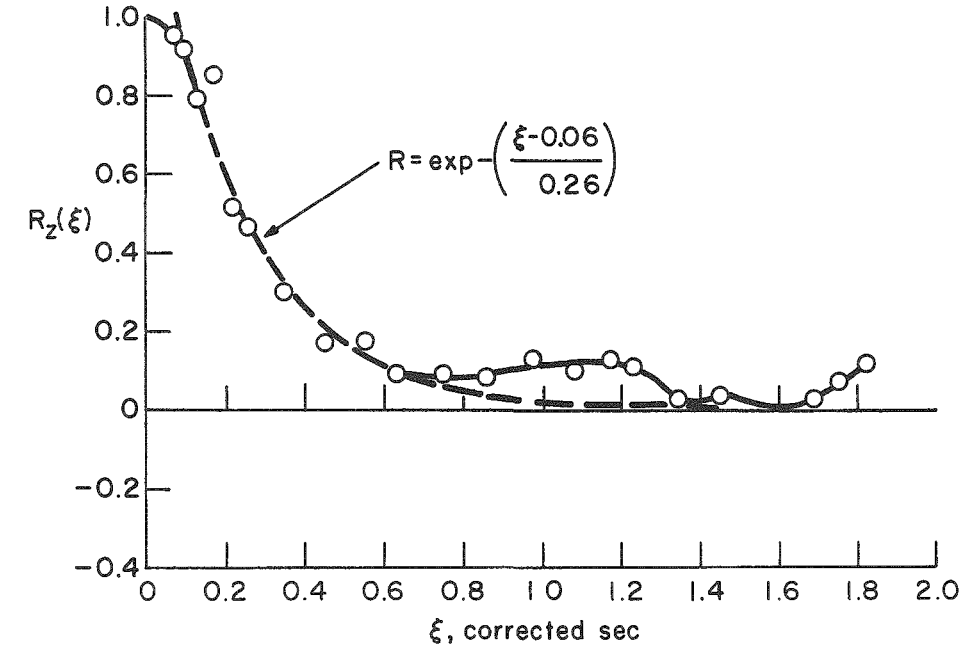

Fig. 22.--Decay curve and correlogram for experiment WS/25/z.

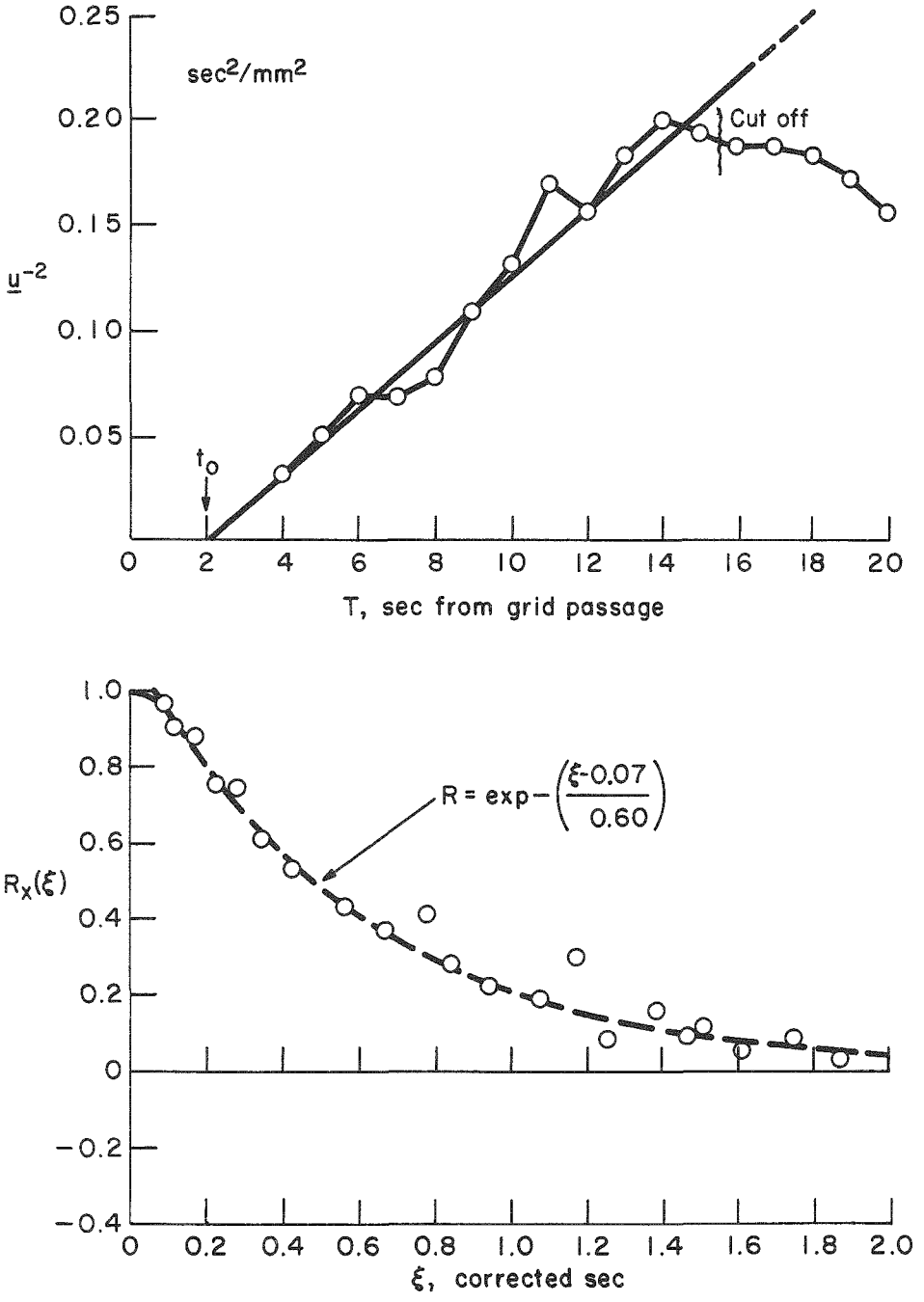

Fig. 23.--Decay curve and correlogram for experiment S/25/x.

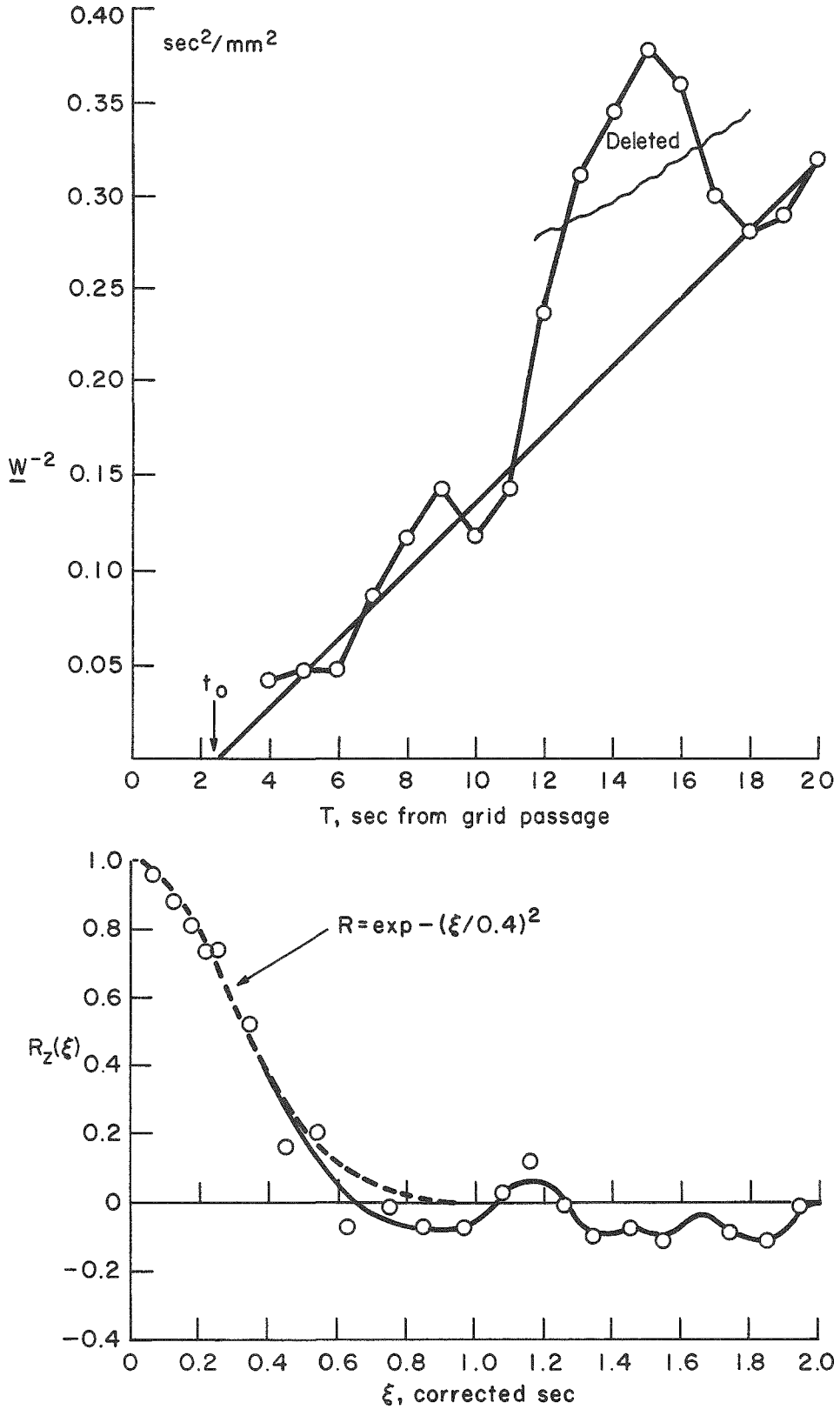

Fig. 24.--Decay curve and correlogram for experiment S/25/z.

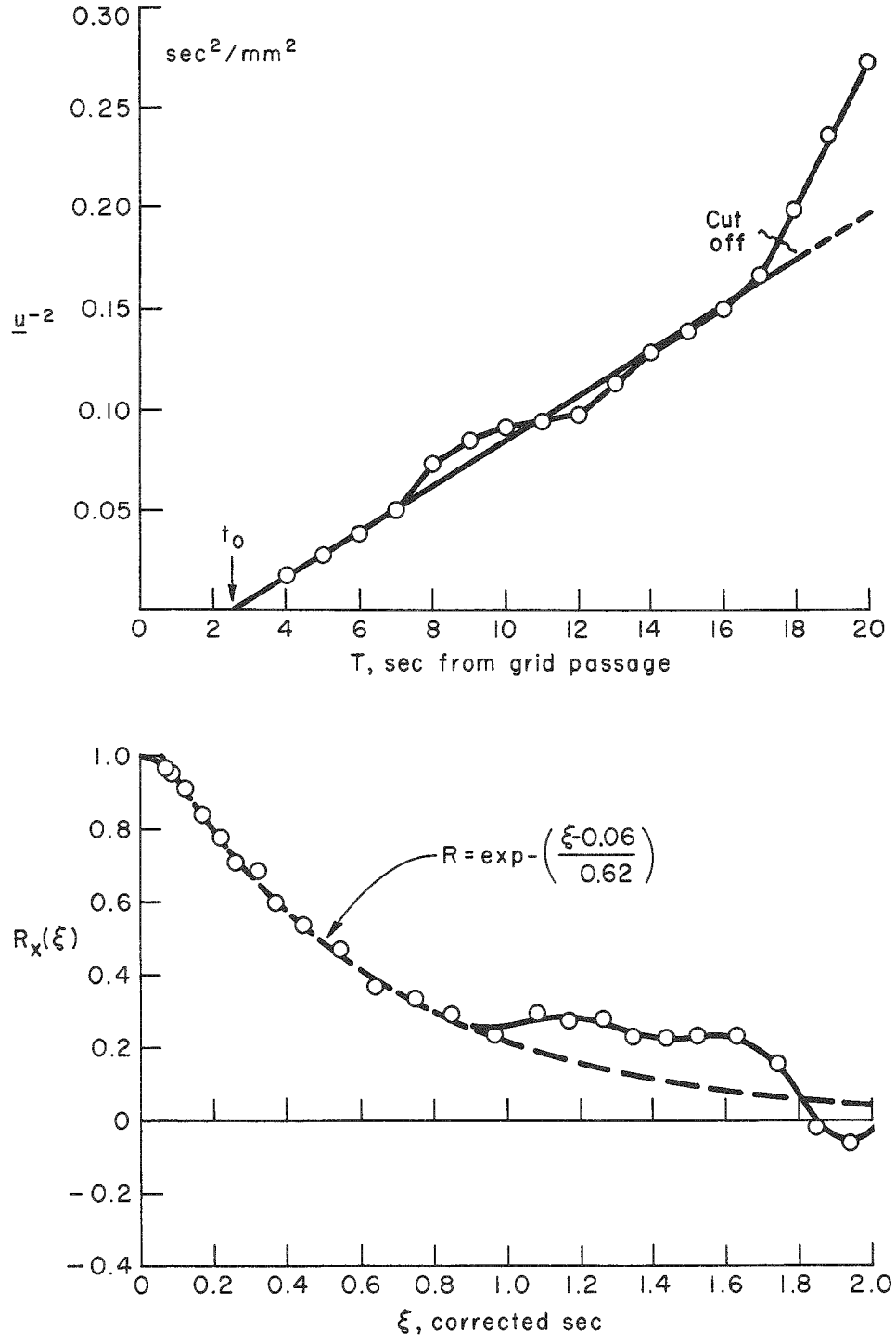

Fig. 25.--Decay curve and correlogram for experiment $S/25/x_y$.

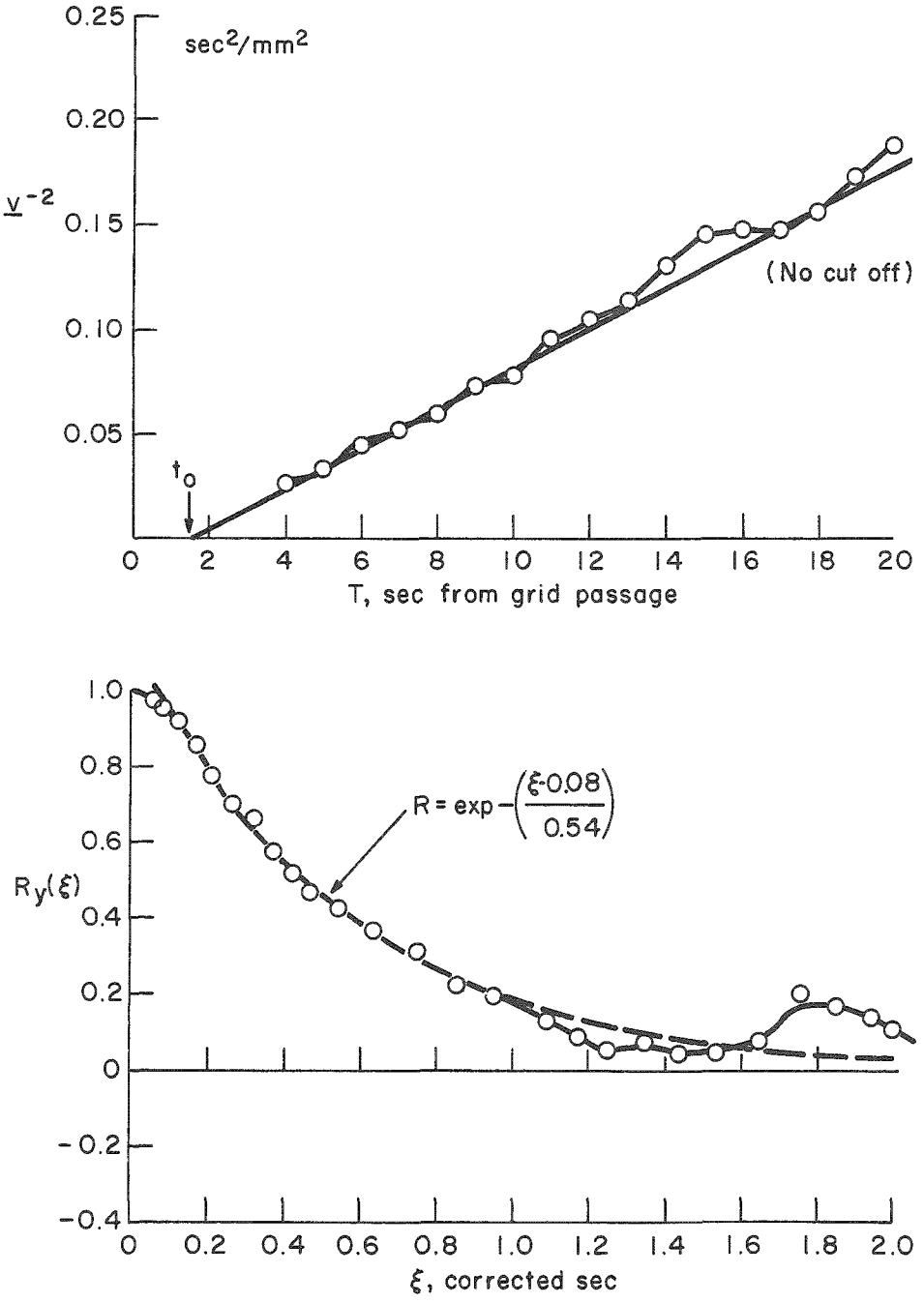

Fig. 26.--Decay curve and correlogram for experiment S/25/y.

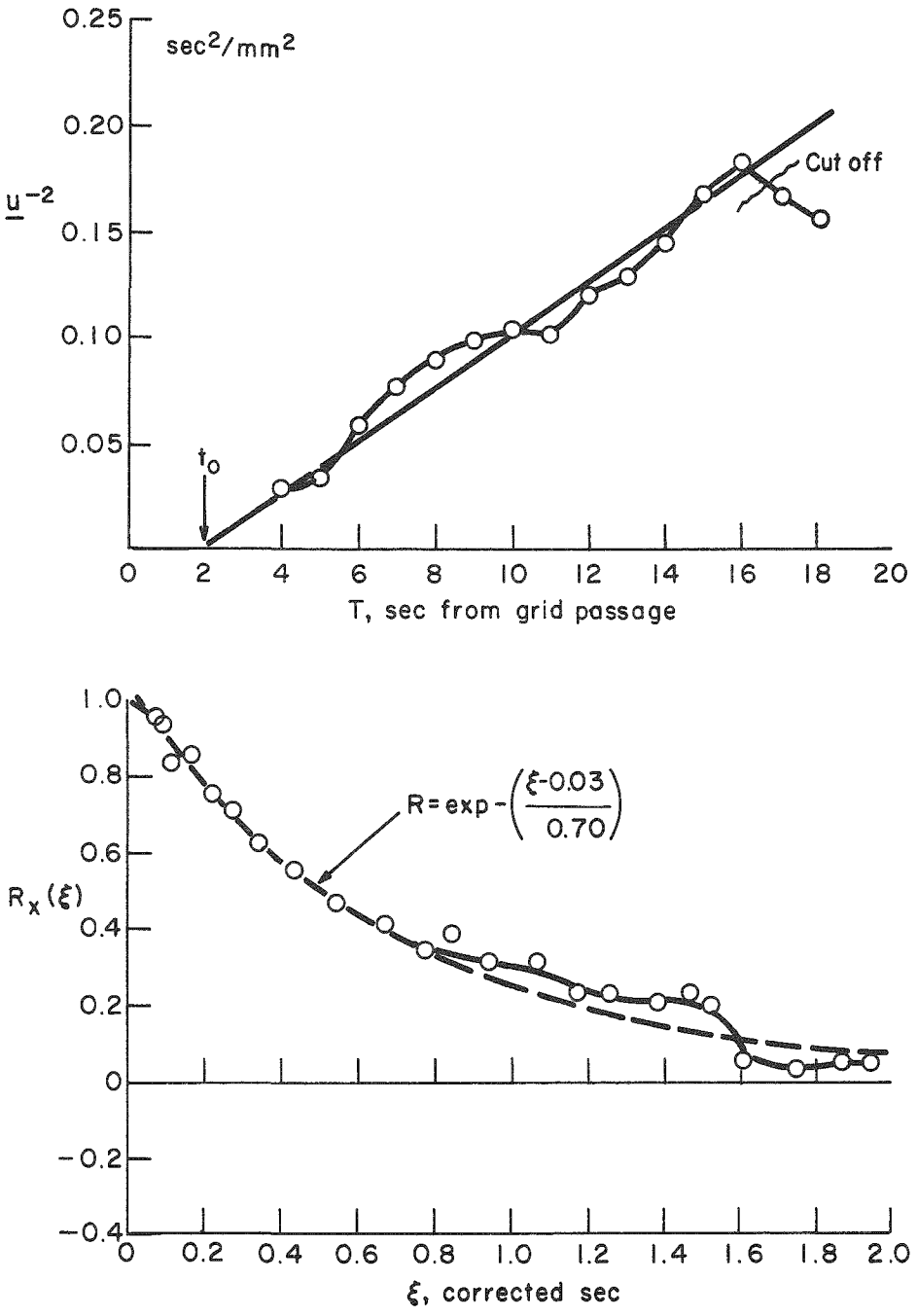

Fig. 27.--Decay curve and correlogram for experiment VS/25/x.

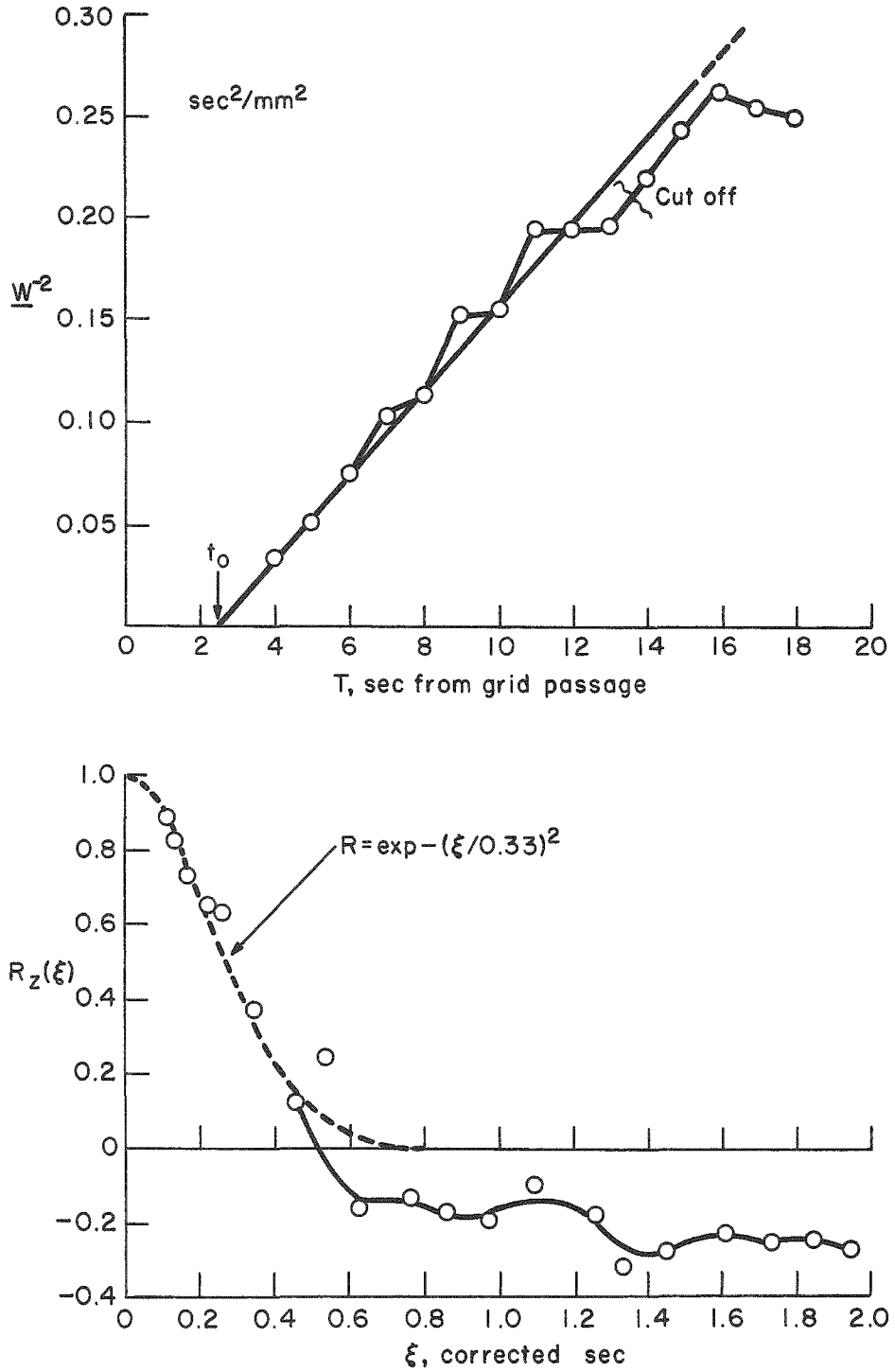

Fig. 28.--Decay curve and correlogram for experiment VS/25/z.

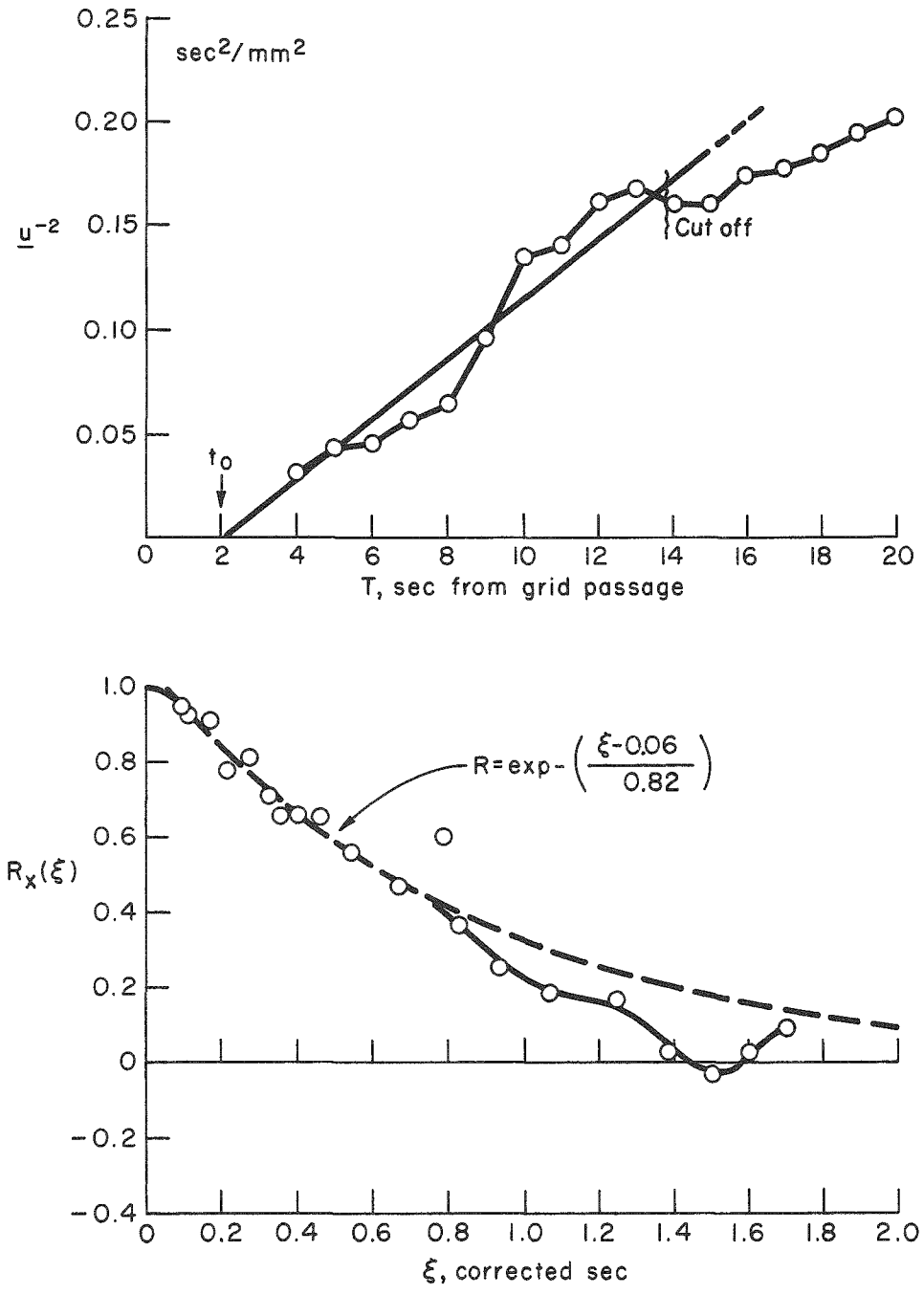

Fig. 29.--Decay curve and correlogram for experiment VS/25/x_y.

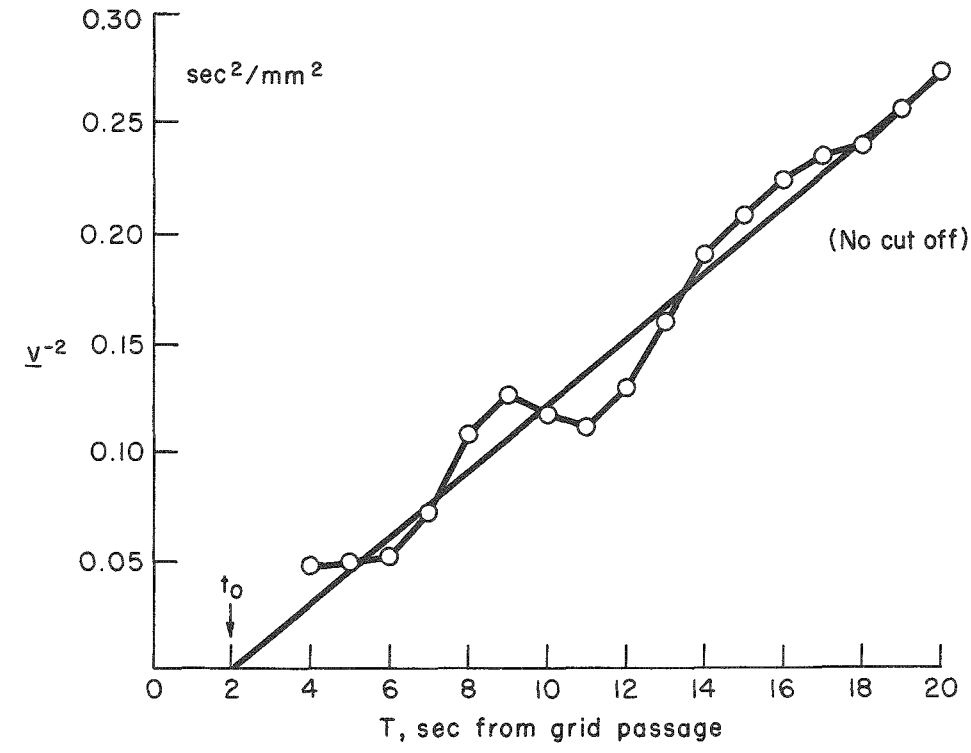

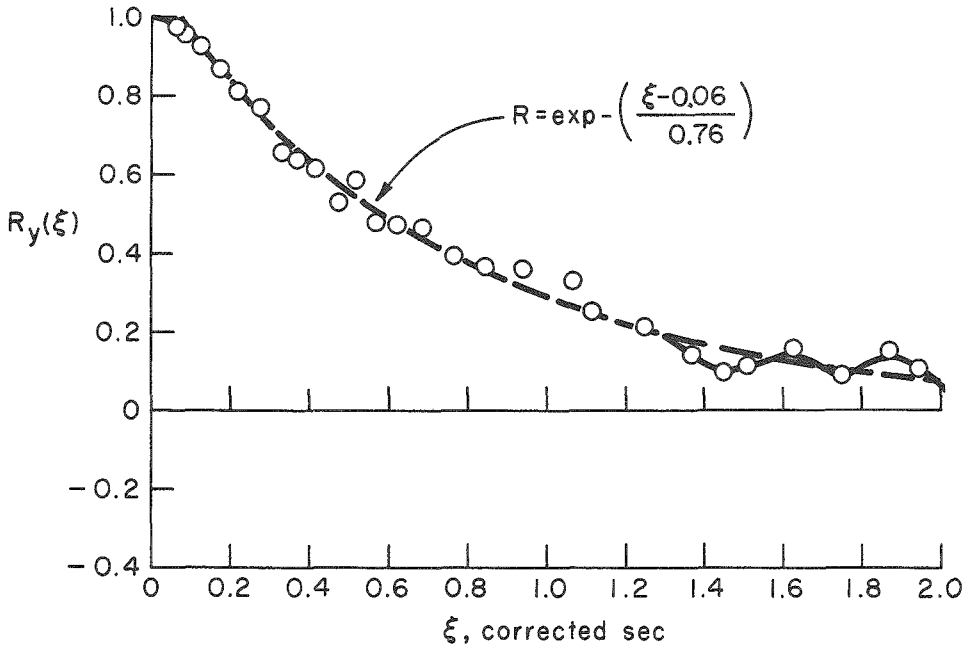

Fig. 30.--Decay curve and correlogram for experiment VS/25/y.

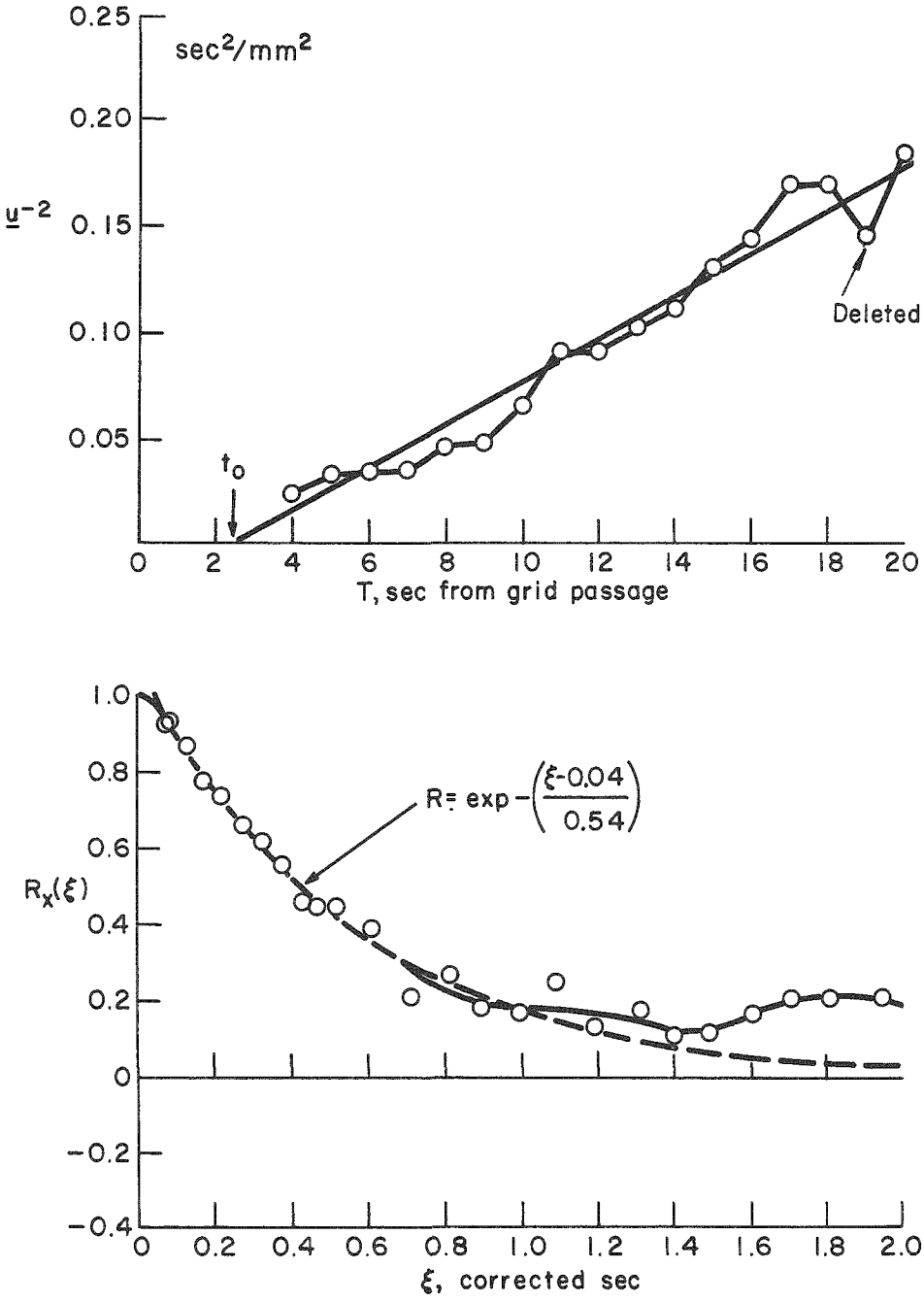

Fig. 31.--Decay curve and correlogram for experiment S/40/x.

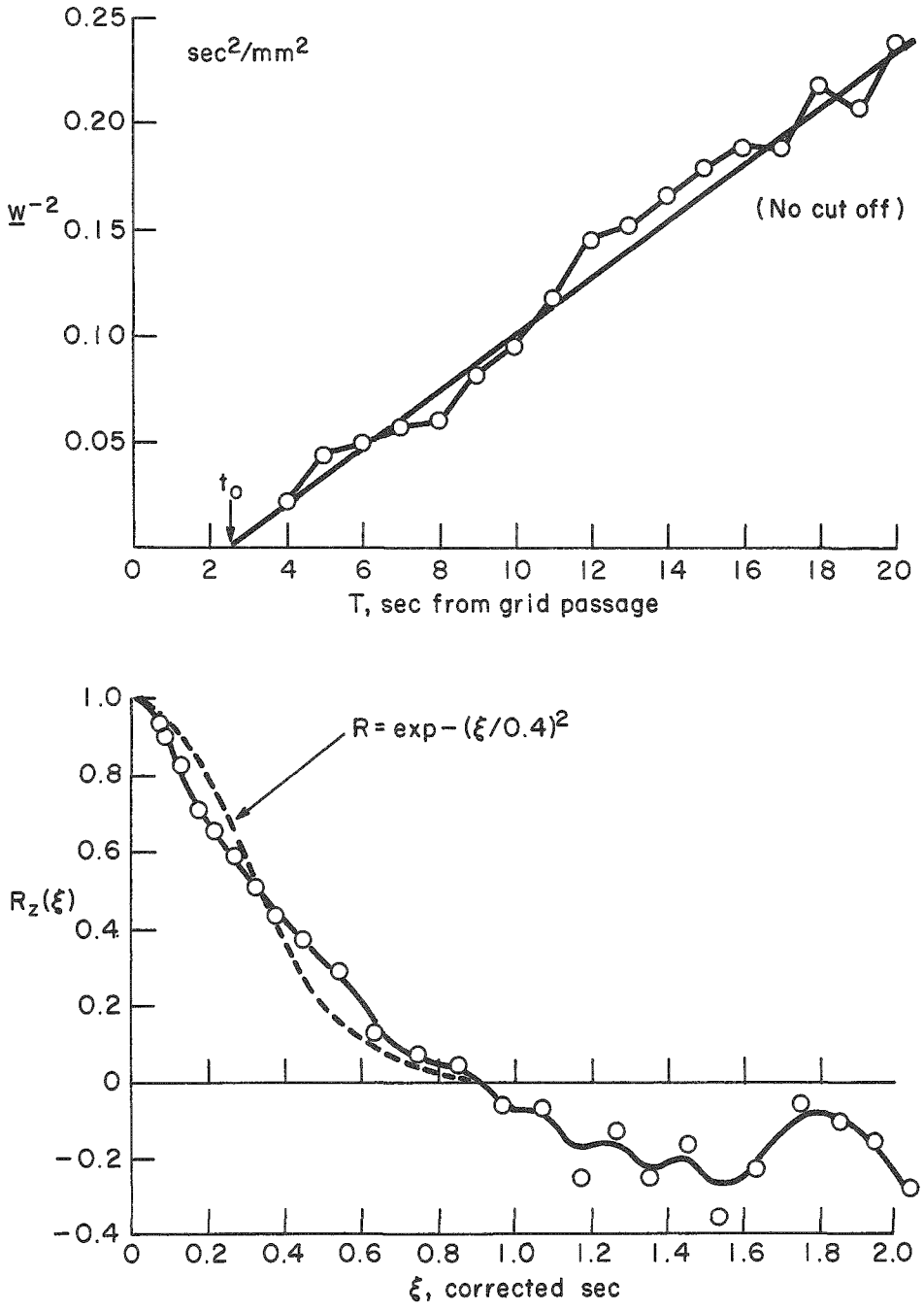

Fig. 32.--Decay curve and correlogram for experiment S/40/z.

varied over a wider range of ±15 per cent, namely (+0.110 ±0.017)°C/cm. The remaining experimental conditions along with the average lapse rates for each case are summarized in Table 8.

TABLE 8.--A summary of experimental conditions and key decay characteristics of the stably stratified experiments

Designator Code, (Fig.)	$d\theta/dz$ (°C/cm)	$Re_g \times 10^{-4}$	Virtual Origin		Data Cut Off
			T(sec)	M	T(sec)
S/12/x, (19)	0.13	0.7	2.5	6	>17
S/12/z, (20)	0.13	0.7	3.5	9	< 5, >17
WS/25/x, (21)	0.03	1.4	2.0	10	>19
WS/25/z, (22)	0.03	1.4	1.5	8	13, 14, >17
S/25/x, (23)	0.12	1.4	2.0	10	>15
S/25/z, (24)	0.12	1.4	2.5	12	12 < T <17
S/25/x_y, (25)	0.16	1.4	2.5	12	>17
S/25/y, (26)	0.16	1.4	1.5	8	none
VS/25/x, (27)	0.30	1.4	2.0	10	>16
VS/25/z, (28)	0.30	1.4	2.5	12	>13
VS/25/x_y, (29)	0.28	1.4	2.0	10	>13
VS/25/y, (30)	0.28	1.4	2.0	10	none
S/40/x, (31)	0.11	2.3	2.5	20	delete 19
S/40/z, (32)	0.11	2.3	2.5	20	none

Under conditions of stable stratification there appeared to be a tendency for the virtual origins of the longitudinal turbulence components to be delayed between 1.0 and 1.5 sec relative to values observed for the same components in neutral experiments. Where t_0 for the x-components of turbulence occurred 1.0 sec after grid passage in three out of four cases with neutral stratification, the introduction of stabilizing density gradients appears to delay the origins of the same components to T = 2.0 or 2.5 sec (cf. Tables 5 and 8). As far as these data indicate, the effect resembles a "threshold response," since in the single weak stable case (WS/25/x) t_0 has already increased to 2.0 sec, while in the two very stable cases (VS/25/x and x_y) t_0 exhibits no further delay. Similar delays in virtual origins of either transverse or vertical components of turbulence were not so well-marked as those

seen in the longitudinal component. As a result, the virtual origins of the two components of turbulence observed in any single experiment tend to be more nearly equal under stably stratified conditions than was the case in neutral conditions.

The effect of increasing Re_g upon the position of the virtual origin relative to the grid appears as it did in the neutral experiments, the combined effects of increased stability and relatively fast flow in experiment S/40/x,z giving a displacement of 20M, the largest observed during the investigation. In the low Re_g range, the long, 3.5-sec delay of the virtual origin of the vertical component again occurs. But under this condition of moderate stability, t_0 for the longitudinal component is delayed 1.5 sec later than that observed in the neutral case; as a result, it precedes the vertical component by only 1.0 sec. Thus, somewhat paradoxically, stable density stratifications decrease the asymmetry observed at low Re_g under neutral conditions. This unexpected influence of stability also appears in the case of moderate Re_g as may be seen in the distribution of turbulent energy components in Table 9.

TABLE 9.--Average turbulence intensities and indices of isotropy observed in the stably stratified experiments; composite N/25/x,y,z data included for purposes of comparison

Designator Code	$d\theta/dz$ (°C/cm)	$Re_g \times 10^{-4}$	Turbulence Intensity (mm^2/sec^2)			Indices of Isotropy	
			$\underline{u}^2$	$\underline{v}^2$	$\underline{w}^2$	$\underline{v}^2/\underline{u}^2$	$\underline{w}^2/\underline{u}^2$
S/12/x,z	0.13	0.7	44		26		0.59
N/25/x,y,z	0.00	1.4	128	88	88	0.69	0.69
WS/25/x,z	0.03	1.4	85		88		1.04
S/25/x,z	0.12	1.4	64		56		0.88
			av: 77				
S/25/x,y	0.16	1.4	90	106		1.18	
VS/25/x,z	0.30	1.4	79		48		0.61
			av: 74				
VS/25/x,y	0.28	1.4	69	66		0.96	
S/40/x,z	0.11	2.2	98		75		0.76

In going from neutral to moderately stable conditions, the vertical, longitudinal isotropy index $\underline{w}^2/\underline{u}^2$ increases from 0.49 to 0.59 at low Re_g, and from 0.69 to 0.88 at the moderate value of Re_g. Comparison of $\underline{u}^2$ at comparable grid Reynolds numbers reveals that, in changing from neutrally stratified conditions to any one of the three strengths of stability, the intensity of the longitudinal turbulence components was sharply reduced. At lower Re_g, increasing stability does not affect the vertical component $\underline{w}^2$ quite so strongly as it does $\underline{u}^2$ (perhaps because it is relatively weak to begin with), hence the tendency toward increased isotropy. At high Re_g (case S/40/x,z), $\underline{u}^2$ and $\underline{w}^2$ are reduced nearly in proportion by the introduction of moderate stability, and the degree of isotropy remains approximately the same as that observed in experiment N/40/x,z ($\underline{w}^2/\underline{u}^2$ = 0.76 as compared with 0.72).

At $Re_g = 1.4 \times 10^4$, Table 9 shows that $\underline{u}^2$ tends to decrease slowly with increasing stability once the initial appearance of weak stability has reduced the turbulence intensity by a third. Thus, $\underline{u}^2$ decreases from 128 to 85 mm^2/sec^2 with a lapse rate increase over isothermal of but 0.03°C/cm; increasing the lapse rate by an additional order of magnitude reduces $\underline{u}^2$ by only an additional 13 per cent. Since the disproportionate initial reduction does not occur in the case of the vertical component of turbulence, the isotropy index $\underline{w}^2/\underline{u}^2$ increases sharply from 0.69 to unity with the introduction of weak stability. With further increase in stability, however, $\underline{w}^2$ decreases as shown in the table, and the energy ratios revert to anisotropic conditions.

The ratio $\underline{v}^2/\underline{u}^2$ in excess of 1.0 obtained in experiment S/25/x,y appears questionable, although the decay curves in this case are exceptionally well-behaved (cf. Figures 25 and 26). The $\underline{v}^2/\underline{u}^2$ ratios for this experiment and for case VS/25/x,y indicate, at any rate, a strong tendency for the preservation of isotropy between the two horizontal components, once the appearance of a slight degree of stability has damped excess energy in the longitudinal component.

Table 10 summarizes the secondary results of the stably stratified experiments. Again, these characteristics of decay-corrected turbulence are discussed in detail later in the chapter, in this case particularly in the section dealing with the influence of fluid stability.

TABLE 10.--Characteristic parameters derived from correlograms of the stably stratified experiments; composite N/25/x,y,z data included for comparison

Designator Code, (Figs.)	Times to Zero (corrected sec)			Lagrangian Scales						Virtual Diffusion Coefficients (cm²/sec)					Pseudomicro-scales (corrected sec)		
				Time (corrected sec)			Length (mm)										
	$\xi_{R_X=0}$	$\xi_{R_Y=0}$	$\xi_{R_Z=0}$	t_x	t_y	t_z	ℓ_x	ℓ_y	ℓ_z	K_y°	K_y°	K_z°	K_y°/K_x°	K_z°/K_y°	λ_y	λ_y	λ_z
S/12/x,z (19, 20)	1.81		1.16	0.70		0.37	4.6		1.9	31.		10.		0.32	0.44		0.31
N/25/x,y,z (13-16)			0.90	0.70*	0.65*	0.39*	7.8	6.1	3.7	88.	57.	34.	0.65	0.39	0.36	0.28	0.26
WS/25/x,z (21, 22)	1.59		1.4	0.56		0.35	5.2		3.3	48.		31.		0.64	0.34		0.26
S/25/x,z (23, 24)	2.0+		0.65	0.67* av: 0.68		0.34	5.4 av: 6.0		2.6	42. av: 52.		19.		0.45	0.41 av: 0.40		0.33
S/25/x,y (25, 26)	1.85	~1.4		0.68*	0.62*		6.5	6.4		61.	66.		1.08		0.39	0.41	
VS/25/x,z (27, 28)	~1.7		0.52	0.73* av: 0.70		0.29	6.5 av: 6.0		2.0	58. av: 52.		14.		0.24	0.29 av: 0.36		0.29
VS/25/x,y (29, 30)	1.45	2.07		0.66	0.76		5.5	6.2		46.	50.		1.09		0.43	0.41	
S/40/x,z (31, 32)			0.91	0.59*		0.37	5.8		3.2	58.		28.		0.48	0.31		0.28

The Unstably Stratified Experiments

The effects of only two degrees of instability at just two grid Reynolds numbers were investigated in the unstably stratified experiments. This limitation was adopted, not only because the range of instability was technically limited by the capacity of the lower heat source, but also because excess heating from below introduced convective motions that could not be removed by simple averaging. The smallest value of Re_g was omitted from this series since the low levels of turbulence produced by the grid moving only 12.5 cm/sec were relatively ineffective in comparison with the convective motions already present; prior to the unstable runs, tracer droplets placed in the tank were observed to move at speeds up to several mm/sec in these circulations.

Lapse rates measured in unstably stratified experiments were found to be very small and quite variable, evidently as the result of continuous overturning taking place within the fluid. Kuo (1961) has

(Text continues on page 111)

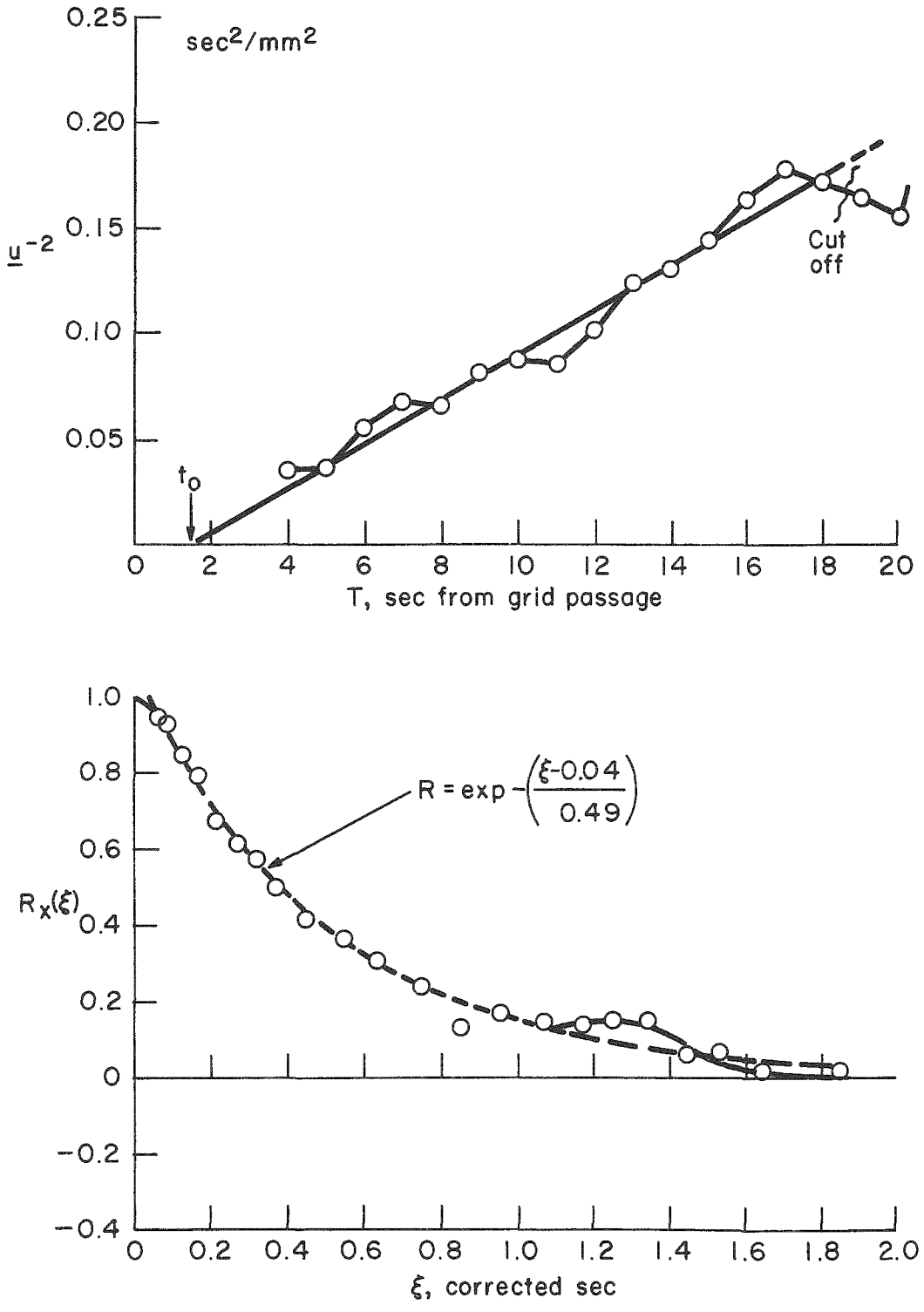

Fig. 33.--Decay curve and correlogram for experiment U/25/x.

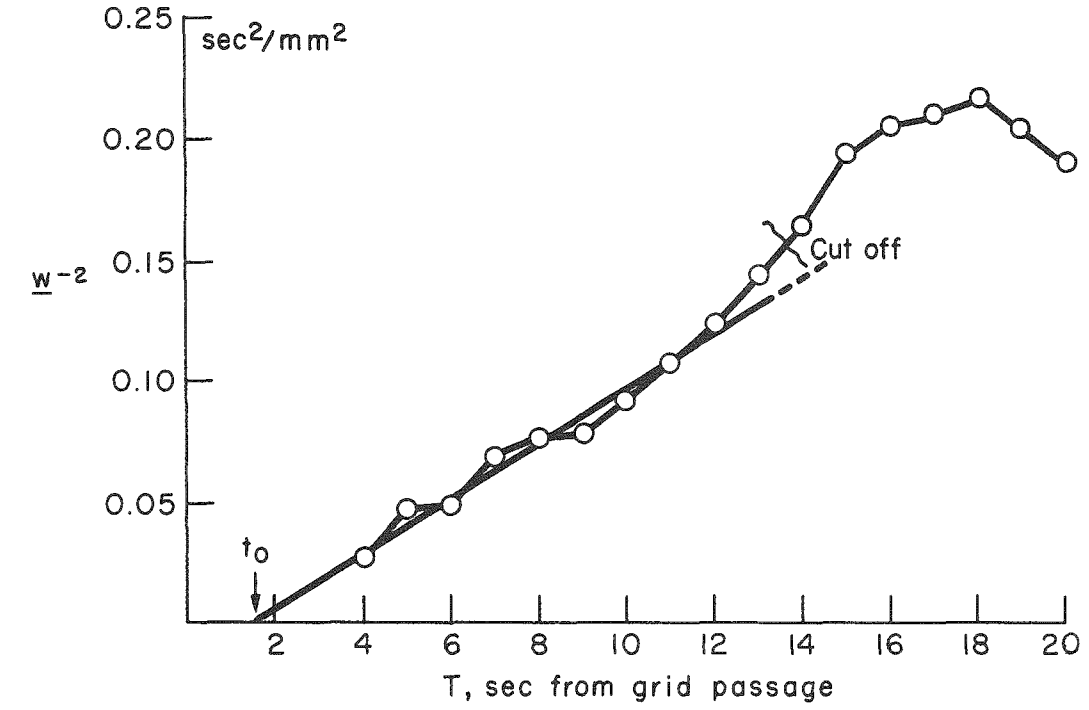

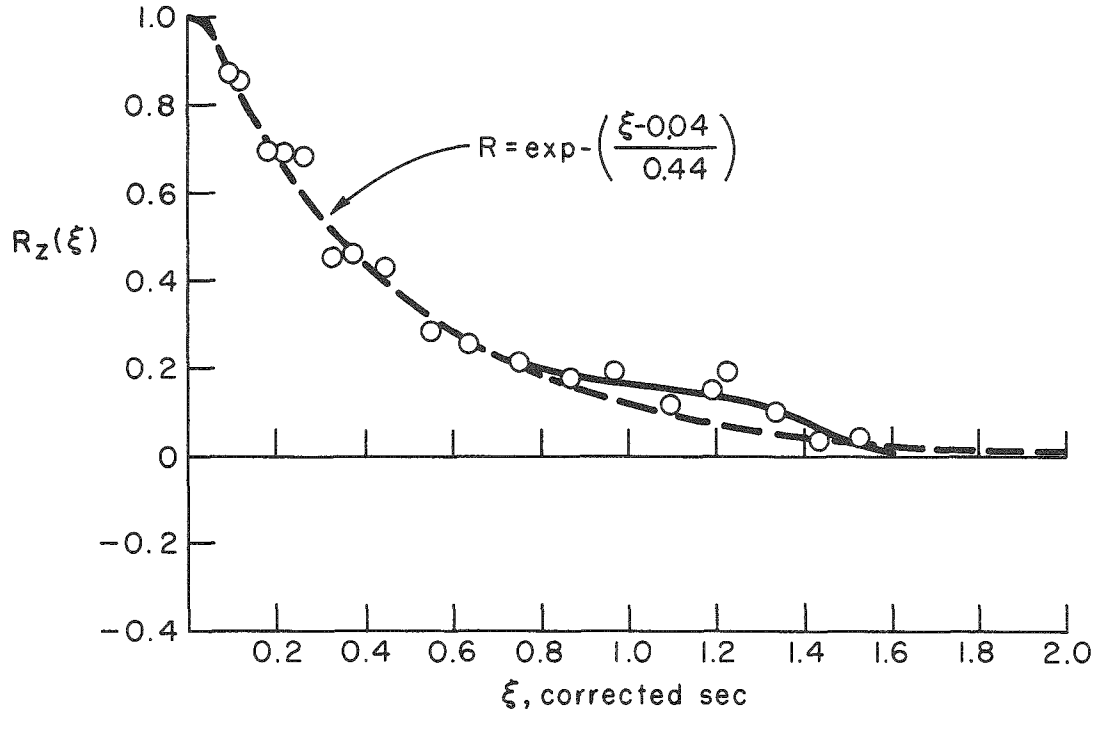

Fig. 34.--Decay curve and correlogram for experiment U/25/z.

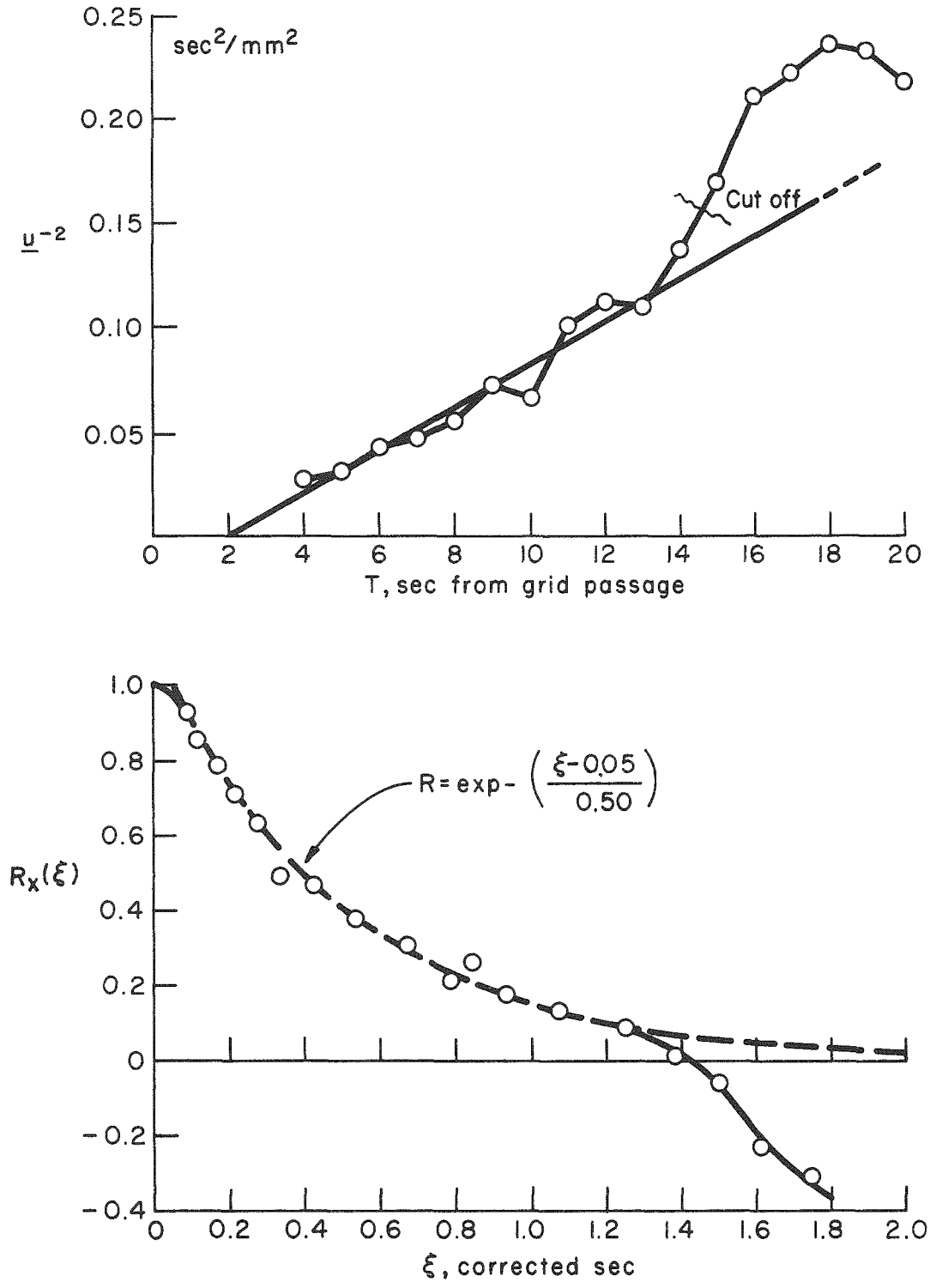

Fig. 35.--Decay curve and correlogram for experiment $U/25/x_y$.

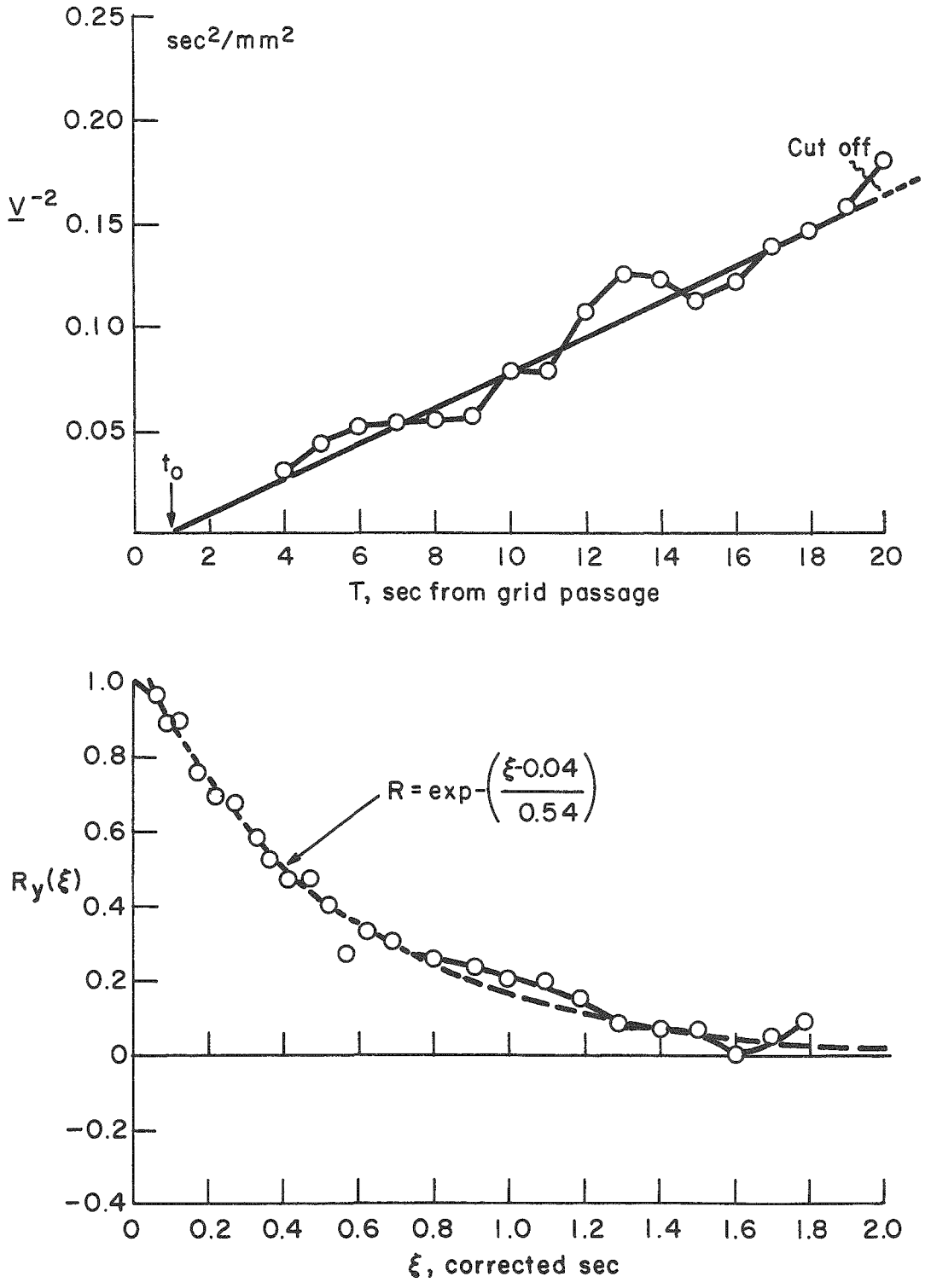

Fig. 36.--Decay curve and correlogram for experiment U/25/y.

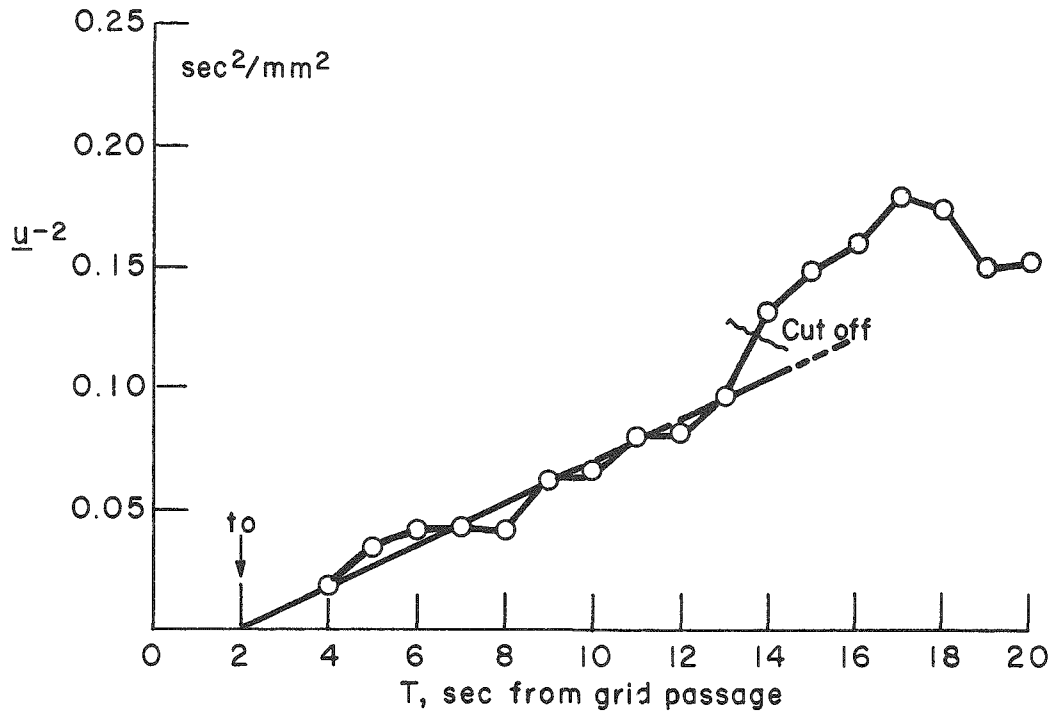

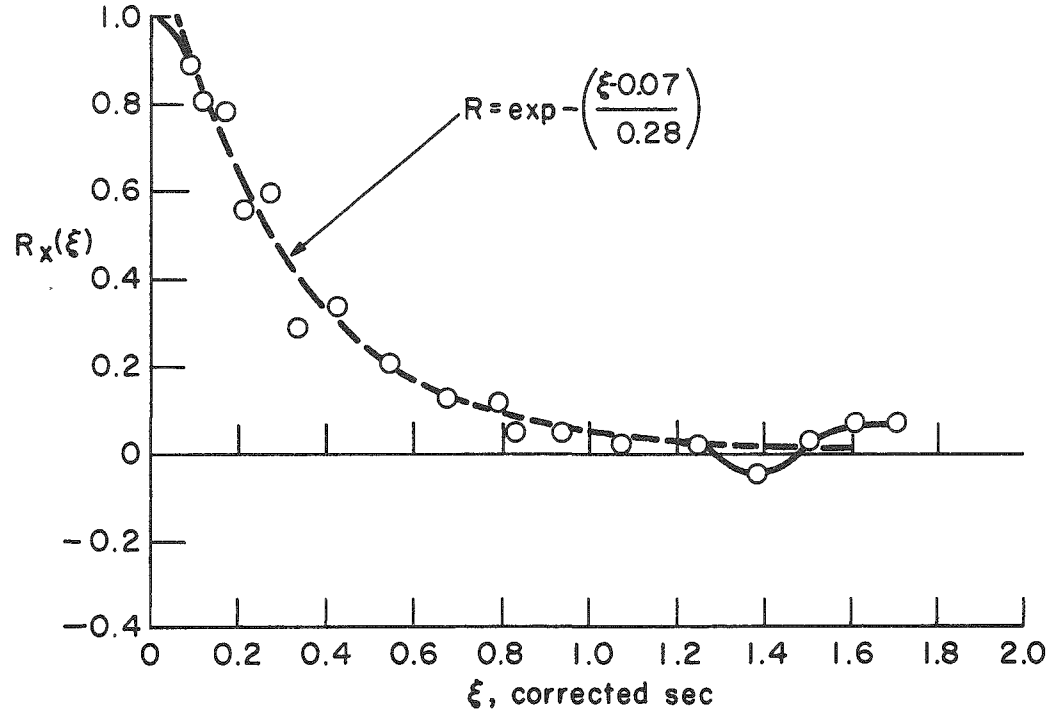

Fig. 37.--Decay curve and correlogram for experiment VU/25/x.

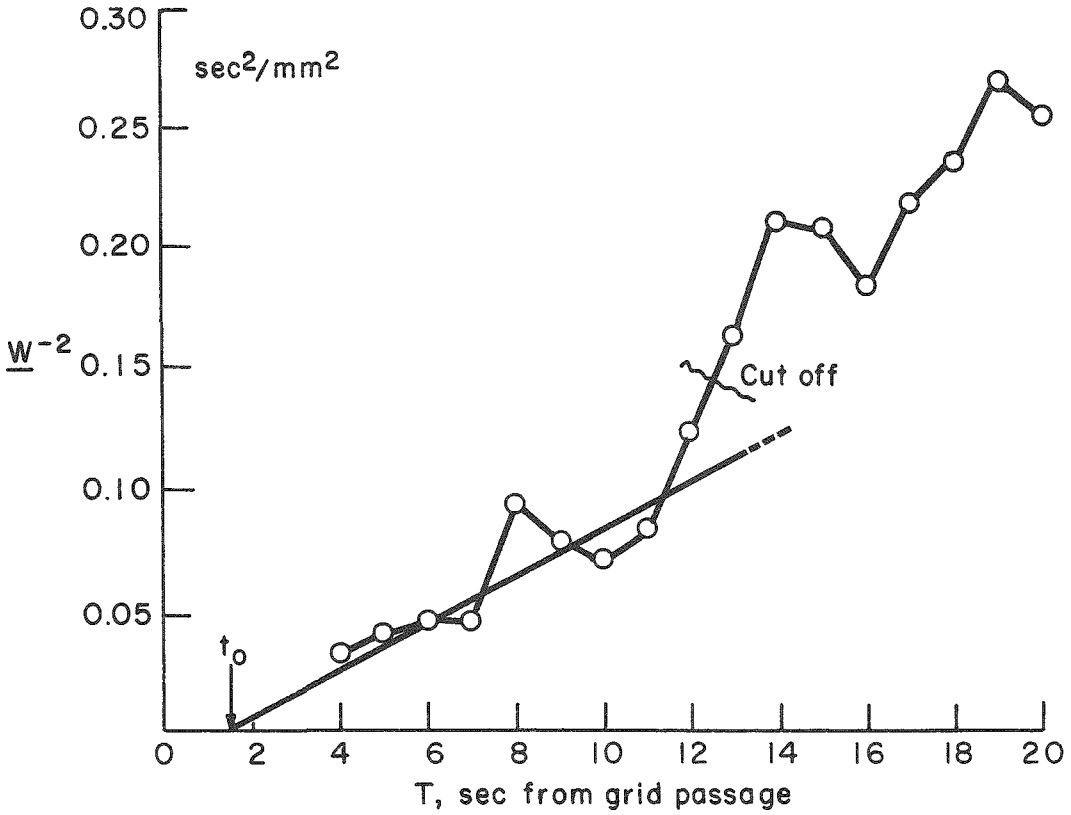

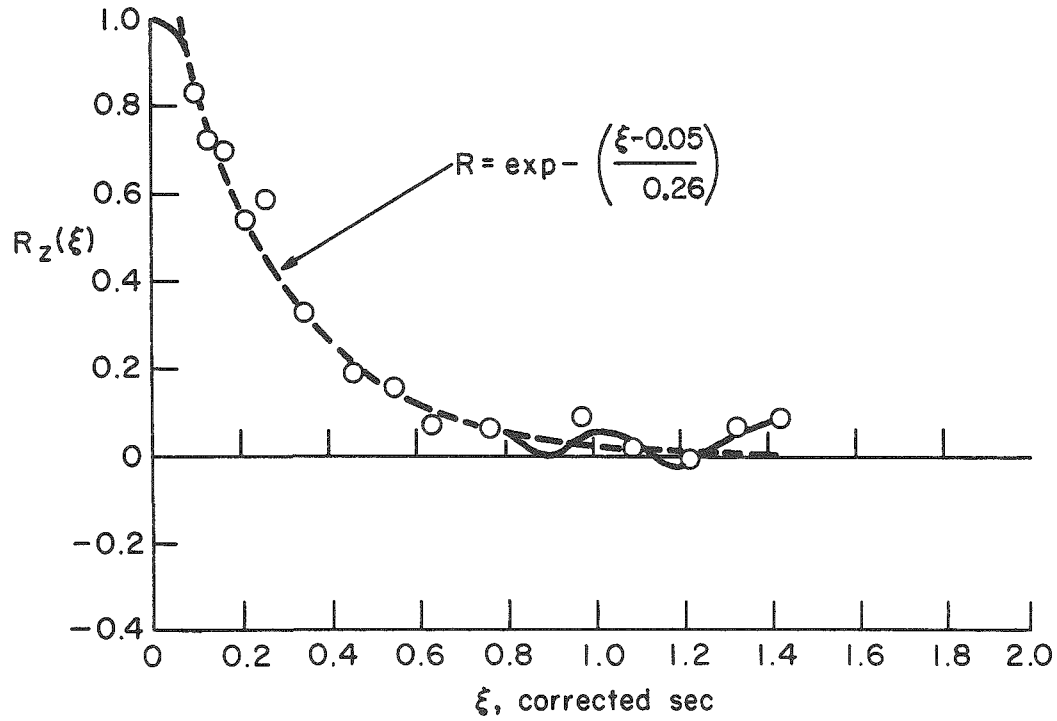

Fig. 38.--Decay curve and correlogram for experiment VU/25/z.

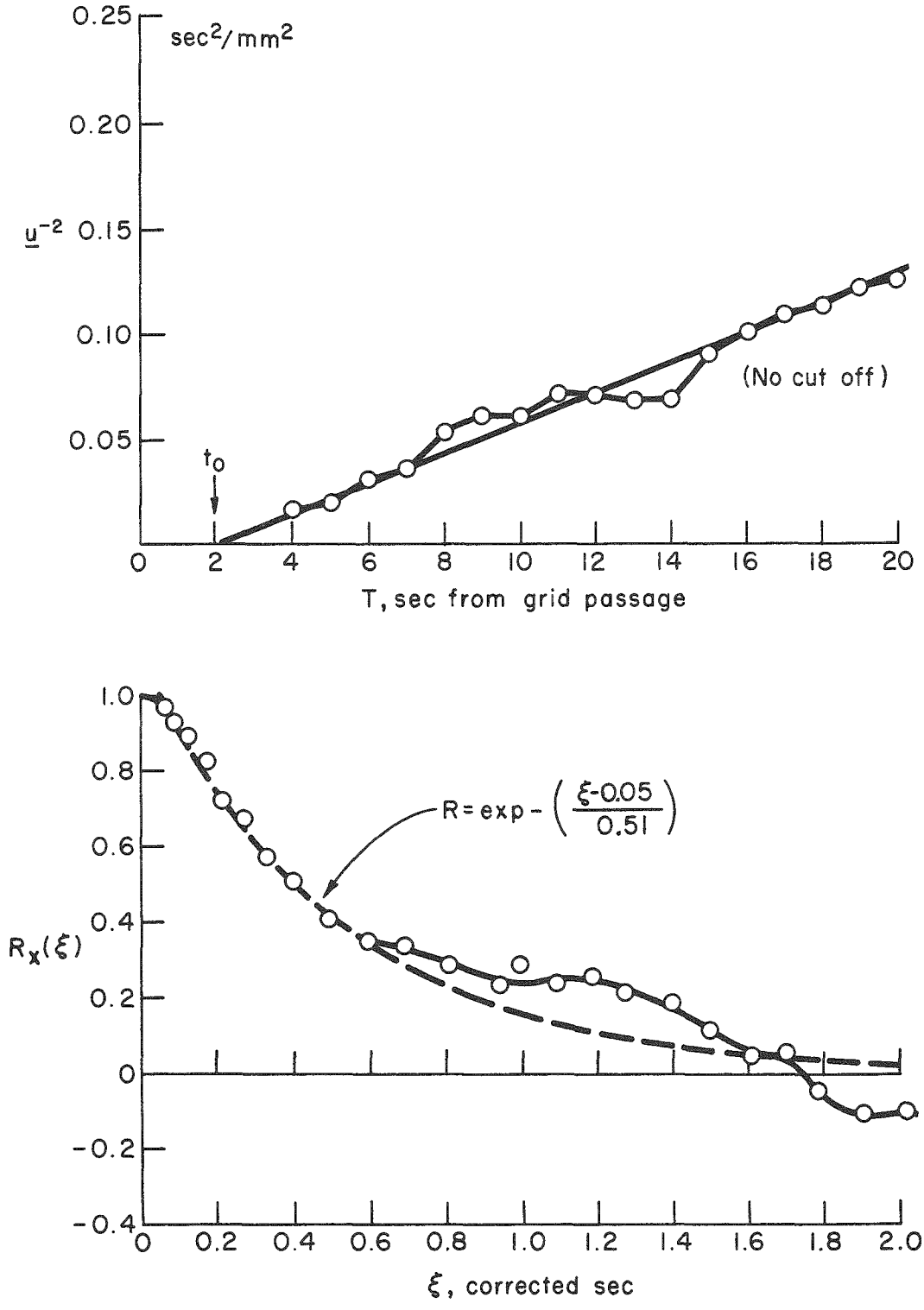

Fig. 39.--Decay curve and correlogram for experiment U/40/x.

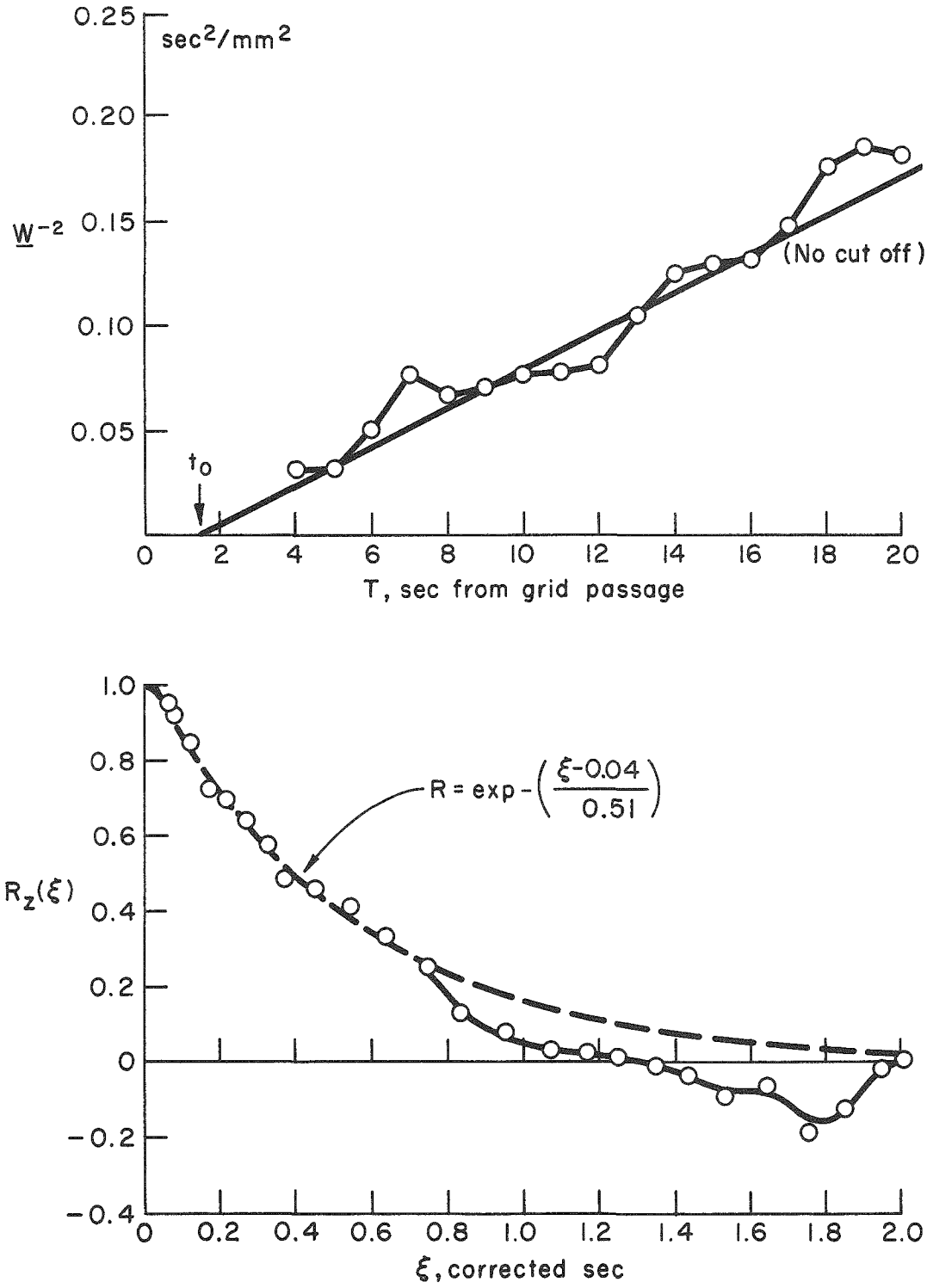

Fig. 40.--Decay curve and correlogram for experiment U/40/z.

shown in a nonlinear, theoretical analysis that once the minimum, critical instability condition necessary to initiate convection has been exceeded, an isothermal region appears in the middle levels of the fluid. When the temperature difference between upper and lower boundary surfaces increases further, this isothermal region grows both upward and downward; consequently, regions of increasingly strong unstable lapse rate become concentrated in increasingly shallow layers immediately adjacent to the boundaries. In this condition, temperature measurements taken across the central regions of the tank (as in these experiments) will show very little in the way of an average vertical temperature gradient, even though the entire body of fluid is in an unstable, supercritically convective state.

A nominally moderate unstable stratification was maintained by placing a moderate voltage across the electrical heaters in the tank base and adjusting the upper heat exchanger until the mean temperature of the water in tank remained constant. With an input of 65 V, this condition was attained when the heat exchanger continuously removed about 500 W. Lapse rates observed during the thirty runs of the three sets of moderately unstable experiments averaged -0.001°C/cm. Increasing the voltage at the base to 100 V required the upper heat exchanger to remove an additional 750 W in order to maintain the average water temperature at a constant value. Under these conditions, the average lapse rate observed during the one "very unstable" experiment approached -0.002°C/cm. Since the relative amounts of energy removed by the upper heat exchanger provide a more representative measure of the relative instabilities than do the lapse rates, these values are listed with the other conditions of the unstably stratified experiments in Table 11.

The influence of grid Reynolds number upon the relative position of t_0 is again apparent in Table 11. At $Re_g = 1.4 \times 10^4$, virtual origins were located at an average of 8 mesh lengths from the grid,

whereas increasing Re_g to 2.2×10^4 moved the virtual origins nearly twice that distance downstream. The proportionately greater energy supplied to the vertical component of turbulence in unstable density distributions appears to eliminate the tendency for its virtual origin to be delayed in comparison with the longitudinal component; whereas in neutral and stable conditions the origins of the z components were usually delayed between 0.5 and 1.0 sec relative to those of the x components, Table 11 shows these circumstances to have been reversed by the introduction of thermal instability, t_0 for the vertical component preceding that of the longitudinal component in two out of three cases.

TABLE 11.--A summary of the experimental conditions and key decay characteristics of the unstably stratified experiments

Designator Code, (Fig.)	Heat Removed (W)	$Re_g \times 10^{-4}$	Virtual Origin		Data Cut Off T(sec)
			T(sec)	M	
U/25/x, (33)	425	1.4	1.5	8	>18
U/25/z, (34)	425	1.4	1.5	8	>13
U/25/x, (35)	540	1.4	2.0	10	>14
U/25/y, (36)	540	1.4	1.0	5	>19
VU/25/x, (37)	1270	1.4	2.0	10	>13
VU/25/z, (38)	1270	1.4	1.5	8	>12
U/40/x, (39)	495	2.2	2.0	16	None
U/40/z, (40)	495	2.2	1.5	12	None

The last column of Table 11 shows that departures from first-period decay rates frequently required data observed late in the unstable experiments to be discarded. On occasion the disturbed regions of decay resembled those previously associated with surge-induced jets in the neutral and stable experiments (see Chapter V), since they began around T = 12 and showed some tendency to return to normal approximately 6 sec later (cf. Figures 34 and 37). In other cases, changes in the decay rate also appeared late in the experiment (e.g., Figures 35 and 38). There is a tendency for these later distortions to occur when the mean-square turbulence fluctuation is observed

to fall below approximately 2.5 mm/sec (i.e., $1/\underline{u}_K^2 \gtrsim 0.16$ sec^2/mm^2 in the decay plots). Since this approximates the order of the velocities observed in thermal eddies prior to grid passage, it seems probable that this final departure from the linear decay law only becomes significant after grid-generated turbulent fluctuations have decayed to the magnitude of the approximately steady-state, thermal motions. Note that in the cases of high grid Reynolds number of Figures 39 and 40, where $\underline{u}_K$ did not fall below 2.5 mm/sec during the experiment, marked final departures were not observed.

Table 12 lists the average, decay-corrected turbulence intensities obtained in the unstably stratified experiments. Note that departure of the lapse rate from isothermal has again effected significant reductions in the intensity of the longitudinal component $\underline{u}^2$; it will be recalled that this was also found to be the case with the first appearance of stable stratification. Once more, a sharp increase in the index of isotropy results, $\underline{w}^2/\underline{u}^2$ increasing from 0.69 to 0.94 with the onset of instability, it having attained a similar value near unity (i.e., 1.04) with the initial introduction of a stable density gradient. These effects of stability changes upon isotropy are discussed further in a later section.

TABLE 12.--Average turbulence intensities and indices of isotropy observed in the unstably stratified experiments; composite N/25/x,y,z data included for purposes of comparison

Designator Code	Heat Removed (W)	$Re_g \times 10^{-4}$	Turbulence Intensity (mm^2/sec^2)			Indices of Isotropy	
			$\underline{u}^2$	$\underline{v}^2$	$\underline{w}^2$	$\underline{v}^2/\underline{u}^2$	$\underline{w}^2/\underline{u}^2$
N/25/x,y,z	0	1.4	128	88	88	0.69	0.69
U/25/x,z	425	1.4	94		88		0.94
U/25/x,y	540	1.4	98	116		1.18	
VU/25/x,z	1270	1.4	117		103		0.88
U/40/x,z	495	2.2	139		108		0.78

Otherwise, Table 12 shows the usual increase in turbulence intensity with grid Reynolds number and the expected tendency toward isotropic conditions with the additional mixing contributed by thermal instability. In the last section of the table, increase of the grid Reynolds number under conditions of relatively weak instability seems to have reversed the trend toward isotropy established at lower Re_g. It would appear that increased levels of mechanical turbulence generated by the faster-moving grid were able to generate departures from isotropy that were too great for the relatively weak thermal mixing to overcome. In fact, $\underline{w}^2/\underline{u}^2 \approx 0.75$ seems to be characteristic of all stability conditions when Re_g attains the highest value used in the investigation.

Table 13 lists the various characteristic parameters of the decay-corrected turbulence fields derived from the correlograms of the unstable experiments. Several difficulties arise in the interpretation of these results; for one, the large asymmetries present in the neutral case make it difficult to detect effects solely due to a change from neutral to unstable conditions. The same problem is present in the interpretation of the results of the stable experiments; but those data cover a wider range of nonisothermal conditions, and stability-dependent trends in the behaviour of the various parameters can be detected without depending too strongly upon the neutral case. These points are among those discussed below in a subsequent section summarizing gravitational stability effects.

TABLE 13.--Characteristic parameters derived from correlograms of the unstably stratified experiments; composite N/25/x,y,z data included for comparison

Designator Code, (Figs.)	Times to Zero (corrected sec)			Lagrangian Scales						Virtual Diffusion Coefficients (mm^2/sec)					Pseudomicro-scales (corrected sec)		
				Time (corrected sec)			Length (mm)										
	$\xi_{R_X=0}$	$\xi_{R_y=0}$	$\xi_{R_Z=0}$	$\mathcal{t}_x$	$\mathcal{t}_y$	τ_z	ℓ_x	ℓ_y	ℓ_z	K_X°	K_y	K_Z°	K_y°/K_X°	K_Z°/K_X°	λ_x	λ_y	λ_z
N/25/x,y,z (13-16)			0.90	0.70"	0.65"	0.39"	7.8	6.1	3.7	88.	57.	34.	0.65	0.39	0.36	0.28	0.26
U/25/x,z (33, 34)	1.80		~1.6	0.52		0.48"	5.0		4.5	49.		42.		0.86	0.28		0.27
U/25/x,y (35, 36)	1.42	~1.6		0.50	0.56		5.0	6.0		49.	65.		1.33		0.32	0.29	
VU/25/x,z (37, 38)	~1.3		~1.2	0.36"		0.30"	3.9		3.0	37.		31.		0.83	0.27		0.21
U/40/x,z (39, 40)	1.74		1.28	0.56"		0.56"	6.6		5.8	78.		60.		0.78	0.33		0.27

Comparison with Water-tunnel Results

The results of the neutrally stratified towing-tank runs compare favourably with those obtained under somewhat similar experimental conditions in a water tunnel by Vanoni and Brooks (1955). It is to be recalled, however, that in the latter investigation an entirely different solution to the problem of utilizing data was obtained from decaying turbulence fields. Vanoni and Brooks used only one velocity product from each of a number of trajectories; for each estimate $R_k(\xi_1)$, velocity samples were taken at times $+\xi_1/2$ and $-\xi_1/2$ measured from a central time that was approximately the same for all trajectories, the method being designed to keep the effects of decay uniform for all $R_k(\xi)$ determinations.

Grids of three different mesh lengths in a flow of constant velocity defined grid Reynolds numbers for the water-tunnel investigation very similar to those used in the towing channel. Table 14 lists the results obtained in these two studies in the form of the times required for $R_k(\xi)$ to fall to zero. Limitations imposed by fast flow relative to the camera in Vanoni and Brooks' experiments prevented the observation of lag times longer than ξ = 1.7 "corrected" seconds ("corrected" in the sense that their method of analysis also determined pairs of lagged products in a manner not intended by the usual definition of ξ).

TABLE 14.--A comparison of times to zero observed in the neutrally stratified towing channel with those found in a water tunnel by Vanoni and Brooks; scales of corrected time in the two experiments are not necessarily the same

Water Tunnel			Towing Channel		
$Re_g \times 10^{-4}$	(corrected sec)		$Re_g \times 10^{-4}$ (Figs.)	(corrected sec)	
	$\xi_{R_x=0}$	$\xi_{R_z=0}$		$\xi_{R_x=0}$	$\xi_{R_z=0}$
0.7	1.90	0.80	0.7 (11, 12)	1.4+	1.22
1.3	1.85	unknown	1.4 (15, 16)	2.0+	0.90
2.7	1.50	1.31	2.2 (17, 18)	1.26	1.15

The two water-tunnel entries in the table larger than 1.7 sec were obtained by linear extrapolation, while the "unknown" value did not fall below R = 0.25. In the towing channel results, the entry 2.0+ refers to case $N/25/x_y$, Figure 15, in which $R_k(\hat{\xi})$ was not observed to fall below 0.10.

The results of these two different investigations cannot, of course, be compared in close detail. Not only were entirely different decay-correction procedures employed, but also Vanoni and Brooks averaged tracer velocities over periods of only 1/60 and 4/60 sec, whereas in the current experiments intervals a full second in duration were used. Further, Vanoni and Brooks centered their decay corrected data about points 100M, 50M, and 25M downstream from the grid for the low, moderate, and high values of Re_g listed in Table 14. These distances correspond to a grid time T ≈ 2.5 sec with the constant flow velocity (50 cm/sec) and the three grid mesh sizes used. In the towing tank, on the other hand, data were taken over an entire range of grid distances between 10 and 100M, the Batchelor decay corrections restoring the observed fluctuations to the approximate intensity and scale of turbulence characteristic of decay time t = 1. Since the virtual origins were observed from 1 to 3 sec after grid passage, the corrected towing tank observations correspond to grid times T from 2 to 4 sec, not a great deal different from the grid time T ≈ 2.5 appropriate to the water-tunnel results.

The fairly close agreement in the magnitude of the times required for the correlograms observed in the two different experiments to fall to zero (if not entirely fortuitous) indicates that the limited spectral sensitivity of the methods of observation employed in the current investigation did not obscure the principal features of the autocorrelation function. The corrected time scales of the two experiments, although not precisely the same, appear to refer their respective results to corrected fields of turbulence similarly located relative to the grids; in other words, correlograms obtained in the two

experiments derive from fields of turbulence corrected to roughly similar states of decay. However, it is difficult to completely assess the comparative effects of the two methods of decay correction; therefore, the separate results obtained should probably not be subject to more than a general comparison of trends within the individual experimental records.

In this regard, note that both experiments find longitudinal, vertical asymmetry: $\xi_{R_{x=0}} > \xi_{R_{z=0}}$ in 5 of the 6 cases in Table 14. The water-tunnel results also show $\xi_{R_{x=0}}$ to decrease with increasing Re_g. Although this does not appear clearly in the times to zero listed for the towing channel, this particular trend may have been obscured by uncorrected mean-flow effects. As will be discussed later, a tendency for the longitudinal component of the Lagrangian scale time to decrease with increasing Re_g is observed in the towing channel in both neutral and stable stratifications. The trend in $\xi_{R_{x=0}}$ observed in the water-tunnel supports this result.

The principal difference between the correlograms determined by the two experiments lies in the smaller radii of curvature of $R_k(\xi)$ near $\xi = 0$ observed in the water tunnel. Five of the six curves given by Vanoni and Brooks tend to remain either exponential or linear well into the region of small ξ, showing little or no tendency to round off near $\xi = 0$. This indication of relatively small microscale can be attributed to the short averaging periods used to determine velocity fluctuations in the water-tunnel experiments, a procedure which enabled the observations of Vanoni and Brooks to extend into significantly higher frequencies than did those of the current investigation. However, it is significant that this difference in procedure does not appear to have affected any other features of correlograms characteristic of the range of grid Reynolds numbers common to both experiments.

Observed Departures from Isotropy

A strong tendency for a significantly larger proportion of the fluctuation energy to appear in the longitudinal component of turbulence occurs under conditions of neutral stratification at all three values of the grid Reynolds number, as can be seen in Table 15. At the intermediate value of Re_g, however, the introduction of either weak stability or weak instability virtually restores the field to isotropy. Stronger stability at the same moderate Re_g tends to distort the field to the anisotropic condition once more, evidently as a result of the selective reduction of the vertical component as negative buoyancy becomes more effective; in Table 9, $\underline{w}^2$ can be seen to decrease steadily with increasing stability. When the stability remains at the same moderate value ($d\theta/dz$ = 0.13°C/cm), increased mixing associated with increasing Re_g initially encourages isotropy; but once Re_g attains the highest value used in the experiments, the index of isotropy falls to ~0.75, a value that appears to be largely independent of the stability condition. It would appear that when the level of mechanical turbulence becomes sufficiently strong, the asymmetric influences of rectangular grid and channel cross section dominate weaker effects favouring isotropy brought about by the changes in gravitational stability.

TABLE 15.--Variation of the vertical, longitudinal isotropy index with lapse rate and grid Reynolds number; results of Vanoni and Brooks included for comparison

$Re_g \times 10^{-4}$	$d\theta/dz$ (°C/cm)						V. and B.
	-0.002	-0.001	0.00	0.03	0.13	0.30	~0.00
0.7			0.49		0.59		0.74
1.4	0.88	0.94	0.61	1.04	0.88	0.61	0.81
2.2		0.78	0.72		0.76		1.12

The possibility that structural asymmetries in the apparatus contribute to the observed departures from isotropy in the neutral case is suggested by the fact that fields of turbulence in the lee of

symmetrical grids in tunnels of symmetrical cross section are generally found to be approximately isotropic, provided Re_g is sufficiently high. Values of Re_g used in the current experiments, though relatively small, are large enough to have generated closer approaches to the isotropic condition in neutral stratifications than were actually observed. This is indicated by the last column of Table 15, in which $\underline{w}^2/\underline{u}^2$ values computed from observations taken by Vanoni and Brooks in a symmetrical, 12 by 12-in. water tunnel at very similar values of Re_g (0.7×10^4, 1.3×10^4, and 2.7×10^4) are shown for comparison. Note that values of the $\underline{w}^2/\underline{u}^2$ ratio obtained in the water tunnel are from 30 to 50 per cent higher than those observed in the towing channel under similar conditions.

Confining attention to the moderate value of Re_g, it can be shown that the sharp reduction of $\underline{u}^2$ observed when the neutral density gradient becomes either slightly stable or slightly unstable does not merely result from the comparison of nonisothermal results to a single sample of abnormally high turbulence intensity for the neutrally stratified case. The N/25/x,y,z data listed in Tables 9 and 12 combine the results of two experiments, one photographed from the side (N/25/x,z, Figures 13 and 14) and the other photographed from above (N/25/x,y, Figures 15 and 16). The first of these gave $\underline{u}^2 = 145$ mm^2/sec^2, whereas $\underline{u}^2 = 110$ mm^2/sec^2 was computed for the second experiment. Further, in the neutrally stratified experiment of the two-dimensional jet studies described in the Appendix, the average, decay-corrected $\underline{u}^2$ was found to be 154 mm^2/sec^2. These high values compare with 85 mm^2/sec^2 obtained in the weak stable stratification (WS/25/x, Figure 21) and with 94 and 98 mm^2/sec^2 obtained in the two sets of runs carried out in weak unstable stratifications (U/25/x,x_y, Figures 33 and 35). Thus, it would appear that at the low and moderate Re_g values, the asymmetric cross section of the apparatus effects maximum departures from isotropy specifically in the neutrally stratified condition.

At the largest value of Re_g used in the experiments, stability changes in the range of these experiments no longer exert a significant effect.

With the onset of instability, the appearance of quasi-isotropic turbulence can be attributed to increased vertical mixing which acts to distribute the turbulent energy more uniformly among all components of the field and to counteract the tendency of the asymmetrical grid and tank cross section to put a larger portion into the longitudinal component. When weak stability first appears, however, a similar restoration of isotropy is difficult to explain.

One possible explanation lies in the "decoupling" effect that one could expect to find associated with reduced vertical mixing in the stable case. Conceivably this could release the central levels of the test section from restrictive influences imposed upon the field of motion by structural asymmetries in the tank and grid. In a manner of speaking, the fluid in the center of the tank cannot sense that the upper and lower boundaries are nearer than those at the side, once vertical mixing has been reduced. As stability increases further, a reduction in $\underline{w}^2/\underline{u}^2$ will eventually appear once the selective damping effects of negative buoyancy become sufficiently important. Very close to the neutral condition, where only small reductions in vertical exchange have occurred, the suggested mechanism requires that the decoupling effect outweigh the effects of selective damping. The observed changes in the vertical component of the virtual diffusion coefficient do not contradict this possibility. In Table 10, the introduction of weak stability can be seen to reduce K_z^* only 13 per cent, from 30 to 26 mm^2/sec; on the other hand, the appearance of weak instability, which is considered to have encouraged isotropy through increased vertical mixing, can be seen in Table 13 to have increased K_z^* by 40 per cent (from 30 to 42 mm^2/sec).

The abrupt changes in the intensity of the longitudinal component of turbulence associated with the departure of the stratification from neutral make it difficult to compare the results of the neutrally

stratified experiments with those conducted under other conditions. However, as will be seen in a later section, the range of stable conditions employed in the experiments enables the influence of stability to be assessed without relying too heavily upon the uncertain results obtained in the neutral case.

Effects of Initial Turbulence Intensity

The effects caused by changing the velocity of the grid and, hence, the grid Reynolds number can be summarized in terms of the observed behaviour of three principal parameters, namely, the average intensity of the decay-corrected turbulence field, $\underline{u}_k^2$, the Lagrangian scale time $\mathcal{t}_k$, and the pseudomicroscale λ_k. As noted previously, the remaining turbulence characteristics depend upon one or more of these three. In Figure 41, nondimensional, relative measures of the vertical and longitudinal components of these parameters, observed under neutral, moderately stable, and moderately unstable conditions, are plotted against the three standard values of the grid Reynolds number. Since observations of the transverse plane were carried out at only one Re_g value, the y components have been omitted from this comparison.

Although, as may be seen in the tables previously given, an increased Re_g generally produced an increase of the absolute intensities of the decay-corrected turbulence fields, Figure 41(a) shows that relative to the energy of the mean flow, the turbulence intensities uniformly decreased. In the figure, $\underline{u}_k^2/\bar{U}^2$ falls most rapidly in the case of the longitudinal component in neutral conditions (N/x), indicating the tendency for increased isotropy with increasing Re_g. At all values of Re_g, the N/x components are the strongest, whereas at any stability condition, the x component is more intense than the z. The difference in energy between the x and z components is greatest in neutral conditions and least in unstable conditions, indicating once more that these conditions are respectively associated with the largest

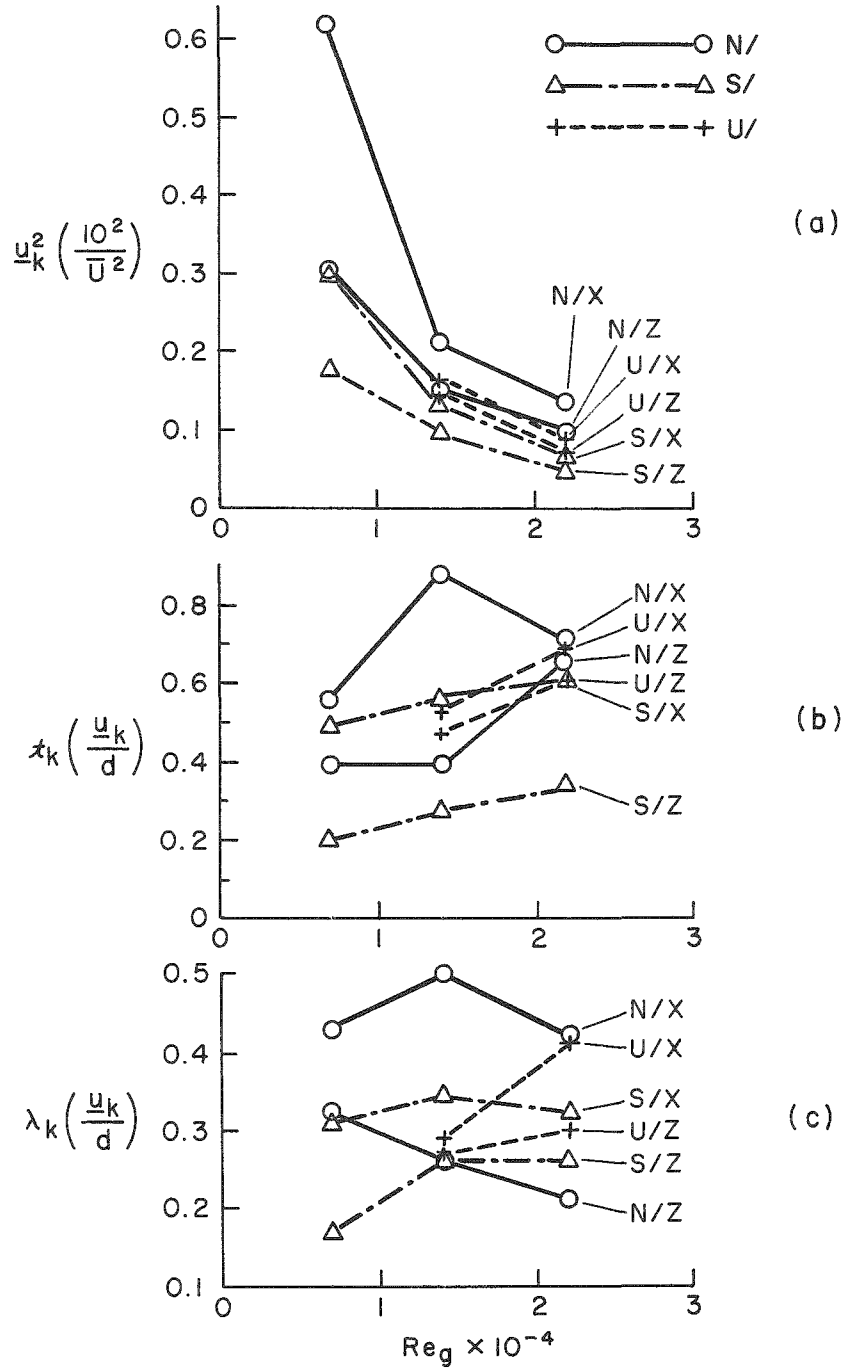

Fig. 41.--A nondimensional presentation of the effects of increasing grid Reynolds number Re_g upon the turbulence intensity $\underline{u}_k^2$, the Lagrangian scale time $\mathcal{t}_k$, and the pseudomicroscale λ_k.

and smallest departures from isotropy. Finally, as might have been expected in view of the effects of buoyancy, the figure shows the vertical component to exhibit the least intensity at each value of Re_g under stable conditions.

From the correlograms it can be seen that the times required for $R_k(\xi)$ to fall to zero varied widely, principally as a result of changes in the general trends of the curves in their later portions that probably resulted from the presence of uncorrected fractions of the mean flow. Lagrangian scale times, as previously noted, are less subject to this source of error since comparatively large changes in the ξ intercept are required to appreciably change the total area under the curve. In cases where the exponential approximation has been used to estimate $\mathcal{t}_{ke}$, errors resulting from uncompensated mean flow are also relatively ineffective, since the exponential function is primarily based upon those portions of the curve that correspond to shorter lag times as discussed in a previous chapter. Thus, even though little systematic behaviour with increasing Re_g can be seen in $\xi_{R=0}$ in either the correlograms or the tables, Figure 41(b) reveals a tendency for nondimensional measures of the Lagrangian time scale to increase with increasing grid Reynolds number. Here $\mathcal{t}_k$ is expressed in terms of a typical eddy period $d/\underline{u}_k$ in which the diameter of a grid bar, d, has been adopted as a representative size for the decay-corrected, root-mean-square fluctuation $\underline{u}_k$.

On the other hand, Table 7 shows a tendency for the absolute magnitudes of both horizontal and the vertical Lagrangian time scales to decrease with increasing Re_g in the neutral condition. This, it will be recalled, parallels the steady decrease in $\xi_{R_x=0}$ observed with increasing Re_g by Vanoni and Brooks in the essentially neutrally stratified flow of the water tunnel (cf. Table 14). Similarly, in the stably stratified case, Table 10 shows that the absolute scale $\mathcal{t}_x$ also decreases with increasing turbulence intensity; however, the vertical

component $\mathcal{t}_z$ remains virtually constant at a comparatively low value. In contrast, the limited data for the unstable condition (see Table 13) shows that both $\mathcal{t}_x$ and $\mathcal{t}_z$ increase as Re_g increases from the moderate to the high value. It is these changes in absolute rather than relative measures of $\mathcal{t}_k$ which can be interpreted in terms of changes in the Lagrangian power spectrum (equation [48] et seq., Chapter V).

In this connection we note first that fields of turbulence generated in the lee of grids at low Re_g are generally found to produce turbulent spectra relatively deficient in small eddies. The effect appears in the tabulated results of the present experiments where the largest absolute measures of pseudomicroscale in Tables 7, 10, and 13 can be seen to be associated with the smallest values of grid Reynolds number; evidently increase of Re_g results in the appearance of proportionally greater amounts of turbulent energy at the high-frequency end of the spectrum. When this energy has been redistributed, the new equilibrium state of the spectrum will show a shift in the frequency n_k of the peak toward that end of the spectrum in which additional energy has been introduced, that is, in this case toward higher frequencies; since $\mathcal{t}_k \propto n_k^{-1}$ (cf. equation [49]), the scale time will decrease.

An increase in n_x from 0 31 to 0.36 cps would account for the observed decrease of $\mathcal{t}_x$ in the neutral condition during the increase of Re_g from the low to the high value. In the case of stable stratification, the observed reduction of $\mathcal{t}_x$ with a similar increase in Re_g corresponds to a smaller shift in n_x from 0.23 to 0.29 cps, the nearly stationary value of $\mathcal{t}_z$ indicates that n_z remains largely unaffected by changes in Re_g in moderately stable conditions.

In the case of unstable stratification, there is some evidence to suggest that the presence of gravitational instability encourages the production of smaller eddies, even at comparatively low values of Re_g. The average of all three components of the pseudomicroscale observed under moderately unstable conditions was only 0.28 corrected second,

whereas in very unstable conditions the average λ_k was an even smaller 0.24 corrected second, the lowest observed for any stability condition (cf. Table 13). This would indicate that significantly smaller eddies were present in the unstable regime.

If such an effect does characterize unstable stratifications, then the possibility arises that moderate increases in Re_g of the order of those employed in the present experiments might not be able to cause significant further increases in the energy of the higher frequencies, for the reason that gravitational instability may have already enabled the small eddy sizes normally involved to be excited at lower Re_g. As a result, the peak in the power spectrum would not be observed to move toward higher frequencies with increasing Re_g; in fact, the peak conceivably could shift toward lower frequencies in response to a general increase in energy over the remainder of the spectrum. In this way, Lagrangian time scales could increase with increasing Re_g, as they seem to have done in Figure 41(b). However, since there is some question concerning the suitability of the decay corrections to unstable stratifications, interpretation of observations obtained under these conditions are not without question.

As can be seen in Tables 7, 10, and 13, absolute measures of the Lagrangian scale lengths ℓ_k largely reflect the monotonic increase in turbulent energy with increasing Re_g; thus, the descending trends in $\mathcal{L}_k$ under neutral and stable conditions are reversed, and ℓ_k generally increases with increase of Re_g. Similarly, the virtual diffusion coefficients K_k^* uniformly increase with increasing Re_g in all stability conditions.

In Table 7, absolute measures of both the longitudinal and vertical pseudomicroscales can be seen to decrease steadily with increasing Re_g in neutral stratifications. This is visibly evident in the correlograms of these cases, for the curvature of the $R_k(\xi)$ curve near $\xi = 0$ markedly increases with increasing Re_g as may be seen by comparing Figures 11, 13, and 17 (cases N/12/x, N/25/x, and N/40/x).

Though less well marked in the relative coordinates of Figure 41(c) (due to the simultaneous reduction in the representative eddy period $d/\underline{u}_k$) the effect is still apparent in the representation of the vertical component N/z.

In stable conditions, the absolute value of the longitudinal pseudomicroscale λ_x decreases in much the same manner. However, the vertical component λ_z remains very nearly stationary at a comparatively low value, a behaviour paralleling that exhibited by the time scale $\mathcal{t}_z$ under similar conditions. The near-constant values of $\mathcal{t}_z$ and λ_z in stable stratifications indicate that, in the vertical component of the field of turbulence, the increased generation of higher frequencies generally associated with increasing Re_g is reduced by the appearance of gravitational stability. Note that this is precisely the reverse of events observed in the unstable condition, where it appears that higher frequencies can be generated at even the lowest experimental value of Re_g.

In the case of unstable stratification, the reversed trend of increasing λ_x, both in the absolute terms of Table 7 and in the relative presentation of Figure 41(c), contrasts with its response to increasing Re_g in either neutral or stable conditions. Along with similarly unusual behaviour on the part of $\mathcal{t}_k$ with increasing Re_g in the unstable cases, this casts further doubt upon the validity of the decay-correction procedures in unstably stratified fluids.

The Effect of Gravitational Stability

Gravitational stability influences are summarized in Figures 42, 43, and 44, in which nondimensional, relative values of a number of parameters observed in experiments at the same moderate grid Reynolds number ($Re_g = 1.4 \times 10^4$) are presented over a range of vertical temperature gradients from -0.001 to +0.30°C/cm. As explained in the last part of Chapter V (equation [50] et seq.), it is convenient to express gravitational fluid stability in terms of the Brunt-Vaisala

parameter N^2, appropriate values of which are listed for the several conditions of the experiment in Table 16. In all but the weak stable case (WS/), the temperature gradients shown are the averages of two essentially identical experiments, differing only in that the one was observed from above the tank while the other was observed from the side.

TABLE 16.--Values of the Brunt-Vaisala parameter N^2 corresponding to temperature gradients observed in the experiments

Designator Code (Figs.)	$d\theta/dz$ (°C/cm)	$N^2 \times 10^3$ (sec^{-2})
U/25/x,y,z (33-36)	-0.001	-0.23
N/25/x,y,z (13-16)	+0.002	+0.46
WS/25/x,z (21, 22)	+0.03	+6.9
S/25/x,y,z (23-26)	+0.14	+32.2
VS/25/x,y,z (27-30)	+0.29	+66.7

For reasons which will become apparent as the discussion proceeds, the results of the nominally very unstable experiments (VU/25/x,z, Figures 39 and 40) are not included in the discussion of stability effects. These were found generally to diverge from trends more or less established by the results of the remaining cases; it seems plausible that the presence of excessively large thermal motions in the very unstable fluid may have been unduly magnified by the decay corrections. Thus it would appear that the use of decay-corrected turbulence fields in unstable regimes should be limited to conditions of very weak temperature gradients.

In Figure 42(a), increasing stability (increasing N^2) can be seen to have caused a general decrease in the relative intensities of all three components of the decay-corrected turbulence fields. The abnormally high value of the longitudinal component $\underline{u}^2$ in conditions of near-neutral stratification (small, positive N^2) is plainly evident, as is the rapid reduction of the same component to the approximate level of

$\underline{w}^2$ with the onset of either negative or larger positive values of N^2. A similar descending trend with increasing stability appears in the transverse component $\underline{v}^2$, but it is more variable than either of the other components. Since there is reason to expect the magnitude of $\underline{v}^2$ to approximate that of $\underline{u}^2$, the value of $\underline{v}^2$ in the moderately stable condition ($N^2M^2/\overline{U}^2 \approx 13 \times 10^{-4}$ in the diagram) would appear to be too high.

An interesting stability dependence of the Lagrangian time scales can be seen in Figure 42(b); nondimensional measures of the horizontal components $\mathcal{t}_x$ and $\mathcal{t}_y$ remain approximately constant or increase slowly with increasing stability, but at the same time the relative value of the vertical component $\mathcal{t}_z$ steadily <u>decreases</u>. The contrasting behaviour of the horizontal and vertical time scales is even more striking when absolute values are compared in Tables 7, 10, and 13; as the stratification becomes increasingly stable, $\mathcal{t}_x$ and $\mathcal{t}_y$ steadily increase from around 0.5 to 0.7 sec or more; over the same stability range, $\mathcal{t}_z$ monotonically decreases from 0.48 to 0.29 sec.

The observed steady increase in the <u>absolute values</u> of horizontal time scales with stability can be interpreted as a steady decrease in the frequency n_k of a peak in the Lagrangian power spectrum, as shown in Chapter V. Equation (49) indicates that n_x, the frequency of the peak in the horizontal spectral component, shifts downward from 0.31 to 0.21 cps as N^2 increases over the full stability range. A nondimensional version of this trend (relative to the representative, decay-corrected eddy frequency $\underline{u}_k/d$) is shown as a solid line in Figure 43. A surprisingly rapid shift toward higher frequencies upon the part of the peak in the vertical component of the Lagrangian power spectrum appears when the vertical time scales are similarly analyzed (see dashed line in Figure 43).

When the stability increases beyond some undetermined moderate value, a significant change takes place in the form of the vertical component of the autocorrelation function. For cases with

values of N^2 near zero (N/25/z and U/25/z, Figures 14 and 34) the exponential form given in equation (38) is clearly appropriate; but, as may be seen in Figures 24 and 28 for cases S/25/z and VS/25/z, the vertical correlograms assume the nature of Gaussian error functions when the stability becomes sufficiently strong; that is,

$$R_z(\xi) \approx \exp - (\xi/a)^2. \tag{51}$$

By integration it can be shown that the scale time for this form of the correlation function becomes

$$\mathscr{t}_{zg} = (a/2)\pi^{1/2}. \tag{52}$$

Further, through cosine transformation and subsequent differentiation of the resulting spectral function to locate the point of zero slope, a procedure analogous to that followed in equations (47) through (49) above, it can be shown that peaks in the vertical component of the Lagrangian power spectra for such cases occur at

$$n_z = [\mathscr{t}_{zg}(8\pi)^{1/2}]^{-1} = [a\pi(2)^{1/2}]^{-1}. \tag{53}$$

These relations were used to determine the two points furthest up and to the right in Figure 43.

Figure 44(a) displays the variation with stability observed in nondimensional measures of the Lagrangian scale lengths ℓ_k and in the virtual diffusion coefficients K_k^* Note that when expressed in terms relative to the representative eddy dimensions d and $\underline{u}_k$, the parameters ℓ_k and K_k^* become identical (cf equations [24] and [25]). The figure shows that the horizontal components $\ell_{x,y}$ and $K_{x,y}^*$ remain approximately constant as the stability increases The vertical components ℓ_z and K_z^*, on the other hand, steadily decrease with increasing stability, since the corresponding components of scale time and turbulence intensity from which they are derived both trend downward.

It should be noted that in nominally very unstable conditions (VU/25/x,z, Table 13) values obtained for these two parameters depart from the trends established in Figure 46(a); ℓ_x = 3.9 mm and

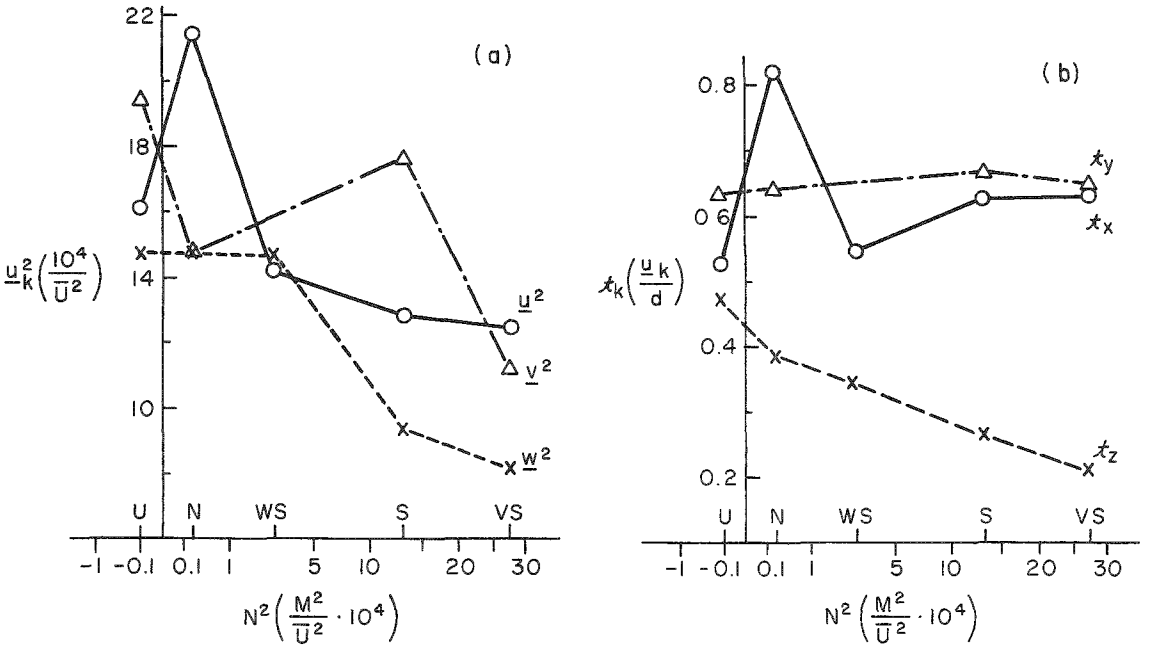

Figure 42.-- A nondimensional presentation of the effects of increasing stability (N^2) upon the turbulence intensity $\underline{u}_k^2$ and the Lagrangian scale time t_k.

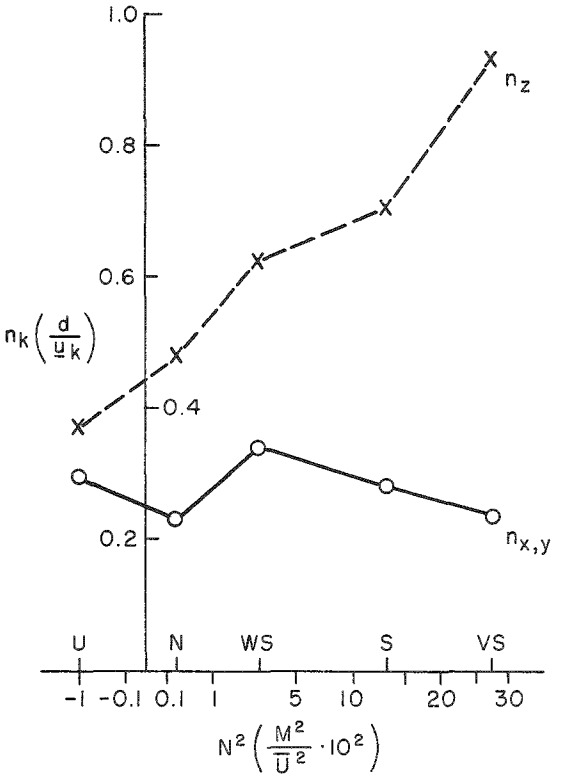

Figure 43.--A nondimensional presentation of the effects of increasing stability (N^2) upon the frequency n_k of the peak in the Lagrangian power spectrum.

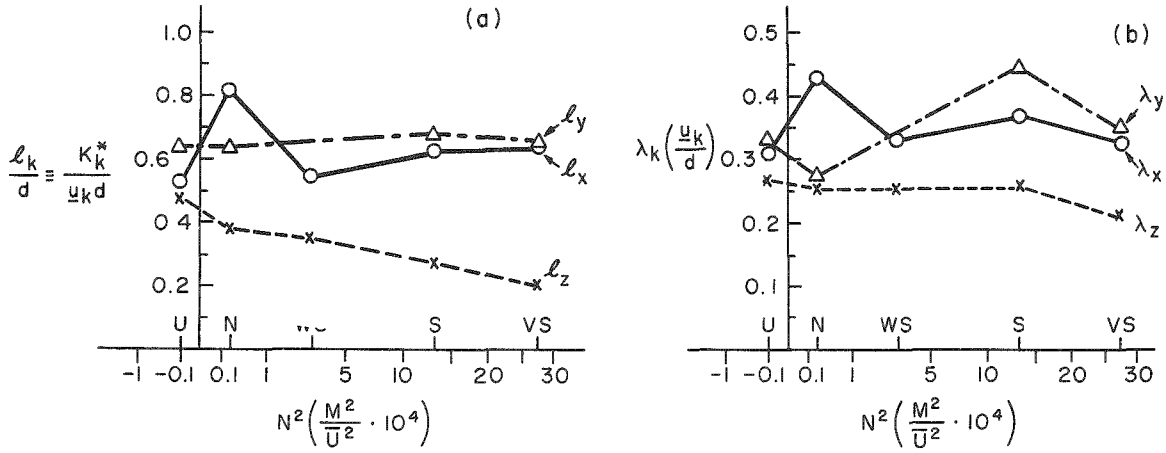

Figure 44.--A nondimensional presentation of the effects of increasing stability (N^2) upon the Lagrangian scale length ℓ_k, the virtual diffusion coefficient K_k^*, and the pseudomicroscale λ_k.

ℓ_z = 3.0 mm observed in this experiment are well below the estimates obtained under conditions of weaker instability in case U/25/x,z. Similarly, the diffusion coefficients K_x^* = 37 mm^2/sec and K_z^* = 31 mm^2/sec are too small; this indication of a decrease in the magnitude of the vertical coefficient of diffusion in a condition of increased instability is one of the principal reasons that the very unstable cases are not considered to have realized decay-corrected fields of turbulence suitable for comparison to the remaining experimental results.

Finally, Figure 44(b) shows that nondimensional measures of the pseudomicroscale (relative to the stability-dependent, characteristic decay-corrected eddy period d/u_k) remain relatively unchanged over the range of N^2. The absolute magnitude of the horizontal components λ_x and λ_y, however, steadily increase with increasing stability, from around 0.3 to as much as 0.4 sec over the experimental range. At the same time, the vertical component λ_z increases only very slightly from 0.27 to 0.29 sec over the same range.

CHAPTER VII

FURTHER INTERPRETATIONS AND CONCLUSIONS

Apart from interpretations peculiar to the nature of the particular model employed in this program of laboratory investigation, the results obtained indicate a number of more general conclusions that can be made relative to the influence exerted by gravitational stability upon the behaviour of the Lagrangian autocorrelation function. But before these are discussed, it is desirable to estimate the scale of motions within the broad spectral range of the atmospheric prototype to which the results of these model experiments might best be expected to correspond. It should be remembered that measurements obtained from the model in this case have evidently been significantly affected by uncompensated mean-flow components and occasionally by failures of the critical assumption upon the nature of homogeneous turbulent decay. At the same time, the prototype atmosphere contains its own peculiar departures from homogeneity, resulting for example from the presence of surface roughness and vertical shear of the horizontal wind, factors for which no analogues were included in the model. Therefore, close similitude between model and prototype cannot be expected, and only general comparisons can be drawn.

General Similarity Considerations

The use of nondimensional equations and the determination of conditions for dynamical similarity has been discussed by Fultz (1951) for the general meteorological problem. It was shown that similitude could be attained by maintaining the magnitude of three dimensionless parameters: a Reynolds number, a Froude number, and a rotational

parameter known as the Rossby number.[1] With regard to the specific problem of atmospheric circulations of relatively small scale, Batchelor (1953) has shown that certain, not unreasonable restrictions upon the field of motion define a class of circulations for which the Richardson number alone is a sufficient criterion for dynamical similarity. Further, these motions can be shown to include those circulations in the lower atmosphere which constitute the principal agents of turbulent mixing during short diffusion times up to 10 min in duration.

Briefly, the discussion proceeds as follows. Initially, consideration is limited to atmospheric motions of scales between 10 km and 10 cm, thus insuring that Coriolis accelerations are negligible; further, it is assumed that the Reynolds number is relatively high, the Mach number small, and that the atmosphere behaves as a perfect gas. Batchelor then writes nondimensional equations of motion, continuity, and energy for the system, and shows that conditions for similarity in this preliminary, general case involve three nondimensional parameters, namely, a Froude number, a pressure coefficient, and the ratio of the specific heats of the fluid medium.

After specifying that the pressure distribution be everywhere similar to that of an "equivalent adiabatic atmosphere" of similar total mass and internal energy, the governing equations are then written in terms of departures of the primary system from this idealized adiabatic condition. This introduces an additional similarity parameter, a density ratio which specifies a characteristic departure of the density from that defined by the equivalent adiabatic atmosphere. It is then required that such departures upon the part of the density of a moving

---

[1]A ratio between characteristic Coriolis and centrifugal accelerations in a rotating system; principally important to the analysis of atmospheric motions on a larger scale, it becomes a controlling factor when circulations approach planetary scale.

fluid parcel remain small; thus, both pressure and density are required to remain closely similar to their counterparts at similar positions in the equivalent adiabatic state. This last enables second-order terms containing the small density departures to be neglected, and Batchelor shows that this simplification enables the Froude number and the density ratio to be combined into a single term with the properties of a Richardson number:

$$\left(\frac{gL}{U^2}\right)\left(\frac{\Delta\rho^*}{\rho^*}\right) = \left(\frac{g}{\rho^*}\ \frac{\Delta\rho^*}{L}\right)\Big/\left(\frac{U}{L}\right)^2 \equiv \mathrm{Ri}.$$

Here L and U are representative scales of length and velocity, ρ^* is the potential density (see equation [55] below), and g is the acceleration of gravity.

At this point the pressure coefficient and the ratio of the specific heats still remain in the continuity equation, specifically in a term describing the change in density of a fluid parcel due to vertical motion. By requiring that the scale of such vertical motion remain small, the continuity equation reduces to $\nabla \cdot u_k = 0$. Thus, under these restrictions, the atmosphere essentially behaves as an incompressible fluid. Further, since this last step eliminates both the pressure coefficient and the ratio of specific heats from the governing equations, the Richardson number remains as the sole criterion for similarity.

The restriction to small-scale vertical motion can be further specified in terms of the vertical distance over which appreciable changes in density occur; that is, the vertical distance over which the velocity of a parcel undergoes appreciable change is required to remain small in comparison with the vertical distance over which density variations are appreciable. Characterizing the latter as a scale height which, for motions near the surface of the earth, is equivalent to the height of the homogeneous (constant-density) atmosphere, Batchelor estimates that conditions for this class of motion will normally be satisfied by atmospheric motions of length scales less than 100 m,

this corresponding to the order of but one per cent of the scale height. In this way it is shown that the Richardson number is a sufficient criterion for similarity relative to the principal scales of eddy motion involved in turbulent diffusion over short time intervals in the atmosphere.

For a truly incompressible fluid, such as the water used in the towing channel experiments, the Richardson number can be written

$$\mathrm{Ri} \equiv g\left(\frac{d\rho}{dz}\right) \Big/ \rho\left(\frac{du}{dz}\right)^2. \tag{54}$$

But in the atmospheric case, even though the field of small-scale motion approximates an incompressible state, the form of Ri which appears in the similarity analysis must still include density terms which refer to standard pressure levels, that is, either the potential density ρ^* or potential temperature θ^* must be used:

$$\rho^* \equiv \rho\left(\frac{p_0}{p}\right)^{\frac{1}{\gamma}}; \qquad \vartheta^* \equiv \theta\left(\frac{p_0}{p}\right)^{\frac{\gamma-1}{\gamma}}. \tag{55}$$

In these expressions, the subscript 0 indicates the value of the reference level and $\gamma \equiv c_p/c_v$ is the ratio of the specific heats at constant pressure and constant volume. Thus, a Richardson number appropriate to the atmosphere can be written as

$$\mathrm{Ri} \equiv g\left(\frac{d\rho^*}{dz}\right) \Big/ \rho^*\left(\frac{du}{dz}\right)^2 = g\left(\frac{d\theta^*}{dz}\right) \Big/ \theta^*\left(\frac{du}{dz}\right)^2. \tag{56}$$

A Richardson Number of Turbulence

One of the difficulties encountered in defining a Richardson number for a specific field of motion lies in the choice of representative scales of velocity and length. Although it often happens that one choice is better than another, the selection is seldom uniquely determined. It is quite possible, as Batchelor points out, for the Richardson

number to have several alternative forms, just as does the Reynolds number. However, in the case of turbulence fields characterized by Lagrangian scales of velocity and length, the choice falls naturally upon the vertical components of these parameters. In fact, the vertical component of the Lagrangian scale length ℓ_z can be seen to represent approximately "the maximum vertical distance over which the velocity can be considered to vary appreciably," while the root-mean-square velocity fluctuation $\underline{u}_z$ constitutes an estimate of the magnitude of that variation.

A Richardson number defined with these representative scales exhibits the desirable characteristics of a bulk parameter since the velocity shears upon which it is based characterize the entire field of motion and do not merely derive from gradients evaluated at a single point; thus the requirement that the Richardson number be recognized as "a reference parameter for the whole flow field, just as is the Reynolds number" (Batchelor, loc. cit.) is fulfilled. Application of Lagrangian turbulent scales in this manner has a close counterpart in the frequent use of Eulerian scales of velocity and length in specifications of "Reynolds numbers of turbulence." Hence, it is appropriate to refer to this form of the Richardson number in similar fashion, that is, as the "Richardson number of turbulence." Thus we define

$$\mathrm{Ri}^* \equiv \frac{g}{\rho}\left(\frac{d\rho}{dz}\right)\Big/\left(\frac{\underline{u}_z}{\ell_z}\right)^2 = \frac{g}{\rho}\left(\frac{d\rho}{dz}\right)\mathcal{t}_z^2, \tag{57}$$

where the last form on the right follows from the Lagrangian scale definitions of equations (23) and (24). Further, from (50) we have $N^2 = (g/\rho)(d\rho/dz)$; therefore (57) can be written as

$$\mathrm{Ri}^* \equiv N^2 \mathcal{t}_z^2. \tag{58}$$

In short, the Richardson number of turbulence as defined here is numerically equal to the square of the Lagrangian scale time reduced to

nondimensional form by the Brunt-Vaisala frequency. This simple result is readily applicable to the atmospheric case, for in the compressible medium we need only write

$$N^2 = \frac{g}{\rho^*}\frac{d\rho^*}{dz} = \frac{g}{\theta^*}\frac{d\theta^*}{dz} \tag{59}$$

and substitute in (58) to obtain the form required for (56) by the Batchelor similarity analysis.

The Similarity Range for the Model

Values of the turbulent Richardson number Ri* appropriate to the five experiments in which $R_z(\xi)$ and hence $\mathcal{L}_z$ were evaluated at the same, moderate value of Re_g (omitting the very unstable case for reasons explained earlier) are presented in Table 17. Although Ri* can be seen to range over two orders of magnitude, we might select the value observed under moderately stable conditions as representative of the more interesting phases of the experiment, there being some question concerning the interpretation of the model results in both neutral and unstable stratifications. Note that this value, $Ri^* \approx 30 \times 10^{-4}$, is approximately the average value obtained in the three stable experiments.

To establish the range of atmospheric conditions most appropriate to model-prototype similarity, vertical Lagrangian time scales that correspond to $Ri^* = 30 \times 10^{-4}$ were computed for a number of

TABLE 17.--Turbulent Richardson numbers attained in the experiments at $Re_g = 1.4 \times 10^4$

Designator Code	$d\theta/dz$ (°C/cm)	$N^2 \times 10^4$ (sec^{-2})	$\mathcal{L}_z$ (corrected sec)	$Ri^* \times 10^4$
U/25/x,z	-0.001	-2.3	0.48	-0.5
N/25/x,z	0.002	+4.6	0.39	+0.7
WS/25/x,z	0.03	+69	0.35	+8.4
S/25/x,z	0.12	+276	0.34	+31.8
VS/25/x,z	0.30	+690	0.29	+58.0

typical atmospheric lapse rates by using equation (59) for N^2 and solving equation (58) for $\mathcal{T}_z$. The results obtained and listed in Table 18 show that, in atmospheric conditions ranging from slight to moderate stability, fields of turbulence characterized by $\mathcal{T}_z$ scales between 2 and 5 sec will be in the similarity range of the model experiments as specified by the criterion $Ri^* \approx 30 \times 10^{-4}$.

TABLE 18.--Lagrangian scale times in the atmosphere corresponding to $Ri^* = 30 \times 10^{-4}$ for several typical lapse rates

Lapse Rate	$d\theta/dz$ (°C/100 m)	$d\theta^*/dz$ (°C/100 m)	$N^2 \times 10^4$ (sec^{-2})	$\mathcal{T}_z$ (sec)
Adiabatic	-1.0	0	0	∞
Standard	-0.65	+0.35	1.2	5.0
Isothermal	0	+1.0	3.3	3.0
Inversion	+1.0	+2.0	6.6	2.1

Vertical time scales of this order appear to be appropriate to fields of turbulence at relatively low levels in stable atmospheres. It is, however, necessary to make this inference indirectly since no direct measurements of this particular parameter seem to have been made. For example, Panofsky and Deland (1959) used Taylor's indirect method to compute estimates of the transverse Lagrangian autocorrelation function from concentration distribution measurements obtained close to the ground during Project Prairie Grass at O'Neill, Nebraska. During daylight hours they found that $R_y(\xi)$ fell to 0.1 at $\xi = 40$ sec; this would indicate that the horizontal scale time was as large as 20 sec in the daytime, unstable condition. On the other hand, $R_y(\xi)$ similarly evaluated at night was found to descend rapidly along a nearly exponential curve, the value of the abscissa at $R = 1/e$ giving the value $\mathcal{T}_y \approx 6$ sec. In view of the relative magnitudes of horizontal and vertical time scales observed to prevail under stable conditions in

the present experiments, it is not unreasonable to estimate a $\mathcal{t}_z$ for the stable atmospheric case in the neighborhood of 3 sec, that is, about half of $\mathcal{t}_y$.

Inoue (1960) has estimated certain characteristics of the behaviour of the vertical autocorrelation function $R_z(\tau)$ more directly, but unfortunately only for an unstable case. From composite photographs of plumes emitted by a factory smoke stack, he found that the vertical dispersive mechanism reached the final, parabolic regime after about 16 sec. Since this represents the time for $R_z(\tau)$ to fall to zero and since the vertical scale time is represented by the area under the correlogram, $\mathcal{t}_z$ can be estimated to have been between, say, one-quarter and one-half as great, that is, something of the order of 4 to 8 sec. Again, the results of the current experiments suggest that under stable conditions, $\mathcal{t}_z$ would have been reduced by as much as one-half; thus, for another estimate of $\mathcal{t}_z$ in stable conditions we obtain a result very similar to that obtained in the previous paragraph, that is, between 2 and 4 sec.

In contrast, Hay and Pasquill (1957) obtained measurements indicating an entirely different order of magnitude for the Lagrangian scales. Concentration distribution measurements taken downstream of a source emitting microscopic tracer particles indicated that $R_z(\tau)$ tended to retain relatively high values for a minute or more, the measurements appearing to indicate that the dispersing particles travelled in nearly straight lines for that length of time. But, as the authors point out, this result can be attributed to the long (30-min) observation periods employed to collect tracer; this procedure allowed the large, slow eddies present at the comparatively high elevations of the experiment to dominate the turbulence statistics, whereas the effects of smaller eddies became obscured by averaging.

Insofar as the turbulent Richardson number can be considered a valid similarity criterion, and to the extent that the methods of decay correction employed in the analysis of the experiments did not

invalidate this similarity, the decay-corrected fields of turbulence used to compute estimates of $R_k(\xi)$ in this investigation can be considered to have been approximately similar to small-scale atmospheric turbulence with the following properties:

a) turbulent Richardson numbers of the order 30×10^{-4};

b) lapse rates between slight and moderate stability ($-0.6 < d\theta/dz < +1.0$ °C/100 m);

c) Lagrangian scale times between 2 and 5 sec. The above conditions most probably obtain

a) over level surfaces at stack height (~50 m) and below, and

b) during short diffusion times (~1 to 10 min) within which turbulence conditions remain quasi-homogeneous.

In all the experiments conducted in unstably stratified conditions, the observed lapse rates were so small ($d\theta/dz = -0.001$°C/cm) and so variable that it is probably not justifiable to base an estimate of Ri* upon them. Moreover, the presence in these experiments of thermal motions that did not decay as rapidly as the turbulent circulations subjected the decay-corrected fields to influences for which there are no counterparts in the prototype atmosphere. Therefore, the unstably stratified regime has not been included in the similarity range.

The limitation to lapse rates no more than moderately stable results from the fact that values of N^2 corresponding to greater stabilities, when taken in combination with vertical time scales of the order of those estimated to occur in stable atmospheres, define greater values of the turbulent Richardson number than those found to characterize the model experiments. There does exist the very real possibility that $\mathcal{K}_z$ falls to very low values in strongly stable stratifications, but to date there are no field observations to support such an argument.

Comparison of Diffusion Coefficients

It is of interest to estimate a scale factor between virtual diffusion coefficients observed in the model and those measured in prototype

atmospheric eddy circulations approximately representative of the similarity range. Atmospheric data suitable to this purpose is provided by the results of a meteorological field investigation conducted in stably stratified flow over level ground at Hanford, Washington (Hilst, 1957). Plumes of smoke released from the 200-ft level of a tower were photographed from above to measure horizontal, cross-wind diffusion rates. In a few experiments, fluorescent tracer particles emitted from the source along with the smoke were collected at a number of points distributed vertically along a balloon cable located 1,000 ft downstream. Results of these simultaneous horizontal and vertical measurements are listed in Table 19.

TABLE 19.--Variances of cross-wind distribution observed in stably stratified flow 1,000 ft from a source at an elevation of 200 ft; after Hilst (1957)

Field Test No.	Standard Ri	$d\theta/dz$ (°C/100 m)	Observed Variance (m^2)		Turbulence $Ri^* \times 10^4$	Diffusion Coeff. (m^2/sec)	
			σ_y^2	σ_z^2		K_y^*	K_z^*
15 A	0.17	2.19	164	169	90	1.64	1.69
13 A	0.54	0.64	85	92	40	0.85	0.92
14 A	1.23	2.64	56	37	100	0.56	0.37

Since all three runs listed in the table took place at similar mean wind velocities, namely, 20 ± 1 ft/sec, the time of diffusion in each case was approximately 50 sec. Values of the horizontal variance (σ_y^2) shown are based upon the assumption of a Gaussian distribution across the visible plume (Hilst's model 1); the vertical variances (σ_z^2) were derived from samples of particle concentration collected along a vertical line through the plume. Horizontal-dispersion measurements were referred to the axis of the plume, which, though meandering horizontally, tended at the same time to remain the same height above the ground. Thus, the effects of horizontal eddies larger than the plume itself were eliminated, and only those of the quasi-homogeneous, smaller-scale eddy circulations were retained. The "Standard

Richardson Number" Ri was derived from wind shears and temperature gradients observed between levels of an instrumented tower and is not to be confused with the turbulence Richardson number Ri*. Estimates of Ri* were based upon N^2 values calculated from the observed lapse rates in combination with an assumed vertical Lagrangian scale $\mathcal{T}_z \approx 3$ sec, in accordance with the previous estimates for a stable atmosphere. Finally, estimates of K_y^* and K_z^* in the last column of Table 19 were derived by assuming the plume at 1,000 ft to be in the final parabolic regime of diffusion. From equation (29) we have

$$K_k^* = \overline{x_k^2}/2T = \sigma_k^2/100, \tag{60}$$

since T = 50 sec.

Comparison of Tables 17 and 19 shows that the turbulent Richardson numbers based upon the assumed value of the Lagrangian scale time, although somewhat larger, are within an order of magnitude of those observed in the model experiments. It is to be noted that the largest value of K_z^* observed by Hilst (test number 15A, 1.69 m^2/sec) compares favourably with observations made by Rider (1954) at a height of 75 cm; those measured in tests 13A and 14A are outside the range of Rider's data, but they do appear to roughly continue the decreasing trend of K_z^* with increasing stability established by Rider's results at lower values of Ri.

For comparison to the model, the value of K_z^* observed in test 13A appears to be the most appropriate, for the moderate degree of stability which prevailed in this case determines an estimated Ri* which closely corresponds to the condition for similarity. Comparing the prototype value $K_z^* = 0.92$ m^2/sec with the average of the estimates observed in the model under moderate and very stable conditions, namely, $K_z^* \approx 16$ mm^2/sec, it can be seen that coefficients of diffusion in the model are scaled down by a factor of the order 10^5. Since the Lagrangian time scales differ by a factor of 10 ($\mathcal{T}_z = 0.3$ corrected

second in the model as compared to $\lambda_z \approx 3.0$ real seconds estimated for the prototype), it follows that the length scales in the model are scaled down by a factor of the order 10^3. Thus, for example, the 15 cm depth of the test section in the model could be considered to correspond to as much as 150 m in a full-scale prototype.

It will be noted that whereas significant differences between K_z^* and K_y^* (or K_x^*) which increased with stability were observed in the model in all stable experiments (cf. Table 10), this form of anisotropy does not appear in the atmospheric measurements of Table 19 until the stability becomes quite pronounced. This indicates a significant difference between the quasi-homogeneous, artificially steady turbulent model and the spatially inhomogeneous but statistically steady lower atmosphere. In the atmosphere, vertical shear of the horizontal wind continuously counteracts the damping effect of a stable density gradient by supplying energy to the vertical component of the turbulence field through the Reynolds stresses. In contrast, negative buoyancy forces which resist vertical fluctuations of grid-produced turbulence in a stably stratified fluid in the model are unopposed by any comparable continuing source of energy. Since the Batchelor corrections can only compensate for normal energy decay, the turbulence field in the model, once subject to the selective damping of stable stratifications, soon becomes anisotropic.

Comparison of Lagrangian and Eulerian Scales

In addition to the general behaviour of $R_k(\xi)$ under various conditions of gravitational stability displayed in the correlograms and summarized in the tables, there are several results of special interest, either because of the manner in which these compare (or contrast) with atmospheric conditions or because they indicate certain features so far unobserved in the atmosphere, but which the model indicates may possibly be present.

The first of these concerns the observed trends with increasing stability exhibited by the Lagrangian time scales; these provide an interesting contrast to the variation of Eulerian length scales with stability recently summarized by Panofsky (1962). Since both the Lagrangian scale of time and the Eulerian scale of length are integrals of their respective correlation functions, their relative magnitudes under similar conditions provide a measure of information with regard to the problem of Lagrangian-Eulerian relationships.

Some inconsistencies have been found in proposed relationships of this kind, and there is evidence to indicate that some of the difficulties arise because the relation between the two systems of reference is stability dependent (Barad, 1959). Results of the current investigation provide indications of further complexities, for whereas the vertical Eulerian and Lagrangian scales are both found to be small and to become smaller with increasing stability, the same cannot be said for the two horizontal components. As may be seen in Table 10 (and to a lesser extent in Figure 42[b]), the longitudinal and transverse components of the Lagrangian time scale both <u>increase</u> as the stability increases. On the other hand, both horizontal components of the Eulerian scale rapidly <u>decrease</u> with increasing stability (cf. Panofsky, <u>loc. cit.</u>, Figure 3). In the unstable condition, horizontal Eulerian scales approach isotropy, as do the Lagrangian scales. But the vertical component of the Lagrangian scale joins in the increased symmetry of the field, increasing over smaller magnitudes of $\mathcal{T}_z$ that prevail in stable and neutral conditions until it nearly equals $\mathcal{T}_x$ and $\mathcal{T}_y$ in the unstable case (see Figure 42 [b]). This is in marked contrast to the vertical Eulerian scale which, although it increases when the instability increases, never approaches the magnitude of the horizontal scales.

Trends with increasing stability exhibited by the absolute magnitudes of both the horizontal and vertical components of the Lagrangian time scale are quite consistent, as can be seen in Table 10. In fact,

except for the value of λ_x measured in near-neutral conditions (where, it will be recalled, the grid-produced fields of turbulence were peculiarly subject to strong departures from isotropy), λ_{xy} and λ_z can each be shown to vary approximately linearly with N, the Brunt-Vaisala stability parameter. This behaviour is clearly evident in Figure 42(b), where plots of λ_k versus an abscissa proportional to the square root of N^2 (i.e., proportional to the absolute value of N) lie nearly along straight lines.

Functional Representation of $R_k(\xi)$

One of the more striking results obtained in this investigation is evidenced by the manner in which these autocorrelation estimates derived from experimental measurements are found to approximate exponential functions closely. In the great majority of cases the calculated points lie along simple negative exponential curves slightly displaced from the origin by the small factor ξ. However, vertical components $R_z(\xi)$ in moderate and strong stable stratifications provide notable exceptions. In the case of relatively weak stable stratification (WS/25/z, Figure 22) the displaced exponential curve still appears adequate; but correlograms derived under more stable conditions (S/12.5/z, Figure 20, S/25/z, Figure 24, and VS/25/z, Figure 28) more closely approximate Gaussian normal error functions of the form $R = \exp-(\xi/a)^2$, in which the constant a is observed to decrease with increasing stability. In case S/25/z, a = 0.40, whereas for VS/25/z, a = 0.33; between these two cases, the Richardson number of turbulence nearly doubles, increasing from 32×10^{-4} to 58×10^{-4}. It will be noted that the correlogram for the case of high Reynolds number (S/40/z) shown in Figure 32 does not fit the Gaussian expression as well as do those for lower Re_g at the same stability, another example in which increased initial turbulence intensity tends to moderate an effect brought about by increased stability.

In consequence of the change in the exponent of e in the functional representation of $R_z(\xi)$ from 1 to 2, the correlogram becomes increasingly convex upward in its early portion and then descends more steeply through regions of medium ξ. This initial tendency for R to remain relatively high becomes more marked as the stability increases. At ξ = 0.2 in Figures 22, 24, and 28, for example, $R_z(\xi)$ can be seen to exhibit values of 0.60 in weak stability, 0.78 in moderate stability, and 0.79 in strong stability.

To the turbulence spectrum, the change in $R_z(\xi)$ from an exponential to a Gaussian form signifies a relative increase in the energy of eddies of medium and moderately small size, while the energy of the largest eddies decreases. The very smallest eddies probably remain relatively unchanged, the small net increase observed in the pseudo-microscale with increasing stability probably and primarily reflecting the increased energy in the moderately small scales.

In terms of plume behaviour, the appearance of a Gaussian form of $R_z(\xi)$ in the more stable stratifications results, of course, in more rapid completion of the transition from the linear to the parabolic diffusion regime. Paradoxically, the change in the shape of the correlogram in regions of small ξ (tending to hold R at higher values) results in the very earliest stages of transition being somewhat delayed (that is, the duration of the initial, conical diffusion regime is actually increased), but this is more than compensated by a subsequent, more rapid decrease in R.

Therefore it appears that when selecting functional forms to represent the Lagrangian autocorrelation function, consideration should be given to normal error functions as once suggested by Frenkiel (1948). More specifically, however, functions of this type appear to be peculiarly appropriate to the vertical component $R_z(\xi)$ in stable stratifications of significant strength. One systematic way of handling this

problem for all three components simultaneously would be to write a general expression of the form

$$R_k(\xi) = \exp-(\xi/a)^b \qquad (61)$$

in which both the Lagrangian scale factor a and the exponent b would be considered stability dependent. By definition, b would remain unity for k = x,y; but for the vertical component k = z, the exponent b would be allowed to increase once the stratification had become stable.

Such an introduction of nonintegral exponents, however, is not likely to be advantageous. The general functions which result in (61) are inconvenient if not intractable, and they would needlessly complicate the analysis of autocorrelation functions. The special cases of integral exponents 1 and 2, on the other hand, define two types of functions which fit a wide variety of correlograms (as evidenced by the results of these experiments), and which have been tabulated over a wide range of independent variables.

Lagrangian-Eulerian Relationships

Eulerian correlation curves evaluated from field data by Panofsky (1962) exhibit the same exponential character found to represent adequately the majority of the Lagrangian correlograms obtained in this investigation. This appears to confirm the widely held impression that correlation functions in the two frames of reference are essentially similar in form and differ only in the scale of their respective independent variables. But, unfortunately for this simple approach, the results of the present investigation also indicate that the vertical component $R_z(\xi)$ undergoes a significant change of form in conditions of moderate stability. Therefore, the concept of a simple scale factor appears to require modification. Of course, there is a possibility that the vertical Eulerian correlation may undergo a similar change of form under similar conditions of stratification. This is certainly a point to be considered for future investigation.

It will also be recalled that the current experimental results indicate that the horizontal Lagrangian time scales increase with increasing stability, whereas in similar circumstances the horizontal Eulerian length scales sharply decrease. This contrasting behaviour also suggests that a simple connection of scale factor between Lagrangian and Eulerian frames will be inadequate; further, it supports the view that whatever relationship does exist must depend strongly upon stability. In addition, in recent studies of fully developed pipe flow Baldwin and Walsh (1961) have found that the relationship is complicated to the extent that the magnitude of the supposed scale factor also depends upon the intensity of turbulence.

Since both gravitational stability and turbulence intensity are experimental variables that are relatively easy to control in the Argonne tank, a comparison of the Lagrangian and Eulerian autocorrelation functions over a range of stabilities and turbulence intensities is one of the experimental programs planned for this facility in the future.

Summary of Principal Results

Results obtained from this program of laboratory investigation can be briefly summarized as follows.

1. The feasibility of employing decay-corrected, homogeneous fields of turbulence produced in the lee of grids as a medium for the study of turbulent diffusion has been shown; in so doing, the usefulness of the decay-correction procedures proposed by Batchelor has been demonstrated.

2. The Brunt-Vaisala stability parameter N^2 has been found to be peculiarly suited to the representation of the effects of gravitational stability in the model since a number of parameters descriptive of the turbulent fields were observed to vary approximately linearly with the absolute magnitude of N.

3. A "Richardson number of turbulence" has been introduced and shown to be a suitable criterion for similarity between the diffusion model in water and an atmospheric prototype; this bulk parameter, a shear-stability ratio defined with Lagrangian scales of turbulent velocity and length, has been shown to be numerically equal to the square of the vertical component of the Lagrangian scale time reduced to nondimensional form by the Brunt-Vaisala frequency.

4. Integrals of the horizontal and vertical autocorrelation functions, the horizontal and vertical Lagrangian scale times, have been found to exhibit opposite behaviour with increasing stability; the horizontal components were found to increase steadily with stability, whereas the vertical component was found to decrease at an equally steady rate.

5. The foregoing behaviour of time scales combined with damping effects exerted by increasing stability upon all components of turbulence approximately alike results in horizontal diffusion coefficients that remain relatively unchanged during conditions of increasing, stability while the vertical diffusion coefficient decreases rapidly.

6. With the exception of the vertical component in stable conditions, Lagrangian autocorrelation functions are found to be represented adequately by exponentials of the approximate form[1] $R_k = \exp-(\xi/a)$, where $a = \mathcal{T}_k$, the Lagrangian scale time. When the stability is sufficiently strong ($N^2 > 10^{-2}$ sec^{-2} in the model experiments), the vertical correlogram assumes the form of the normal error function, $R_z(\xi) = \exp-(\xi/a)^2$, in which the scale time is $\mathcal{T}_z = a(\sqrt{\pi}/2)$.

---

[1] More properly, the correlograms approximately correspond to the compound form given in equation (38).

7. The contrasting variations with stability exhibited by Lagrangian and Eulerian scales indicate that the relationship between these two reference systems will show a pronounced dependence upon stability; what is more, the change in the functional form of $R_z(\xi)$ observed in the stable case suggests that, in this region at least, it may not be possible to regard Lagrangian-Eulerian relations as simple scale factors between their independent variables.

The significance of these laboratory results in the absence of confirmation by atmospheric observations is of course limited. But they do point to a number of areas which full-scale field investigations might well investigate. For example, the paradoxical, divergent behaviour shown by the horizontal and vertical Lagrangian scale times could be studied over a range of stability conditions in the atmosphere by adapting the composite-photographic method of Inoue (1960), using vertical as well as horizontal views to estimate $\mathcal{t}_y$ as well as $\mathcal{t}_z$. It would also be useful to investigate the value of the parameters N^2 and Ri* to full-scale atmospheric-diffusion problems. The turbulent Richardson number, because of its nature as a true bulk parameter, could conceivably contribute to the resolution of difficulties of the kind that frequently arise when standard Richardson numbers are evaluated by means of differences in mean wind between successive levels within a turbulent boundary layer. Average shears defined by turbulent length and velocity scales representative of the field as a whole might be expected to be more relevant to, for example, problems concerning the intensification or decay of turbulence than is the shear of the average horizontal flow measured between arbitrary levels.

APPENDIX

THE MEAN FLOW PROBLEM

Upon closer examination, the problem of the mean circulation in the towing tank was found to be quite a complicated one. Not only was the longitudinal drift found to consist of more than one component, but also its distribution in the vertical was found to vary with the stability of the fluid. Matters were further disturbed by the fact that the appearance of jetlike vertical profiles in the longitudinal drift was observed to be associated with significant departures from the normal process of homogeneous turbulent decay. Although no procedures capable of entirely eliminating these difficulties were found, studies of the mean flow did result in the adoption of certain methods of experiment and analysis which enabled the principal investigation to avoid their worst consequences.

Components of the Mean Flow

Mean-flow circulations set up by a single passage of the grid through fluid initially at rest were found to be made up of two components occurring simultaneously, one oscillatory and the other steady. The oscillatory component, a longitudinal surge with a period between 6.5 and 7.0 sec, was initially excited by the acceleration of the grid from rest and subsequently reflected back into the test section by the far end of the tank. Additional complication of the experiment by a counterpart rarefaction wave was avoided by decelerating the grid only after the last observation had been completed. Both phase and amplitude of the surge component were found to be intimately associated with the starting position and rate of acceleration of the grid; therefore care was taken to reproduce these initial conditions accurately throughout

each experimental series. The grid was always started from a position 125 cm upstream of the center of the test section, and the acceleration from rest was duplicated for each run of a given set by means of the electrically driven speed control.

What appeared to a steady drift through the test section in the direction of grid movement was actually part of a large, toroidal secondary circulation that filled the entire tank. Consisting of a uniform flow down the central axis accompanied by compensating return flows near the boundaries, this circulation was maintained by the drag exerted on the fluid by the grid during its passage along the tank. The strength of the drift component was found to depend not only upon the speed of the grid, but also upon the clearance at its outer edges, that is, upon the unobstructed cross-sectional area available to the return flow. In practice, the grid was centered in the tank by adjusting the mounting struts, clearances at the sides and bottom being kept as uniform as possible. In addition, the depth at which the upper lids floated above the grid was adjusted just before each series of runs.

Another form of "mean flow" important to the determination of the vertical turbulent fluctuations and, eventually, to the computation of $R_z(\xi)$ took the form of slow, steady rise or fall of tracer droplets slightly lighter or heavier than their surroundings. This buoyant component was held to a practical minimum ($< \pm 1.0$ mm/sec) by careful adjustment of tracer mixtures. Except in a few cases, tracer from the same batch was employed for all runs of a particular series. In any case, variation of the buoyant drift from run to run remained quite small; therefore, removal of the average of all vertical displacements observed at similar times by the computer program can be considered to have eliminated this effect adequately.

Thus, every effort was made to insure that the amplitudes and phases of the mean flow components would be uniform from one run to the next in each experimental series.

The Mean Profile

The field of observation in the test section did not include fluid nearer than 10 cm to the upper and lower boundaries of the tank. Although return flows were initially confined to the vicinity of these boundaries, they deepened with time; as a result, these circulations tended to progressively intrude into the field of view in the later stages of the experiment. It was necessary to determine the extent of this effect in order to avoid selecting trajectories whose mean drift components were unduly affected by it. In other words, it was desired that trajectories only be selected from those regions in which the mean drift profile remained approximately flat.

Photographs for profile evaluations were obtained by arranging the camera to take time exposures, one second in length, every other second, while the electronic flash was programmed to fire three times in an asymmetrical sequence (** *) that made it possible to identify both the speed and direction of each tracer droplet (see Figure 7). A rectangular sampling-grid placed over each photograph divided the field of view into 6 levels with 10 sampling squares per level. With the aid of the Benson-Lehner OSCAR, the horizontal displacement of the one tracer droplet image located nearest the center of each square was then measured. Then by averaging the displacements observed at each level, estimates of the profile were obtained.

Figure 45 presents mean profiles obtained in this way with 25-cm/sec grid speeds in neutral, moderately stable, and slightly unstable stratifications. Each profile shown is the mean of five individual profiles obtained from five independent realizations of the turbulence field under identical experimental conditions. With the exception of the uppermost levels in all cases and the intermediate levels in stable conditions, the profiles are fairly flat. On the basis of these results, the selection of trajectories was restricted to the central two-thirds of the field of view, avoiding those levels in which the drift began to

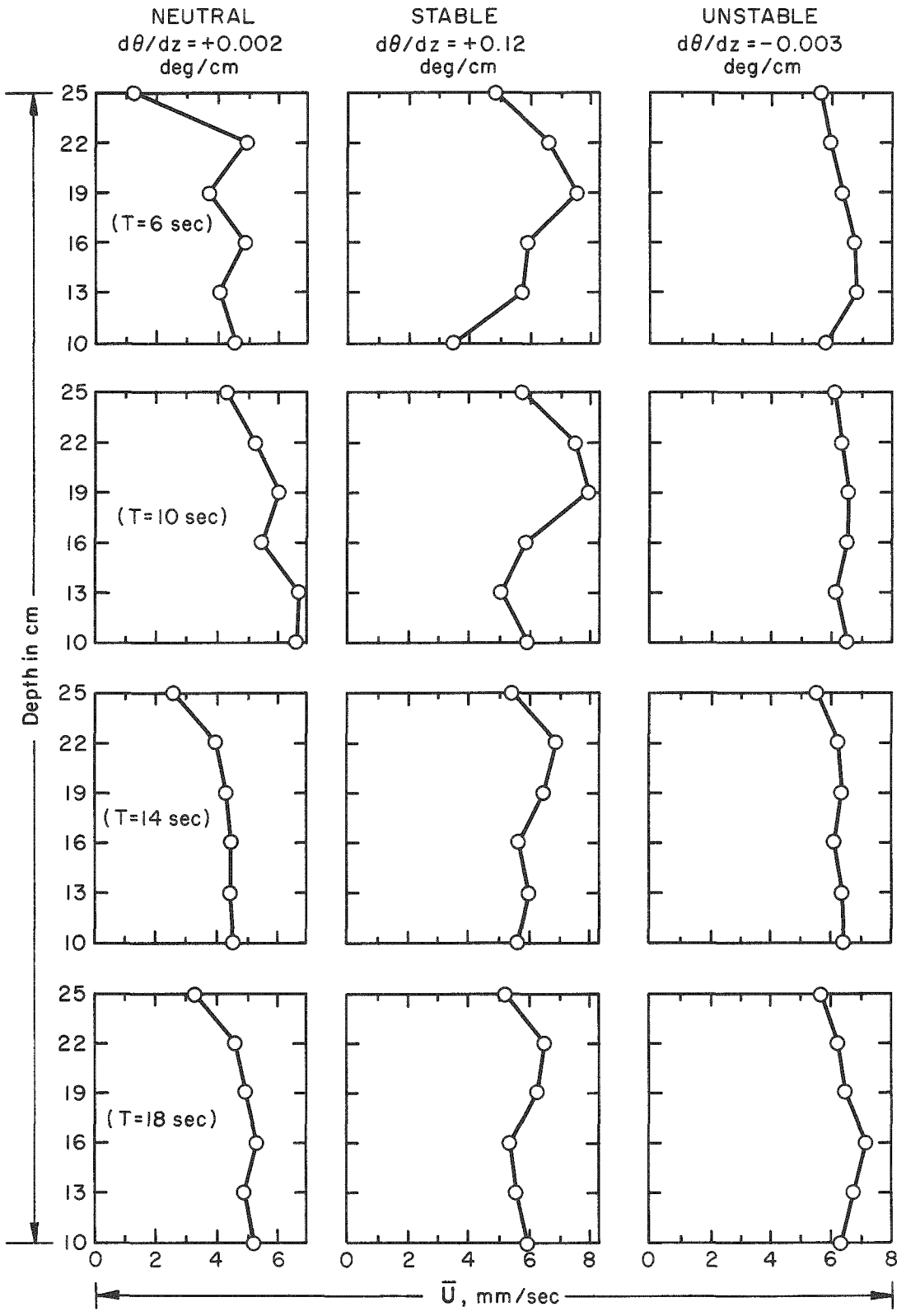

Fig. 45.--Successive vertical profiles of the mean longitudinal drift; grid speed = 25 cm per sec.

change too rapidly with depth late in the experiment. For the stable case, however, the observed early occurrence of marked jet maxima required further investigation.

Two-dimensional Jets in Stable Stratification

The marked tendency for the horizontal momentum to concentrate vertically into two-dimensional (x, z) jets shortly after grid passage posed a special problem. Results of preliminary trajectory measurements and calculations of $R_k(\frac{1}{2})$ indicated that the presence of such velocity maxima in the drift profiles would restrict the extension of the Lagrangian studies into the more strongly stably stratified regimes. To investigate this possibility, a separate study of the jet phenomenon was carried out. A more complete description of the study appears elsewhere (Frenzen, 1960), but a brief summary follows.

Results obtained in the two-dimensional jet investigation are not entirely applicable to the present study, specifically with regard to the time of appearance and the intensity of the jets. This is due to the fact that Lagrangian trajectories were observed in a test section located well upstream for reasons discussed earlier, whereas the observations of the jet study were made in the center of the tank, a region in which the jets both formed more readily and reached greater strengths. However, this study did show that undesirable effects of strong jets could be largely avoided provided the stability was not too strong and provided observations were terminated sufficiently early.

The occurrence of relatively strong two-dimensional jets late in the stable cases appears to be related to the vertical concentration of momentum which theoretical analyses by Long (1959) and Yih (1959) have shown to occur in slow flow of stably stratified fluids when the circulation can be characterized by a critical value $(1/\pi)$ of a ratio of the inertial and gravitational forces known as the internal Froude number:

$$Fi^2 \equiv \frac{\bar{\rho} u^2}{d} \Big/ \bar{\rho} g \left(\frac{\Delta \rho}{\bar{\rho}} \right) = \frac{u^2 \bar{\rho}}{g d \Delta \rho}, \tag{62}$$

where u and d are representative measures of horizontal velocity and vertical length (e.g., the velocity and depth [Δz] of a jet) and the other symbols have their familiar meanings. Note that Fi^2 is the reciprocal of the Richardson number.

In the Argonne tank a bulk measure of Fi was evaluated from successive one-second time-exposure photographs of the same kind employed in the evaluation of the mean profiles (cf. Figure 7). Average vertical shears distributed over the entire field were determined first by measuring the horizontal displacements of tracer droplets located nearest the centers of a 10 by 10, square sampling grid, and then calculating the average difference between displacements observed in squares located one above the other. With the vertical distance between sampling levels representing the dimension d, the average of the local shears gave u/d, whereas the mean temperature and lapse rate determined $\frac{1}{\bar{\rho}} \frac{\Delta \rho}{d}$. These were combined in measures of Fi characteristic of velocity fields produced by the grid in a series of experiments over a range of stable stratifications. As one might expect in decaying turbulence, the value of this Froude number was found to decrease with time, the decay proceeding in accordance with a power-law relationship of the form $Fi = at^{-b}$. On a log-log plot, both the intercepts a and the negative slopes b of this family of Fi decay curves were found to decrease in a fairly regular manner with increasing stability. This made it possible to summarize the experimental observations of the trends in Fi in the form of the approximate, empirical nomogram reproduced in Figure 46.

Strong two-dimensional jets and a near-collapse of the turbulent decay process (the decay rate abruptly decreasing to approximately $\underline{u}^2 \propto t^{-1/2}$, cf. last few points of Figure 47) were found to be closely

associated with the attainment of the lower value designated on the nomogram, Fi = 0.6, eight observations lying within ±0.04 of this value. Because of the choice of d, the definition of Fi used here differs from that of Long and Yih by a factor of 2; consequently, this lower critical value corresponds very closely to the theoretical value $1/\pi = 0.32$. Note, however, that this terminal state never was allowed to appear in the trajectory experiments, since comparatively weak stabilities and relatively short periods of observation were employed. In terms of the nomogram, the trajectory observations were terminated well before Fi fell to 0.6.

Departures from Homogeneous Decay

The ordinate Fi = 1.0 is also marked for special attention on the nomogram of Figure 46. In the two-dimensional jet experiments, values of Fi near unity gave some appearance of indicating the onset of a regime of accelerated turbulent decay in stable stratifications; but as a reproducible criterion, it left much to be desired. Increased rates of decay were observed in only 6 out of 10 cases, while the values of Fi associated with their beginnings were scattered from 1.3 to 0.7. However, similar regions of accelerated decay were subsequently indicated in many of the trajectory experiments, and there is reason to believe that the effect is genuine. It does not simply arise from errors in measurement or analysis.

Initially, this disturbed decay effect was thought to be associated with an intermediate regime of accelerated, "nonviscous" decay (see Chapter III), somehow influenced by the stability to occur earlier and closer to the grid in a region normally occupied by normal, first-period decay. This interpretation principally arose from the fact that the rate of decay observed approximately equaled that theoretically predicted for the intermediate period, namely, $\underline{u}^2 \propto t^{-10/7}$. However, subsequent trajectory experiments have eliminated the association of this effect with the stable regime, for it has been found under neutral

and unstable conditions as well. Further, close examination and re-analysis of one of the most pronounced examples obtained in the two-dimensional jet studies (shown in the log-log plot of Figure 47) indicates that, rather than representing an alternate regime of homogeneous turbulent decay, the appearance of accelerated decay in these experiments is associated with systematic departures of the turbulent fields from homogeneity.

Increased decay first appears near decay time $t \approx 12$ sec in the figure. Examination of the distribution of energy across various levels in the test section shows that excess disappearance of turbulent energy after that time principally occurs near the level of maximum velocity in the profile. The data are not conclusive, for the experiments were not designed to investigate this point; ten samples per level cannot lead to an accurate estimation of energy. Be that as it may, these results are cited in order to illustrate what appears to be a systematic departure of the fields of turbulence from homogeneity in the region of apparent overall increased decay.

At t = 10.5 in Figure 47, several seconds before the decay curve exhibits an increase in slope[1] in excess of the normal characteristic of the initial period; the total variance of all observations taken from all ten levels was 9.1 mm^2/sec^2. In the same photograph, the variance of just the two levels containing a weak relative jet maximum located just below the central level was 9.0 mm^2/sec^2; the combined variance of the two levels bounding the jet above and below was 7.9 mm^2/sec^2, while the combined variance of the four levels bounding the foregoing three (i.e., two above and two below) was 8.8 mm^2/sec^2. Thus, prior to the appearance of the region of disturbed decay, the

---

[1] References to changes in the slope of decay curves here refer to plots of the reciprocal of the root-mean-square fluctuation, u^{-1}, versus the decay time t; thus, increased slope corresponds to increased decay rate and vice versa.

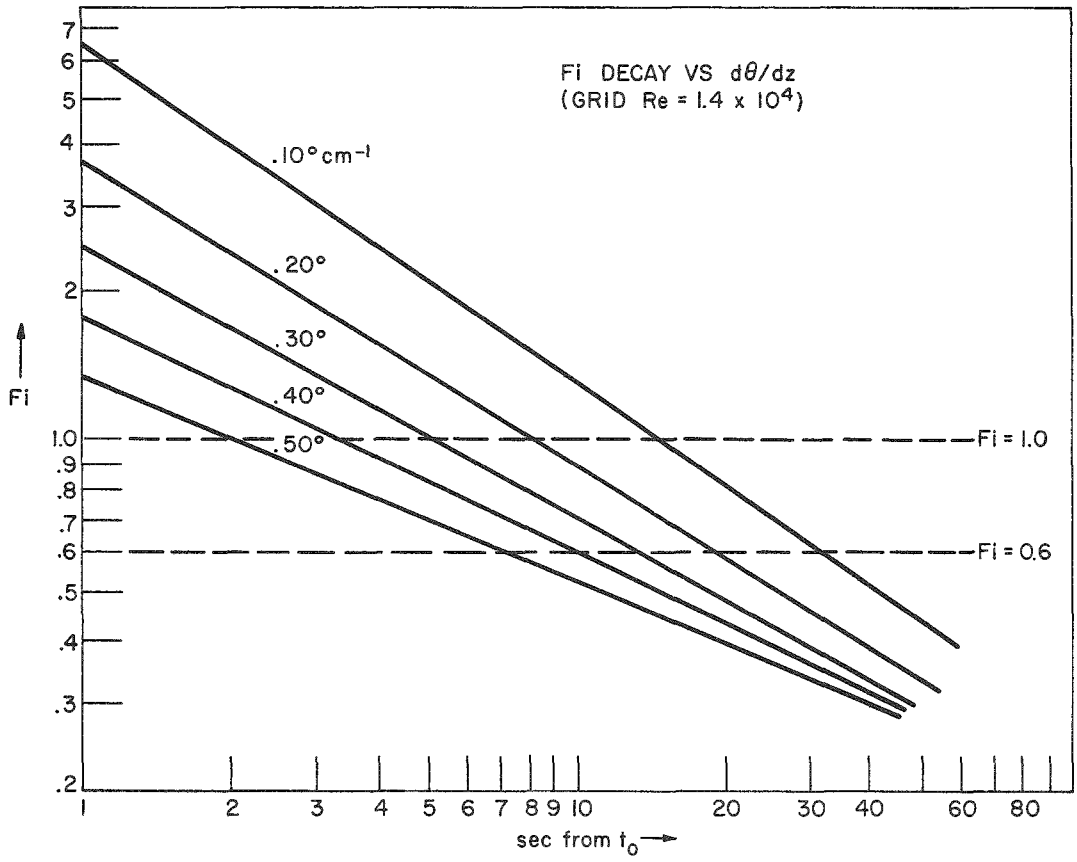

Fig. 46.--Nomogram representing the approximate observed decay of the internal Froude number in the two-dimensional jet experiments.

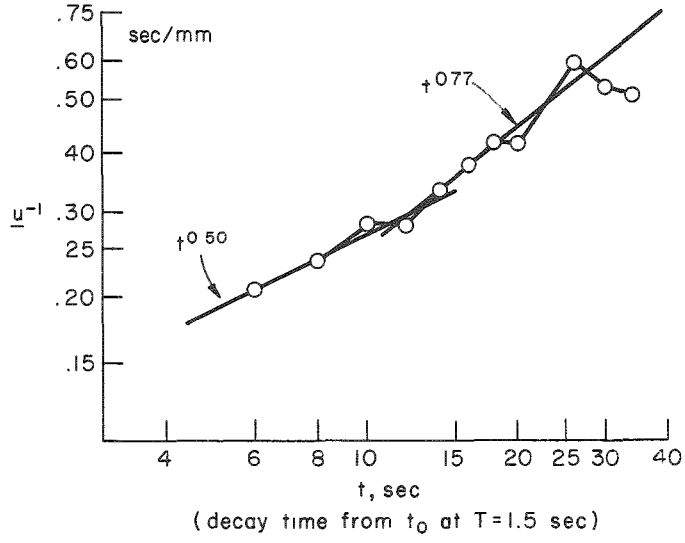

Fig. 47.--Observed change in the rate of decay of the longitudinal component of turbulence with the onset of the inhomogeneous condition; lapse rate approximately neutral, grid-speed, 25 cm per sec.

vertical distribution of turbulent energy was fairly uniform (i.e., flat within 10 per cent.).

On the other hand, at time t = 18.5 (5 sec after the decay curve deflects upward), this was no longer the case. By this time, decay had reduced the overall variance of the ten levels to 3.7 mm^2/sec^2; but two levels containing a moderately strong jet in the center of the tank showed a combined variance of only 2.7 mm^2/sec^2; the two on either side of the jet had a slightly larger variance equal to 3.3 mm^2/sec^2, while the two on either side of the central four showed a markedly larger variance of 5.9 mm^2/sec^2. In the remaining four levels (the upper and lower two) the variance decreased again to 3.4 mm^2/sec^2. Thus, energy changes from level to level now exceed a range of ±35 per cent. If the linear energy decay of the earlier portions of the experiment had continued until this later time, the overall variance would have been in the neighbourhood of 6.0 mm^2/sec^2, very close to the maximum observed in the third and eighth levels on either side of the central jet (i.e., in the region of maximum mean shear).

From the available data it is difficult to determine just how this selective disappearance of energy among the levels in the test section might occur. However, trajectory data decay curves such as that obtained for case N/25/z indicate that what in some cases appears to be the establishment of a monotonic increase in the rate of turbulent decay may only be the beginning of a temporary disturbance. In Figure 14 for this case, note that the decay slope begins to increase near T = 8 sec but returns to normal near T = 14 sec. Since this 6-sec period is approximately that of the surge, and since the disturbance first appears very near to the time of the arrival of the reflected surge in the test section, it seems likely that the apparent increased decay effect is associated with the surge component.

Successive profile measurements show that the surge takes the form of a local intensification of the toroidal drift circulation; the

velocities of both the main downstream current in the core and the secondary return flow along the boundaries increase. Even in neutral stratifications this tends to produce periodically something approaching a broad jet maximum in the complete profile, only a portion of which is seen in the test section. Note in Figure 45 that at grid time T = 10 sec in the neutral case (this being close to the time of the maximum surge) the entire visible portion of the profile is shifted toward higher velocities. Since the lid exhibits little vertical motion in this region (between 1.0 and 1.5 m from the end clamps), the net flow through the test section must remain approximately unchanged; therefore, return flows above and below the visible section of the complete profile must simultaneously undergo similar, but opposite, intensification. Evidently, this appearance of a broad jet in the neutral case is sufficient to disrupt the homogeneity of the turbulence field in much the same way as is accomplished by narrower, more intense jets in stable conditions; for disturbed periods of decay, approximately synchronized with the surge maximum, are frequently observed in both neutral and stable stratifications.

Locally increased rates of turbulent decay have been observed in wind tunnels under conditions deliberately designed to produce inhomogeneous fields of turbulence (Townsend, 1956, pp. 51-56). But in such experiments, the maximum rates of dissipation of turbulent energy occur in regions of maximum turbulence intensity, an association tending to return the field to homogeneity. On the other hand, local variations in rates of decay in the current experiments, initially at least, appear to remove the turbulence field even further from the homogeneous condition; in order to have attained the vertical energy distribution found late in the experiment of Figure 47, maximum disappearance of turbulent energy must have taken place at levels of minimum turbulence intensity during at least a part of the period preceding the time of observation.

Even with the limited information available, it seems fairly certain that the form of inhomogeneous turbulent decay observed in the wind-tunnel experiments is not involved to a significant degree in the disturbed periods of decay observed in the towing tank. Rather, it would appear that a significant fraction of that portion of the limited turbulence spectrum observed by the methods of observation employed in these studies supplies energy directly to the jet in the central levels of the towing channel, and probably to the upper and lower return jets as well. If this is the case, the mechanisms involved in this transfer of turbulent energy to the mean circulation are of considerable interest to other meteorological problems; hence, this feature is certainly worthy of further study.

Finally, note that the profiles for the unstable case in Figure 45 remain the flattest of all, showing neither a marked jet maximum nor a significant overall increase in velocity at the time of arrival of the surge. As may be seen in Figures 33 through 40, this increased uniformity (the result, no doubt, of increased vertical exchange) is associated with somewhat more consistent behaviour upon the part of the decay curves. In the eight cases measured in the unstable regime, there are only two fairly well-marked deviations in decay slope near T = 10 sec, and these are somewhat less pronounced than the majority of those observed in stratifications other than unstable.

Whatever may be the details of the mechanism of this distortion in homogeneous decay, to the principal experiment it contributed an effect that it was necessary to avoid, since any departure from the decay characteristics of the initial period would invalidate the basic assumption of the Batchelor corrections. For this reason, when results of the initial computer run for any experiment revealed large departures from the first-period decay slope, the data corresponding to the observations in doubt were deleted from the input of the autocorrelation computation. Data exhibiting moderate departures from the linear decay law were sometimes retained, but individual

correlation estimates based upon these were reviewed for consistency relative to their neighbors in corrected time. Where the results appeared doubtful, they also were deleted.

It remains to be explained why the accelerated decay effects appear in the results of some experiments and not in others. A clue to the answer to this question lies in the results of experiment $N/25/x_y$, shown in Figure 15. Here the observed velocity fluctuations determine a decay curve with one of the most clearly marked changes of slope found during the investigation. Photographs for this case were taken from above the tank under circumstances of improved lighting that made it possible to collimate the illumination into a centered range of depths significantly narrower than that viewed by the camera mounted at the side of the tank in previous experiments. In addition, tracer droplets in the vertical-view cases were initially distributed in a centrally located horizontal, rather than vertical, plane. As a result, a larger number of the trajectories selected for measurement in these cases tended to be located near the central levels of the tank, within the region of jet maxima and, hence, within the region of maximum departures from homogeneity. In contrast, trajectories selected from side-view cases were generally distributed over a wider range of depths, both because of the vertically wider field of illumination and because of the initial tracer distribution in a vertical plane. Thus, in side views, the proportion of selected trajectories which lay in the regions of accelerated decay became a matter of chance.

A similar relationship could obtain between any two experiments in which trajectories selected for measurement for one lay, by chance, more closely grouped about the central levels than in another. Consequently, the more or less random appearance in the experiments of periods of significantly accelerated decay can probably be attributed to the random vertical distribution of the selected trajectories about the central regions of inhomogeneity.

REFERENCES

Angell, J. K., 1960: An analysis of operational 300 mb transosonde flights from Japan in 1957-58. J. Meteorol., 17, 20-35.

Angell, J. K., and D. H. Pack, 1960: Analysis of some preliminary low-level, constant volume balloon (tetroon) flights. Mo. Wea. Rev., 88, 235-248.

Angell, J. K., and D. H. Pack, 1962 Analysis of low-level constant volume balloon (tetroon) flights from Wallops Island. J. of Atmos. Sci., 19, 87-98.

Baldwin, L. V., and T. J. Walsh, 1961: Turbulent diffusion in the core of fully-developed pipe flow. Am. Inst. Chem. Eng. J., 7, 53-61.

Barad, M. L., 1959: Analysis of diffusion studies at O'Neill; in Advances in Geophysics, 6, Frenkiel, F. N., and P. A. Sheppard, eds., loc. cit., 389-398.

Batchelor, G. K., 1952: Diffusion in a field of homogeneous turbulence. II. The relative motion of particles. Proc. Camb. Phil. Soc., 48, 345-362.

Batchelor, G. K., 1953: The conditions for dynamical similarity of motions of a frictionless perfect-gas atmosphere. Quart. J. Roy. Meteorol. Soc., 79, 224-235.

Batchelor, G. K., 1956: Turbulent diffusion; in Surveys in Mechanics. Batchelor, G. K., and R. M. Davies, eds. Cambridge Univ. Press, Cambridge, 352-399.

Carslaw, H. S., and J. C. Jaeger, 1959: Conduction of Heat in Solids, 2nd ed. Clarendon Press, Oxford, 510 pp.

Collis, D. C., 1948: The diffusion process in turbulent flow. Rpt. A-55, Comm. Sci. and Ind. Res., Div. of Aero., Melbourne, Australia, 18 pp.

David, F. N., 1938: Tables of the Correlation Coefficient. Cambridge Univ. Press, Cambridge, 55 pp.

Eckart, C., 1960: Hydrodynamics of Oceans and Atmospheres. Pergamon Press, New York, 290 pp.

Edinger, J. G., 1951: A technique for measuring the detailed structure of atmospheric turbulent flow; in Geoph. Res. Pa. No. 19, Hewson, E. W., ed., loc. cit., 241-261.

Frenkiel, F. N., 1948: On the kinematics of turbulence. J. Aeronauts Sci., 15, 57-64.

Frenkiel, F. N., 1953: Turbulent diffusion; in Advances in Applied Mechanics, 3, von Mises, R., and T. von Karman, eds. Academic Press, New York, p. 61.

Frenkiel, F. N., and P. A. Sheppard, eds., 1959: Advances in Geophysics, 6, Proc. of Oxford Symp., 1958. Academic Press, New York, 471 pp.

Frenzen, P., 1960: The Argonne meteorological model towing tank. ANL-6297, pp. 109-113.

Fultz, D., 1951: Non-dimensional equations and modelling criteria for the atmosphere. J. Meteorol, 8, 263-267.

Gifford, F., 1955: A simultaneous Lagrangian-Eulerian turbulence experiment. Mo. Wea. Rev., 83, 293-301.

Gifford, F., 1959: Statistical properties of a fluctuating plume model; in Advances in Geophysics, 6, Frenkiel, F. N., and P. A. Sheppard, eds., loc. cit., 117-137

Haltiner, G. J., and F. L. Martin, 1957: Dynamical and Physical Meteorology. McGraw-Hill Book Co., Inc., New York, 470 pp.

Hay, J. S., and F. Pasquill, 1957: Diffusion from a fixed source at a height of a few hundred feet in the atmosphere. J. Fluid Mech., 2, 299-310.

Hewson, E. W., ed., 1952: International Symposium on Atmospheric Turbulence in the Boundary Layer. Geoph. Res. Pap. No. 19, Geoph. Res. Dir., A.F.C.R.C., Cambridge, Mass., 530 pp.

Hilst, G. D., 1957: Observations of the diffusion and transport of stack effluents in stable atmospheres. Ph.D. dissertation, The Univ. of Chicago.

Inoue, E., 1951: On the Lagrangian correlation coefficient for turbulent diffusion and its application to atmospheric diffusion phenomena; in Geoph. Res. Pap. No. 19, Hewson, E. W., ed., loc. cit., 397-412.

Inoue, E., 1960; On the shape of stack plumes. Mem. on Meteor. Res., Jap. Meteor. Soc., 11, 332-339.

Kalinske, A. A., and C. L. Pien, 1944: Eddy diffusion. Ind. Eng. Chem., 36, 220-223.

Kuo, H. L., 1961: Solution of non-linear equations of cellular convective heat transport. J. Fluid Mech., 10, 611-634.

Lin, C. C., 1961: Statistical theories of turbulence; in Turbulent Flows and Heat Transfer, Lin, C. C., ed., Princeton Univ. Press, Princeton, pp. 196-253.

Long, R. R., 1959: The motion of fluids with density stratification. J. Geophys Research, 64, 2251-2263.

Mickelsen, W. R., 1955. An experimental comparison of the Lagrangian and Eulerian correlation coefficients in homogeneous isotropic turbulence. NACA Tech. Note No. 3570, 42 pp.

Moses, H., and J. H. Willett, 1955: Five-year climatological summary, July 1949 to June 1954. ANL-5592, 390 pp.

Panofsky, H. A., 1962: Scale analysis of atmospheric turbulence at 2m. Quart. J. Roy. Meteor. Soc., 88, 57-69.

Panofsky, H. A., and R. J. Deland, 1959: One-dimensional spectra of atmospheric turbulence in the lowest 100 meters; in Advances in Geophysics, 6, Frenkiel, F. N. and P. A. Sheppard, eds., loc. cit., 41-62.

Pasquill, F., 1962: Atmospheric Diffusion. Van Nostrand, London, 297 pp.

Rider, N. E., 1954: Eddy diffusion of momentum, water vapor, and heat near the ground. Phil. Trans. Roy. Soc. A246 481-501.

Roberts, O. F. T., 1923: The theoretical scattering of smoke in a turbulent atmosphere. Proc. Roy. Soc. (London) A104, 640-654.

Stewart, R. W., and A. A. Townsend, 1951. Similarity and self-preservation in isotropic turbulence. Phil. Trans. Roy. Soc. (London) A234, 359-386.

Sutton, O. G., 1947: The theoretical distribution of airborne pollution from factory chimneys. Quart J. Roy. Meteor. Soc., 73, 426-436.

Sutton, O. G., 1953: Micrometeorology. McGraw-Hill Book Co., Inc., New York, 333 pp.

Taylor, G. I., 1921. Diffusion by continuous movements. Proc. Lon. Math. Soc., 20, 196-212.

Taylor, G. I., 1935: Statistical theory of turbulence. Parts I-IV. Proc. Roy. Soc. (London) A151, 421-478.

Taylor, G. I., 1938: The spectrum of turbulence. Proc. Roy. Soc. (London) A164, 476-490.

Townsend A. A., 1956: The Structure of Turbulent Shear Flow. Cambridge Univ. Press, Cambridge, 315 pp.

Uberoi, M. S., and S. Corrsin, 1953: Diffusion of heat from a line source in isotropic turbulence. NACA Rpt. No. 1142, 90 pp.

United States Weather Bureau, 1955: Meteorology and Atomic Energy. U.S. Govt. Printing Off., 169 pp.

Vanoni, V. A., and N. H. Brooks, 1955: Rpt. No. E-46, Hydro. Lab., Cal. Inst. of Tech., 51 pp. (ASTIA Reprint AD 66182).

Washburn, E. W., et al., eds., 1926-1933: International Critical Tables. Nat. Res. Council, New York, 8 vol.

Webb, E. K., 1955: Autocorrelations and energy spectra of atmospheric turbulence. Tech. Pap. No. 5, Comm. Sci. and Ind. Res. Org., Div. of Meteor. Phys., Melbourne, Australia, 28 pp.

Yih, C. S., 1959: Effect of density variation on fluid flow. J. Geophys. Research, 64, 2219-2223.